Simulation of Wind-Forced Responses over the Newfoundland Shelf

by

© Zhimin Ma

A thesis submitted to the School of Graduate Studies in partial fulfillment of the requirements for PhD of Science

Department of Physics and Physical Oceanography
Memorial University of Newfoundland

August, 2015

St. John’s Newfoundland

Abstract

A three-dimensional finite volume coast ocean model (FVCOM) is applied to understand better the wind forced oceanic responses over the Newfoundland Shelf including its embayments, especially during hurricane events. The hurricane-ocean model is applied over the Newfoundland Shelf to examine the mechanism that results in the significant coastal sea level rise and sea surface temperature drop. Model is coupled with Holland hurricane wind model to represent well the fast moving hurricanes. Hurricane induced coastal trapped waves are found through the analysis of tide-gauge sea level and currents. Turbulent mixing is the dominant process causing the sea surface temperature (SST) drop. The model is further applied to investigate the different oceanic response during Hurricane Igor (2010) and Hurricane Leslie (2012) on Placentia Bay. The model results agree reasonably well with field observations on sea level, near-surface currents and sea surface temperature (SST). The two hurricanes feature significant different tracks, radius and maximum sustainable wind, causing opposite shifts in inner bay circulation. The peak storm surge is significantly influenced by local atmospheric forcing during Leslie, but predominately due to remote forcing during Igor. Baroclinicity is important for the hurricane-induced inertial oscillation in the near-surface currents. The barotropic simulation results in a significant underestimate of the near-surface currents, including the inertial oscillation. FVCOM is finally applied off Eastern Newfoundland to study the circulation and hydrographic variability in 2000 and 2001. The model results along the eastern Newfoundland coast agree reasonably well with observations of sea level and currents. The model surface circulation patterns and temperature distributions in Trinity

Bay in spring and summer reveal seasonal differences along the coast. Summer circulation shows significant upwelling along the western side of the bay, together with the emergence of two eddies in the bay. The generation of these eddies reveals the importance of nonlinear dynamics. The stratification along the Newfoundland coast shows the spatial differences and the seasonal and inter-annual change of stratification due to the wind stress and heat flux.

Acknowledgment

I would like to thank Prof. **Guoqi Han** and Prof. **Brad de Young** for the assistance and guidance during my graduate program.

Thanks to Dr. Brad de Young for providing the observed data for comparison.

Thanks to Dr. Changsheng Chen for providing the FVCOM source code.

Table of Contents

List of Tables

List of Figures

List of Symbols

σ	sigma coordinate from 0 to -1
ξ	free surface elevation(m)
D	water depth plus sea level(m)
H	bottom depth(m)
K_m	vertical turbulent viscosity(m^2/s)
K_h	vertical diffusivity (m^2/s)
ρ	potential density(kg/m^3)
A_m	horizontal viscosity(m^2/s)
A_h	horizontal diffusivity(m^2/s)
T	potential temperature(^{o})
S	salinity(psu)
q^2	twice the turbulent kinetic energy (m^2/s^2)
l	turbulent length scale
u	eastward velocity(m/s)
v	northward velocity(m/s)
ω	sigma coordinate vertical velocity(m/s)
κ	von Karman constant=0.4

1. Introduction

1.1 Newfoundland Shelf and Its Embayments

The Newfoundland Shelf is located in the Northwest Atlantic, including the Grand Banks, Placentia Bay, Bonavista Bay, Trinity Bay, Conception Bay and other important coastal embayments. The ocean circulation and hydrography of the Newfoundland Shelf is strongly influenced by the Labrador Current, the North Atlantic Current, surface heat flux and ice formation and melting (Loder et al., 1998). Wind stress, atmospheric pressure perturbation and net freshwater flux at the sea surface also affect the circulation and hydrography in this region. With the interaction between the cold, fresh Labrador Current and warm, salty North Atlantic Current waters, there are stronger seasonal variations in temperature and salinity over the Newfoundland Shelf than the Labrador Shelf. The relatively shallow Newfoundland Shelf plays an important role in the seasonal heat flux budget, resulting in significant marine ecosystem fluctuations (Bradbury et al., 2000).

The Grand Banks of Newfoundland, which is the largest component of the Newfoundland Shelf, covers the region with a horizontal dimension of about nearly 500 km of longitude and 600 km of latitude. The Bank is separated from the coast by the Avalon Channel (Fig.1-1). The average depth of the bank is around 80 m. The mean circulation is weak around 0.05 m/s on the central bank (Han et al., 2008), but strong around 0.3 m/s during wind events such as hurricanes (Ma et al., 2015). The strong winds result in significant vertical mixing over the bank and lead to sudden change in sea surface temperature by 6^{o}C (Han et al., 2012a). The equator-ward flowing shelf-edge Labrador Current meets the polar-ward receded North Atlantic Current at the tail of the

Grand Banks. The inshore Labrador Current flows through the Avalon Channel into Placentia Bay and onto the southwestern Newfoundland Shelf (Han et al., 2008, 2011).

Placentia Bay is located in the south Newfoundland (See Fig. 1-1 PB) and is bordered by the Burin Peninsula to the west and the Avalon Peninsula to the east. The mouth of the bay extends over 100 km towards the head of the bay, with a deep basin in the central bay. The mean circulation is anti-clockwise and driven by the inshore Labrador Current that flows through Avalon Channel (Hart et al., 1999; Schillinger et al., 2000; Bradbury et al., 2000). deYoung et al. (1993b) demonstrated the importance of wind to circulation in coastal embayments such as Placentia Bay. They also suggested that non-local forcing should be taken into account in bay studies. During summer, upwelling events exist along the head and western side of the bay.

Trinity Bay is one of several large embayments along the east coast of Newfoundland (See Fig. 1-1 TB). The bay is 30 km wide at the mouth and extends 70 km from the mouth to the head of bay. The mean circulation pattern is suggested by Tittensor et al. (2002, a and b) with eddies existing at the centre of the bay, a clear inflow at the northwestern mouth of bay and an outflow at the southeastern mouth of bay. Floating sea ice from the northern Labrador Shelf frequently flows into the bay during winter and therefore the melting ice could keep cold and fresh surface water until summer. Predominant westerly winds during summer cause upwelling along the western side of the bay and downwelling along its eastern side (Yao,

1986).

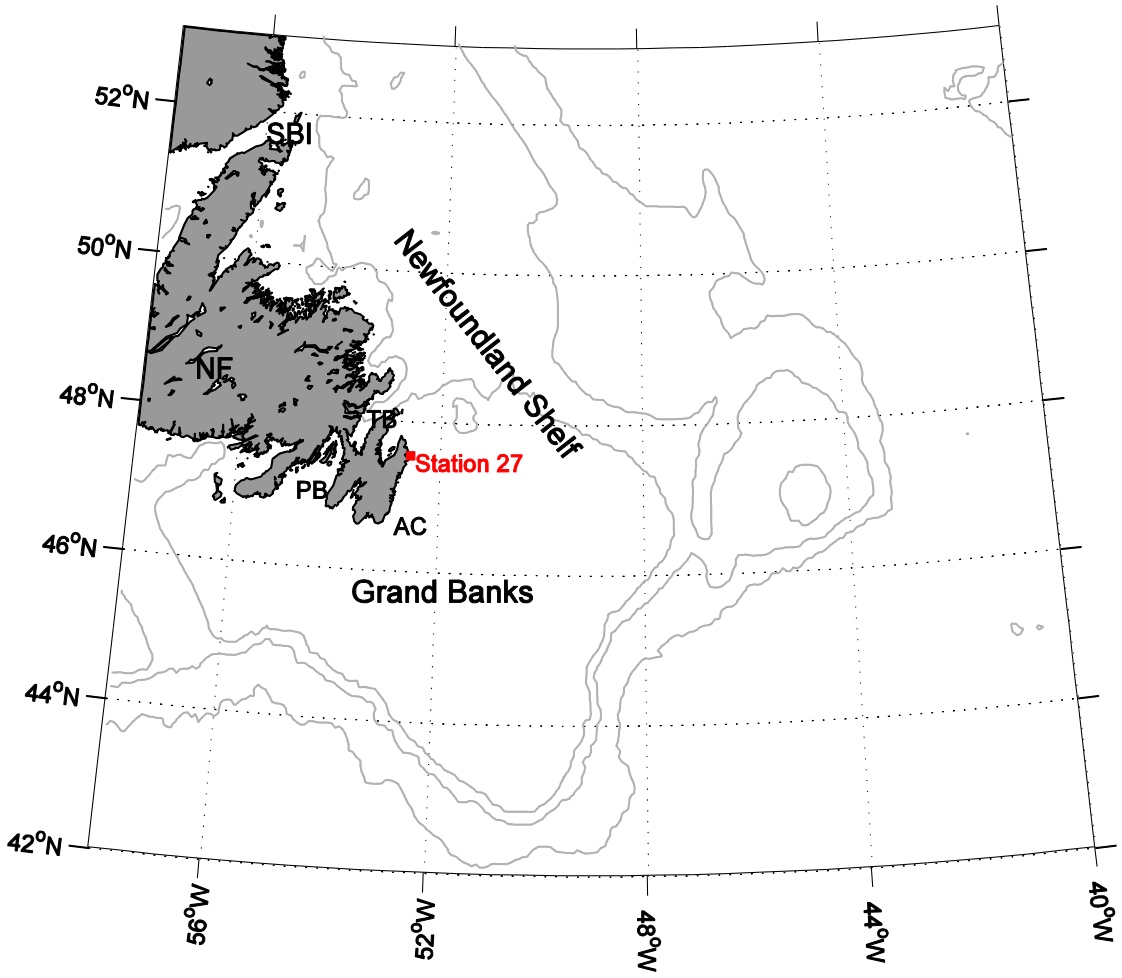

Fig. 1-1: Map showing the topography of Newfoundland Shelf. SBI is the Strait of Belle Isle. PB is the Placentia Bay and TB is the Trinity Bay. AC is the Avalon Channel. The grey lines are 200, 1000 and 3000m.

1.2 Oceanographic Study over the Newfoundland Shelf and Its Limitation

Over the past two decades, efforts based on *in situ* observations have been made on the Newfoundland Shelf to better understand the circulation and hydrography variability (Colbourne et al., 1997), and even to monitor the short time scale wind response. Four tide gauge stations are located along the Newfoundland coast. They are located at

Bonavista, St. John's, Argentia and St. Lawrence from north to south along the coast (see Fig. 1-1). The St. John's tide gauge station is located inside the harbor and the dataset collected at this station can be traced back to 1935. Station 27 (see Fig. 1-1) is located at 47.55^{o} N and 52.59^{o} W (8 km southeast to St. John's), with a water depth of 176 m. This station is unique due to its long historical record tracing back to 1946 for vertical hydrographic profiles, together with biological and chemical data as well. Since the late 1990s, temperature and salinity data at Station 27 have regularly been collected by the Northwest Atlantic Fisheries Centre through the Atlantic Zone Monitoring Program (AZMP) of Fisheries and Oceans Canada (www.Meds-sdmm.dfo-mpo.gc.ca/isdm-gdsi.azmp-pmza/index-egn.html). The AZMP program also collects hydrographic data along the Bonavista and Flemish Cap transects over the Newfoundland Shelf.

The surface circulation and its wind forced response of coastal embayment are of interest because of the convergence or divergence of the flow due to the wind set up and the influence of low-frequency travelling continental shelf wave (de Young et al., 1993a). As early as 1987, observational monitoring inside the embayments on the Newfoundland Shelf started. Weak tides and weak mean flows were found in Conception Bay by Aggett et al. (1987) and deYoung and Sanderson (1995). Since then, Hart et al. (1999) and Scillinger et al. (2000) documented the observed mooring stations in 1998 and 1999 summer in Placentia Bay to examine the mean circulation pattern and monitor the real-time hydrographic variation at different depths. Recently, extensive efforts have been made to understand the physical, chemical and biological processes of Placentia Bay for example through the Smart Bay Project launched by the Marine Institute of Memorial

University in early 2000s (http://www.smartbay.ca/). The Smart Bay Project regularly collects oceanographic data at three fixed stations located inside Placentia Bay. In 2001 and 2002, Tittensor et al., (2002a and b) analyzed the observational data on the circulation and hydrography in Trinity Bay. The ADCP and mooring data suggest small scale circulation inside of the bay, together with the non-linear advection and the significant summer upwelling at the western side of bay.

There have been a number of numerical studies on ocean dynamics over the Newfoundland Shelf and its embayments including Placentia Bay and Trinity Bay, e.g., Hannah et al.'s (1995) linear models for the Grand Banks circulation, Tang et al.'s (1996) diagnostic modeling for the Labrador Shelf, Sheng and Thompson's (1996) diagnostic calculation of summer surface circulation. Greenberg and Petrie (1988) simulated barotropic mean circulation in the Grand Banks region with a numerical model, and showed notable discrepancies between observed and modeled flows. Greatbatch et al. (1996) applied a barotropic, shallow-water model of the North Atlantic to investigate the synoptic sea level variability. Han (2005) investigated the barotropic wind-driven circulation over the Newfoundland and Labrador shelf using a three-dimensional finite element model and demonstrated the importance of wind-driven transport over the Newfoundland Shelf. Han et al. (2008) examined the seasonal variability of the Labrador Current and shelf circulation off Newfoundland using a semi-prognostic model. Han et al. (2011) improved the model performance in reproducing the seasonal variation of currents and transport over Newfoundland Shelf. Urrego-Blanco and Sheng (2012) simulated the seasonal and inter-annual variability over the eastern Canadian continental shelf by applying the spectral nudging method. Wu et al. (2012) examined the seasonal and annual

mean variation on the Labrador Current currents and its freshwater transport. Ma et al. (2012) applied a finite volume model over Placentia Bay to reproduce the circulation and hydrography variability in 1999. These modelling studies provide us the basic knowledge of circulation and hydrograph over Newfoundland Shelf.

1.3 Hurricanes induced response over the Newfoundland Shelf

Given the increase of global sea-surface temperature, both the total number of tropical cyclones and the proportion of intense tropical cyclones have increased notably since 1970 (Webster et al., 2005; Emanuel, 2005). Hurricane-induced storm surges may be aggravated by accelerated sea-level rise (Han et al., 2015). Theoretical explanations on the oceanic responses to a moving storm have been provided (Greatbatch, 1983; Gill, 1984), focusing on the inertial oscillation in the wake of a storm. Gill (1984) argued that a pumping mechanism forcing vertical motions was induced by the localized of convergence and divergence when storm passed. This vertical motion was impacted by the initial stratification and the parameterization of the storms. Greatbatch (1983) found that the rapid transition from the maximum of downwelling to the maximum of upwelling were associated with the along-track advection; while the displacement of the maximum response to the right with the cross-track advection. Modelling studies of hurricanes impacts on storm surge in the coastal waters have been quite frequent over the past decade. (e.g. Resio and Westerink, 2008; Shen et al., 2006; Weisberg and Zheng, 2006a, b; Westerink, 2008). Storm surge calculation was the primary purpose for these numerical simulations. Insights into surge mechanism were also examined in numerical experiments. Weisberg and Zheng (2006 a, b; 2008) and Rego and Li (2010) investigated the coastal inundation and surge propagation along a coastal embayment. Xie et al. (2004)

discussed inundation algorithms and flooding velocities using the Princeton Ocean Model forced by an idealized Category-3 hurricane. Shen et al. (2006) simulated Hurricane Floyd's storm tide of September 1999 in Chesapeake Bay, with a substantial dataset for validation and concluded that water levels inside the bay can be explained by the superposition of the surge propagated into the bay and that generated by local wind forcing.

Hurricanes or tropical storms pass across the Newfoundland Shelf occasionally from August to October, resulting in strong near-surface current and storm surge along with significant drops in sea surface temperature (hereafter SST) and enhancement of vertical mixing, e.g. Han et al. (2012a). Han et al. (2012a) showed a sharp sea surface temperature decrease around $6\,^{o}C$ from buoy observations under Hurricane Igor. The occurrence of a phytoplankton bloom over the Grand Banks was attributed to the mixed-layer deepening and upwelling associated with the strong wind stress curl. With the same hurricane, Han et al. (2012b) also found that the storm surge along the East Newfoundland coast was associated with a continental shelf wave generated. However, monitoring both spatial and temporal effects of hurricanes and tropical storms is limited. We can overcome this gap through the application of ocean modelling with reconstructed winds from a hurricane wind model. As such we can improve our understanding of the physical and biological response to extreme weather events in such under-observed regions.

Numerical simulation of ocean’s responses to spatially uniform wind or hurricanes winds over the Newfoundland Shelf has been initiated since 1980s. Yao (1986) examined

the responses of currents to the wind in Trinity Bay. deYoung and Tang (1990) discussed and simulated baroclinic near-inertial currents on the Grand Banks induced by a storm using a two-layer idealized model. Using a linear barotropic model, Tang et al. (1997) investigated four types of wave motions for an idealized moving storm off Newfoundland and Labrador. Mercer et al. (2002) modelled the barotropic response to a storm, explaining the mechanism for coastal sea level change associated with a fast moving storm passing over the Grand Banks. However, previous modelling studies during hurricanes were based on an idealized storm and were from a barotropic perspective. To understand both the barotropic and baroclinic response a fully prognostic and baroclinic ocean model under realistic atmospheric forcing is required.

1.4 Objective

The goal of this thesis is to develop a three-dimensional baroclinic ocean model that can better simulate seasonal evolution from spring to fall and oceanic responses during storms and explain physical mechanisms on the oceanic responses to winds. To accomplish this goal, three steps are performed. The objectives of the first step are to simulate a hurricane event over the Newfoundland Shelf including the storm-induced surge and SST decreasing and to examine mechanisms of these oceanic responses by developing a three-dimensional (3D) high resolution ocean model. The model domain covers the Newfoundland Shelf and the southern Labrador Shelf. The second step of the study, focusing on Placentia Bay is to examine the different responses during Hurricanes Igor in 2010 and Hurricanes Leslie in 2012. The objective of this study is to explain mechanisms for significant sea level rise and for hurricane-induced inertial oscillation.

The final step is to reproduce the seasonal sea level and temperature variability in Trinity Bay and over the adjacent eastern Newfoundland Shelf. The objectives of the final step are to examine the evolution of hydrography and surface circulation in response to seasonal wind events and to understand underlying mechanisms.

1.5 Outline of Thesis

As opposed to a traditional thesis format, this thesis is composed of three journal articles (one published, two submitted). Some materials in the articles may have been presented in the introduction. Each article has its own reference list, with a separate reference list for the entire thesis. The original research papers of this thesis appear in Chapters 3, 4 and 5. Chapter 2 describes the basic equations of the circulation model and its boundary conditions at surface and bottom. Chapter 6 provides a summary and concludes with thoughts for future work.

2. Hydrodynamic Equations

2.1 Basic Equation

The numerical model used for this study is an unstructured grid, finite-volume, three-dimensional, primitive equation, finite-volume coastal ocean model (FVCOM; Chen et al., 2003). In general, two numerical methods are used in ocean modelling. One is the finite-difference method (Blumberg and Mellor 1987; Blumberg 1994) and the other is finite-element method (Lynch and Naimie 1993; Naimie 1996). The finite difference approach is computationally more efficient, but is less capable of resolving the complicated coastal boundary. Using a triangular mesh, the finite element method can more easily and most accurately fit the irregular coastaline. This method, however, had difficulty to conserve mass and momentum. The finite volume method integrates the momentum and tracers through individual unit control volumes and is solved numerically by flux through the volume boundaries to guarantee the conservation of mass and momentum.

FVCOM (version 3.1.4) is a generalized coordinate, free surface, hydrostatic model. It uses time splitting method for computational efficiency including the internal mode and external mode. External mode is constrained by its Courant-Friedriches-Levy (CFL) condition. A second order accuracy, fourth order Runge-Kutta time stepping scheme is used for the external time integration, while the first order Euler time stepping scheme is selected for the internal time integration. A second order accurate upwind scheme is used for the spatial flux calculation for momentum and tracer values (Kobayashi et al., 1999; Hubbard, 1999). For a more accurate estimation of sea level, currents, and the salt and temperature flux, velocity variables are placed at centroids, while all scalar variables are placed at nodes.

The basic equations are presented in a terrain following, generalized coordinate system in order to obtain a smooth representation of irregular variable bottom topography. The coordinate transformation is defined as $\hat{g} = \hat{g}(x, y, r, t)$ where x and y are defined as the eastward and northward axes, and r varies from -1 at the bottom to 0 at the surface. r can be specified as a sigma, hybrid or more generalized function. An example for a hybrid coordinate is shown in Fig. 2-1.

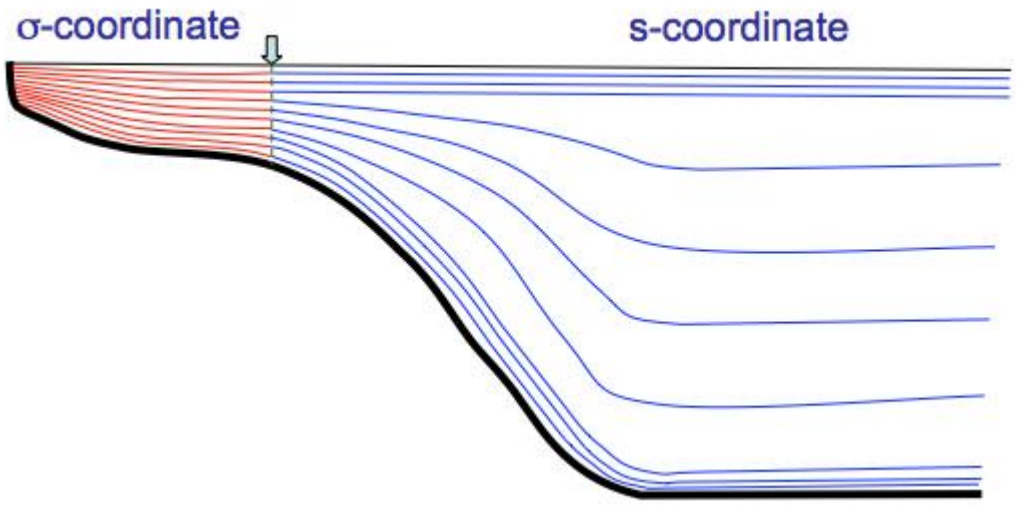

Fig. 2-1: An example of a hybrid coordinate consisting of σ- and *s*-coordinates. The dashed line indicates a transition location of two coordinates at which all layers are uniformly divided in the vertical. (FVCOM manual, 2011)

Under this coordinate system, the momentum and continuity equations are given as (2-1) - (2-3), where u, v, ω are the eastward, northward and upward velocity, K_m is the vertical eddy viscosity, and ρ is the potential density; and thermodynamic equations are as (2-4)-(2-6), where T and S are the temperature and salinity, K_h is the vertical diffusivity and $\hat{H}$ is the heat source term.

$$\frac{\partial J}{\partial t}+\frac{\partial Ju}{\partial x}+\frac{\partial Jv}{\partial y}+\frac{\partial \omega}{\partial r}=0 \tag{2-1}$$

$$\frac{\partial uJ}{\partial t}+\frac{\partial u^2 J}{\partial x}+\frac{\partial uvJ}{\partial y}+\frac{\partial u\omega}{\partial r}-fvJ$$
$$=-gJ\frac{\partial \xi}{\partial x}-\frac{J}{\rho_o}\frac{\partial \mathrm{P}_a}{\partial x}-\frac{gJ}{\rho_0}[\int_r^0 J(\frac{\partial \rho}{\partial x}+\frac{\partial \rho}{\partial r'}\frac{\partial r'}{\partial x})dr']-\frac{1}{\rho_o}(\frac{\partial qJ}{\partial x}+\frac{\partial qA_1}{\partial r})+\frac{\partial}{\partial \sigma}(\frac{K_m}{J}\frac{\partial u}{\partial r})+JF_u \tag{2-2}$$

$$\frac{\partial vJ}{\partial t}+\frac{\partial v^2 J}{\partial y}+\frac{\partial uvJ}{\partial x}+\frac{\partial v\omega}{\partial r}+fuJ$$
$$=-gJ\frac{\partial \xi}{\partial x}-\frac{J}{\rho_o}\frac{\partial \mathrm{P}_a}{\partial y}-\frac{gJ}{\rho_0}[\int_r^0 J(\frac{\partial \rho}{\partial y}+\frac{\partial \rho}{\partial r'}\frac{\partial r'}{\partial y})dr']-\frac{1}{\rho_o}(\frac{\partial qJ}{\partial y}+\frac{\partial qA_2}{\partial r})+\frac{\partial}{\partial r}(\frac{K_m}{J}\frac{\partial v}{\partial r})+JF_v \quad (2\text{-}3)$$

$$\frac{\partial TJ}{\partial t}+\frac{\partial TuJ}{\partial x}+\frac{\partial TvJ}{\partial y}+\frac{\partial T\omega}{\partial r}=\frac{\partial}{\partial \sigma}(\frac{K_h}{J}\frac{\partial T}{\partial r})+J\hat{H}+JF_T \quad (2\text{-}4)$$

$$\frac{\partial SJ}{\partial t}+\frac{\partial SuJ}{\partial x}+\frac{\partial SvJ}{\partial y}+\frac{\partial S\omega}{\partial r}=\frac{\partial}{\partial r}(\frac{K_h}{J}\frac{\partial S}{\partial r})+JF_s \quad (2\text{-}5)$$

$$\rho=\rho(T,S,p) \quad (2\text{-}6)$$

where $J=\frac{\partial z}{\partial r}$, A_1 and A_2 are coordinate transformation coefficients defined as $A_1=J\frac{\partial r}{\partial x}$ and $A_2=J\frac{\partial r}{\partial y}$. In the generalized terrain-following coordinate system, the horizontal diffusion terms are defined as:

$$DF_x\approx\frac{\partial}{\partial x}[2A_mH\frac{\partial u}{\partial x}]+\frac{\partial}{\partial y}[A_mH(\frac{\partial u}{\partial y}+\frac{\partial v}{\partial x})] \quad (2\text{-}7)$$

$$DF_y\approx\frac{\partial}{\partial y}[2A_mH\frac{\partial v}{\partial y}]+\frac{\partial}{\partial x}[A_mH(\frac{\partial u}{\partial y}+\frac{\partial v}{\partial x})] \quad (2\text{-}8)$$

$$D(F_T,F_S,F_{q^2},F_{q^2l})\approx[\frac{\partial}{\partial x}(A_hH\frac{\partial}{\partial x})+\frac{\partial}{\partial y}(A_hH\frac{\partial}{\partial y})](T,S,q^2,q^2l) \quad (2\text{-}9)$$

where A_m and A_h are the horizontal eddy and thermal diffusion coefficients, respectively.

2.2 Vertically Integrated Equation (External mode)

The vertically integrated equation (2-10 to 2-12) illustrates the external mode based on the mode splitting method (Madala and Piacsek, 1977). The external mode is for the fast moving motion, while the internal mode is responsible for the slow moving motion. Since a fast moving gravity wave exists in the ocean, sea level should be computed for the external mode. Because sea level is proportional to the gradient of the water transport,

it can be computed using the vertically integrated equations. Then the 3D internal model equations can be solved for a given sea level.

$$\frac{\partial \xi}{\partial t} + \frac{\partial (\bar{u}D)}{\partial x} + \frac{\partial (\bar{v}D)}{\partial x} = 0, \tag{2-10}$$

$$\frac{\partial \bar{u}D}{\partial t} + \frac{\partial (\bar{u}^2 D)}{\partial x} + \frac{\partial (\bar{u}\bar{v}D)}{\partial y} - f\bar{v}D = -gD\frac{\partial \xi}{\partial x} - \frac{D}{\rho_o}\frac{\partial \mathrm{P}_a}{\partial x}$$
$$-\frac{g}{\rho_0}\int_{-1}^{0}\{J[\int_{r}^{0} J(\frac{\partial \rho}{\partial x} + \frac{\partial \rho}{\partial r'}\frac{\partial r'}{\partial x})dr']\}dr' - \frac{1}{\rho_o}\int_{-1}^{0}(\frac{\partial qJ}{\partial x} + \frac{\partial qA_1}{\partial r})dr' + \frac{\tau_{sx} - \tau_{bx}}{\rho_0} + D\overline{F}_u + G_x, \tag{2-11}$$

$$\frac{\partial \bar{v}D}{\partial t} + \frac{\partial (\bar{v}^2 D)}{\partial y} + \frac{\partial (\bar{u}\bar{v}D)}{\partial x} + f\bar{u}D = -gD\frac{\partial \xi}{\partial y} - \frac{D}{\rho_o}\frac{\partial \mathrm{P}_a}{\partial y}$$
$$-\frac{g}{\rho_0}\int_{-1}^{0}\{J[\int_{r}^{0} J(\frac{\partial \rho}{\partial y} + \frac{\partial \rho}{\partial r'}\frac{\partial r'}{\partial y})dr']\}dr' - \frac{1}{\rho_o}\int_{-1}^{0}(\frac{\partial qJ}{\partial y} + \frac{\partial qA_2}{\partial r})dr' + \frac{\tau_{sy} - \tau_{by}}{\rho_0} + D\overline{F}_v + G_y, \tag{2-12}$$

where G_x and G_y are defined as

$$G_x = \frac{\partial \bar{u}^2 D}{\partial x} + \frac{\partial \bar{u}\bar{v}D}{\partial y} - D\tilde{F}_x - [\frac{\partial \bar{u}^2 D}{\partial x} + \frac{\partial \bar{u}\bar{v}D}{\partial y} - D\overline{F_x}], \tag{2-13}$$

$$G_y = \frac{\partial \bar{v}^2 D}{\partial y} + \frac{\partial \bar{u}\bar{v}D}{\partial x} - D\tilde{F}_y - [\frac{\partial \bar{v}^2 D}{\partial y} + \frac{\partial \bar{u}\bar{v}D}{\partial x} - D\overline{F_y}], \tag{2-14}$$

and the horizontal diffusion terms are approximately given by

$$D\tilde{F}_x \approx \frac{\partial}{\partial x}[2\overline{A_m}H\frac{\partial \bar{u}}{\partial x}] + \frac{\partial}{\partial y}[\overline{A_m}H(\frac{\partial \bar{u}}{\partial y} + \frac{\partial \bar{v}}{\partial x})], \tag{2-15}$$

$$D\tilde{F}_y \approx \frac{\partial}{\partial y}[2\overline{A_m}H\frac{\partial \bar{v}}{\partial y}]+\frac{\partial}{\partial x}[\overline{A_m}H(\frac{\partial \bar{u}}{\partial y}+\frac{\partial \bar{v}}{\partial x})], \quad (2\text{-}16)$$

$$D\overline{F_x} \approx \frac{\partial}{\partial x}\overline{2A_mH\frac{\partial u}{\partial x}}+\frac{\partial}{\partial y}\overline{A_mH(\frac{\partial u}{\partial y}+\frac{\partial v}{\partial x})}, \quad (2\text{-}17)$$

$$D\overline{F_y} \approx \frac{\partial}{\partial y}\overline{2A_mH\frac{\partial v}{\partial y}}+\frac{\partial}{\partial x}\overline{A_mH(\frac{\partial u}{\partial y}+\frac{\partial v}{\partial x})}, \quad (2\text{-}18)$$

The overbar "-"denote the vertical integration. $\bar{u}$ and $\bar{v}$ are vertical averaged eastward and northward velocity. τ_{sx} and τ_{bx} are the surface and bottom stress.

Equation (2-10), (2-11), and (2-12) are the continuity and momentum equations expressed in the generalized terrain-following coordinate system. The right hand side of the momentum equations contains the barotropic, inverse barometer effect, baroclinic, wind stress, horizontal diffusion and dispersion terms separately.

2.3 Horizontal Mixing Coefficient

The horizontal mixing coefficient in FVCOM can be selected as a constant value or following the Smagorinsky eddy parameterization method (Smagorinsky, 1963). The diffusion coefficient of momentum and tracer value can be expressed by (2-21) using the Smagorinsky horizontal diffusion scheme.

$$A_m = 0.5C\Omega\sqrt{(\frac{\partial u}{\partial x})^2+0.5(\frac{\partial v}{\partial x}+\frac{\partial u}{\partial y})^2+(\frac{\partial v}{\partial y})^2} \quad (2\text{-}21)$$

where C is a constant parameter from 0.1 to 0.2 and Ω is the area of the individual momentum control volume or the tracer control volume.

The vertical turbulent model can be referred to each paper in Section 3, 4 and 5.

2.4 Velocity and Temperature Boundary Treatment at the Surface and Bottom

a) Surface and bottom currents boundary condition are as follows

$$(\frac{\partial u}{\partial r},\frac{\partial v}{\partial r}) = \frac{J}{\rho_0 K_m}(\tau_{sx},\tau_{sy}) \qquad \text{at the surface } r=0,$$

$$(\frac{\partial u}{\partial r},\frac{\partial v}{\partial r}) = \frac{J}{\rho_0 K_m}(\tau_{bx},\tau_{by}) \qquad \text{at the bottom } r=-1,$$

where τ_{sx}, τ_{sy}, $\tau_{bx} = C_d\sqrt{u^2+v^2}u$, and $\tau_{by} = C_d\sqrt{u^2+v^2}v$ are the x and y components of surface wind and bottom stresses. $D=H+\xi$. The drag coefficient C_d in FVCOM is determined by matching a logarithmic layer to the model at a height z_{ab} above the bottom. $C_d = \max[\frac{\kappa^2}{\ln(\frac{z_{ab}}{z_o})},0.0025]$, where $\kappa = 0.4$ is von Karman's constant and z_o is the bottom roughness parameter (Chen et al., 2004).

A zero normal velocity was specified at the land boundary.

b) Surface and bottom condition for temperature

The surface and bottom boundary conditions for temperature are

$$\frac{\partial T}{\partial r} = \frac{J}{\rho c_p K_h}[Q_n(x,y,t) - SW(x,y,\xi,t)], \text{ at } \quad r=0 \qquad (2\text{-}22)$$

$$\frac{\partial T}{\partial r} = -\frac{A_H \tan\alpha}{K_h/J + A_H \tan\alpha \frac{\partial r}{\partial n}}\frac{\partial T}{\partial n}, \text{ at } r=-1$$

where $Q_n(x,y,t)$ is the surface net heat flux and $SW(x,y,\xi,t)$ is the short wave flux incident at the sea surface. α is the slope of the bottom bathymetry, and n is the horizontal coordinate (Pedlosky 1974; Chen et al., 2004).

Knowledge of the distribution of solar radiation in the upper ocean is important for modeling physical processes. To simulate the heat flux penetration process, Kraus (1972) first suggested an absorption profile for short wave radiation as a close simulation. This penetration procedure of the shortwave radiation can be expressed as an exponential equation involving two attenuation lengths. However, this assumption yields a poor approximation in the upper ocean. Based on the observations, downward radiation effects upon the upper ocean in conjunction with wind stress conditions have been improved by (Simpson 1981, a, b). Based on their conclusion, Chen et al., 2003 suggested that this approach leads to a more accurate prediction of near surface temperature. The shortwave profile scheme used in the present study is given by (2-23).

$$\hat{H}(x,y,z,t) = \frac{SW(x,y,0,t)}{\rho c_p}\left(\frac{R}{a}e^{z/a} + \frac{1-R}{b}e^{z/b}\right) \qquad (2\text{-}23)$$

where SW is the shortwave radiation, R is the ratio of the red component of the electromagnetic radiation in the total shortwave radiation and a and b are attenuation lengths for longer and short (blue-green) wavelength components of the shortwave irradiation.

3.0 Changes to the Code

Surface salinity is restored to the monthly mean climatology. A correction term has been added into the salinity equation as follows.

$$\frac{\partial SJ}{\partial t} + \frac{\partial SuJ}{\partial x} + \frac{\partial SvJ}{\partial y} + \frac{\partial S\omega}{\partial r} = \frac{\partial}{\partial r}\left(\frac{K_h}{J}\frac{\partial S}{\partial r}\right) + JF_s + \frac{1}{T_R}J(S - S_c) \qquad (2\text{-}24)$$

where S_c is the monthly mean salinity and T_R is the restoring time scale.

Connecting Text

The first research article addressed the first step, describing the oceanic response over Grand Banks to Hurricane Igor.

The core of the hurricane ocean model was to construct the hurricane wind field that can well resolve the hourly wind including its magnitude change. Holland's hurricane model is usually considered in constructing the hurricane wind field, keeping the maximum sustainable wind and minimum center air pressure. Simulated results were compared against observations based on tide-gauge, mooring, and satellite data. The physical mechanics resulting in the high sea level surge at St. John's were further examined. The coast trapped wave was found and the travelling wave speed was calculated based on coastal elevation and vertical averaged current. The mechanisms in producing salient sea surface temperature drop over Grand Banks were investigated.

This research paper has been written with the intention of being submitted to the *Journal of Geophysical Research*.

3. Oceanic Responses to Hurricane Igor over the Grand Banks: a modelling study

Zhimin Ma[1], Guoqi Han[2] and Brad de Young[1]

[1] Department of Physics and Physical Oceanography, Memorial University of Newfoundland, St. John's, Newfoundland, Canada.

[2] Biological and Physical Oceanography Section, Fisheries and Oceans Canada, Northwest Atlantic Fisheries Centre, St. John's, Newfoundland, Canada.

3.1 Abstract

A three-dimensional (3-D) baroclinic finite-volume ocean model (FVCOM) was developed to examine the oceanic response to Hurricane Igor over the Grand Banks of Newfoundland. Hurricane Igor generated a storm surge of almost 1 m at St. John's and about 0.7 m at three nearby coastal tide gauge stations (Bonavista, Argentia and St. Lawrence). The surge magnitude from the 3-D baroclinic model agrees approximately with tide-gauge observations at all four stations, slightly better than that from an alternative 3-D barotropic case. The sudden drop of sea surface temperature caused by the storm, approximately 6^{o}C as observed by buoys, is well simulated by the baroclinic model with a k-ε turbulence closure. A sensitivity case with the Mellor-Yamada turbulence closure significantly underestimates sea surface cooling. The model solution shows that the largest surge occurred between Bonavista and St. John's. Further analysis suggests the generation of a free continental shelf wave after the storm made landfall, with the peak surge propagating from St. John's to St. Lawrence. The storm-induced sea surface cooling is mainly associated with turbulent mixing.

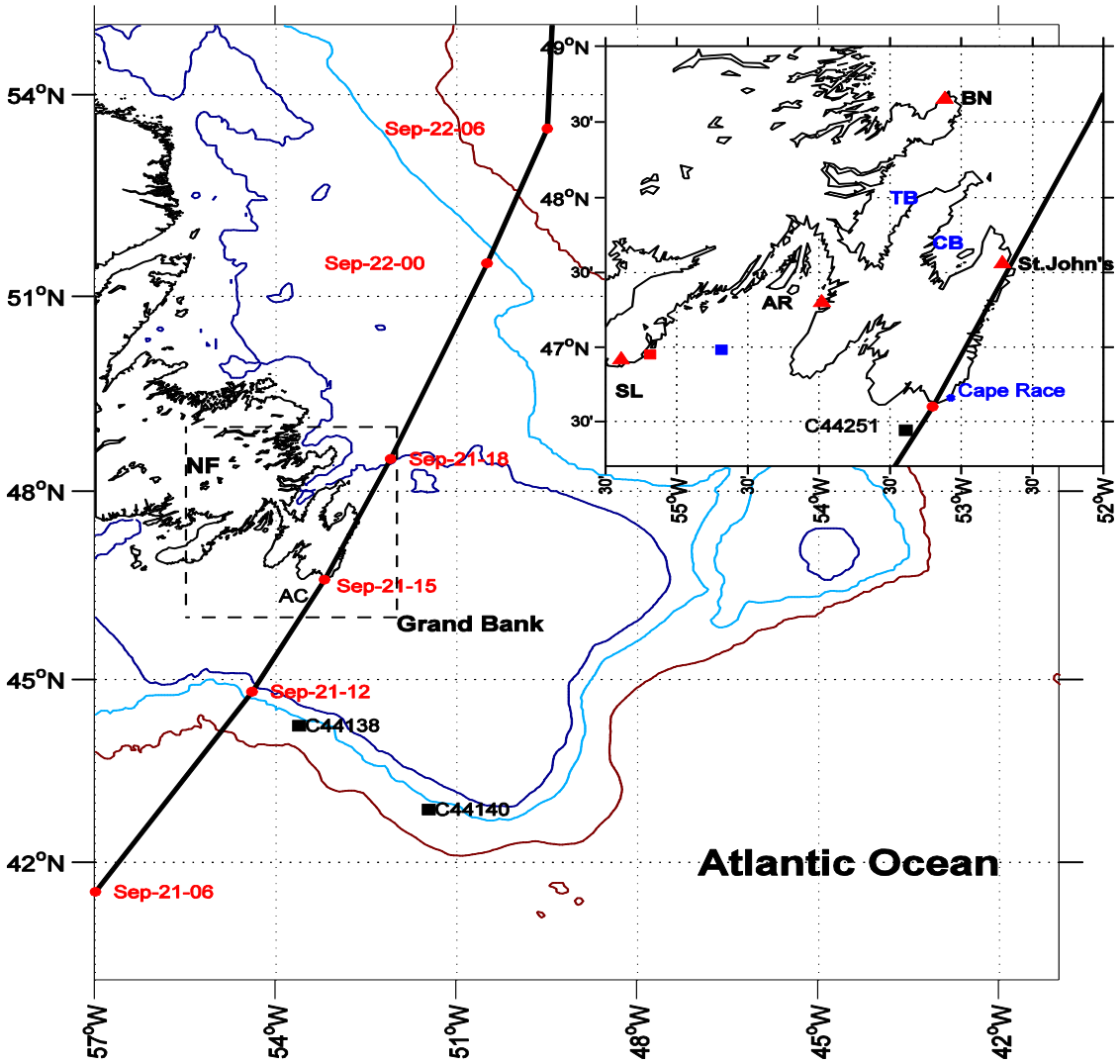

Fig. 3-1: Hurricane Igor track (black thick line) and bathymetry (200 m, 1000 m and 3000 m) over Newfoundland shelf. Tide-gauge stations (red triangles) include St. John's, Bonavista (BN), Argentia (AR) and St. Lawrence (SL). Locations of buoys are depicted in black squares. Current buoy location is blue square. TB and CB indicate the Trinity Bay and Conception Bay, separately. CR is the Cape Race. AC is the Avalon Channel. Red square is the location where the model current and sea level are shown in Fig. 3-13.

3.2 Introduction

The Grand Banks of Newfoundland, located in the northwest of Atlantic Ocean, extend nearly 500 km wide and 600 km long of the mid-latitude. Situated southeast of Newfoundland, the Banks are separated from it by the Avalon Channel (Fig. 3-1). With

the influence of different water masses, the cold fresh Labrador Current and the warm salty Gulf Stream, the shallow Grand Banks play an important role in regional climate variability and marine ecosystem function.

Occasionally from August to October, hurricanes or tropical storms passing by the Banks result in a storm surge, along with drops in sea surface temperature (SST) and enhancement in vertical mixing. In Sep-21, 2010, Hurricane Igor, the most intense hurricane in Newfoundland in recent decades [*Pasch and Kimberlain*, 2011], hit this area, crossed over the Newfoundland Shelf, heading north into the Labrador Sea. The SST observed at a buoy on the Grand Banks showed a sharp decrease of $6\,^{o}\mathrm{C}$ [*Han et al*., 2012a]. Two strong storm surges were captured at the St. John's tide gauge station with a time difference of 11 hours [*Han et al*., 2012b]. The occurrence of a phytoplankton bloom over the Banks was thought to be attributed to the mixed-layer deepening and upwelling associated with the strong wind [*Han et al.*, 2012a].

Historically, scientists have used observations to explore the physical mechanisms of the oceanic response over the Newfoundland Shelf to the storm forcing. With wavelet and cross-wavelet analyses, *Thiebaut and Vennell* [2010] analyzed a fast continental shelf wave with data observed from six tide-gauges located along the Newfoundland coastal under hurricanes. *Han et al.* [2012a] used satellite altimetry and tide-gauge data studied storm surges off Newfoundland caused by Hurricane Igor. They found that the storm surge was associated with a continental shelf wave generated by Hurricane Igor. However, monitoring both spatially and temporally the effects of hurricanes and tropical storms over the Grand Banks are limited, because there are few direct observations.

Therefore, ocean modelling has become increasingly important to improve our understanding of the physical and biological response to extreme weather events in such under-observed regions.

Modelling studies of hurricane impacts on storm surge and upper ocean's responses in the coastal waters have been quite frequent over the past decade. [e.g. *Resio and Westerink*, 2008; *Shen et al.*, 2006; *Weisberg and Zheng*, 2006a,b; *Westerink et al.*, 2008]. *Weisberg and Zheng* [2006 a,b; 2008] and *Rego and Li* [2010] investigated the coastal inundation and surge propagation along a coastal embayment. *Xie et al*. [2004] discussed inundation algorithms and flooding velocities using the Princeton Ocean Model forced by an idealized Category-3 hurricane. *Shen et al*. [2006] simulated Hurricane Floyd's storm tide of September 1999 in Chesapeake Bay, with a substantial dataset for validation and concluded that water levels inside the bay can be explained by the superposition of offshore surge propagation into the bay and local wind forcing. Focusing on the Newfoundland Shelf, *deYoung and Tang* [1990] discussed and regenerated baroclinic near-inertial currents on the Grand Banks induced by a storm using a two layer idealized model. Using a linear barotropic model, *Tang et al*. [1997] investigated the four types of wave motions with a barotropic response for an idealized moving storm off Newfoundland and Labrador. *Mercer et al*. [2002] modelled the barotropic response to a storm, determining the mechanism for a storm-generated wave effect on coastal sea level associated with a fast moving storm passing over the Grand Banks. However, these modelling studies were based on an idealized storm case and focused on an idealized barotropic perspective. *Sheng et al.* [2006] modelled upper ocean response to Hurricane Juan over the Scotian Shelf using a three-dimensional (3-D) baroclinic model. The sea

surface cooling was reproduced reasonably well but the storm surge was not.

Most of the above studies are based on either two-dimensional (2-D) depth averaged model or a 3-D barotropic model. *Weisberg and Zheng* [2008] showed an improvement of storm surge simulation by their 3-D barotropic model over a 2-D depth-averaged model in the Tampa Bay, Florida. From our knowledge, studies on coastal ocean's response to hurricanes based on 3-D baroclinic models are limited. In this study, we will apply a state-of-the-art finite-volume coastal ocean model [FVCOM, *Chen et al.*, 2003] to understand the baroclinic ocean responses to Hurricane Igor over the Grand Banks. Our main objectives are (1) to establish a 3-D high resolution baroclinic ocean model that can realistically simulate storm-induced oceanic responses and (2) to investigate features of storm surge, sea surface cooling and mixed-layer deepening and impacts of baroclinicity and turbulence parameterization. In section 3.3, we will describe the model setup, boundary conditions, forcing data, initial conditions and solution procedure. Section 3.4 will present comparisons between the model and observations and further describe circulation and hydrography. Section 3.5 discusses the mechanisms underlying coastal sea level propagation and sea surface cooling associated with the storm. Finally, in section 3.6, we will present the summary and conclusions.

3.3 Circulation models, forcing, initial and open boundary conditions

3.3.1 FVCOM (3.1) Ocean Circulation Model and Mesh

The FVCOM model [*Chen et al.,* 2003] used in this study combines the advantages of horizontal grid flexibility and computational efficiency. Thus, this model is highly suitable for the present study area with an irregular complex coastal-line, reaching

from shallow waters to the steep topography of the shelf break. A hybrid s-coordinate is chosen to better resolve the surface isopycnal layers and bottom topography. To account for the effect of atmospheric pressure on sea level, an atmospheric pressure gradient term is added into the momentum equation. A k-ε second-order turbulence model from the General Ocean Turbulence Model (GOTM; available at http://www.gotm.net) is also included with this model. No normal flow to solid boundaries is applied at the lateral boundaries.

The storm surge effect is forced directly by wind stress and atmospheric pressure, but also is influenced by the continental shelf geometry and bathymetry. Thus, any storm simulation should include a domain large enough to contain the meteorological forcing fields and remote effects through coastally trapped wave propagation. The current model domain covers the southern Labrador Shelf including the Grand Banks, Newfoundland Shelf and the adjacent deep ocean (Fig.3-1). With 33,863 unequally spaced nodes and 64,480 elements, the horizontal resolution is typical 5 km over the shelf and 1-2 km along the coast and shelf edge (Fig.3-2). Vertically, 41 levels are non-uniformly distributed with a transition depth of 80 m. Model uses uniform coordinate when water depth is less than 80 m. The first layer depth is within 1 m of the surface both for the shelf areas and the deep ocean. We use topography from the Canadian Hydrographic Service for the shelf part and etopo5 for the deeper ocean (www.ngdc.noaa.gov). The bathymetry has been smoothed to minimize the pressure gradient errors [*Mellor et al.*, 1993] with a volume conserving technique within each triangle. This technique limits the depth difference for three vertices at each triangle [*Foreman et al.*, 2009]. On the basis of Courant-Friedrichs-

Levy (CFL) numerical stability condition, model equations are solved with an integration time step of 1 s for the external mode and the internal time is 10 s.

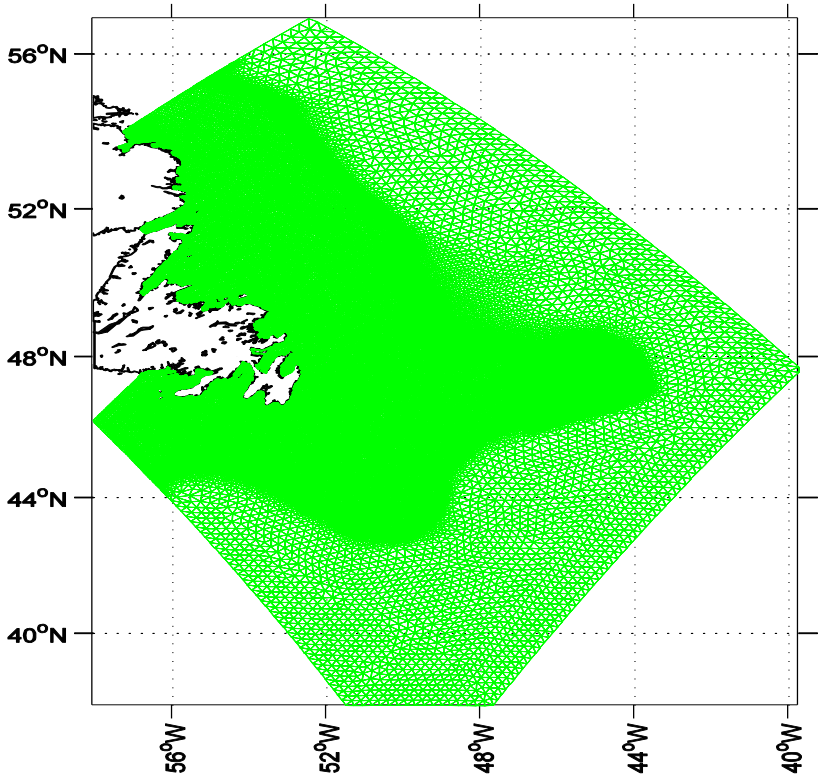

Fig. 3-2: Mesh with 33863 nodes over Newfoundland Shelf and Grand Banks. The resolution is around 1-2 km along the coastal and shelf edge. The Shelf and Banks are covered by 5 km unstructured triangular.

3.3.2 Forcing and Hurricane Igor Wind Model

The model is forced by winds, heat fluxes and air pressure at the sea surface. We used spatially variable wind stress, air pressure, relative humidity, cloud cover, air temperature, dew point temperature and short-wave heat flux from NOAA/OAR/ESRL PSD, Boulder, Colorado, USA, (www.esrl.noaa.gov/psd) over the entire computational domain. The North American Regional Reanalysis (NARR) project is an extension of the NCEP Global Reanalysis which is run over the North American Region. The NARR model uses the very high resolution NCEP Eta Model (32 km/45 layer) together with the Regional Data Assimilation System (RDAS), with output 8 times daily. The heat flux data were calculated from MATLAB code including different functions to calculate the long-wave radiation, latent heat flux and sensible heat flux. A revised equation from *Li et al.* [2006] was used to calculate the albedo, including the white cap effect [*Monahan and MacNiocaill*, 1986], while the formulas from the Tropical Ocean and the Global Atmospheric Program (TOGA)-Coupled Ocean Atmospheric Response Experiment (COARE) [*Fairall et al.*, 1996] was used to calculate the sensible and latent heat fluxes. The formulation of *Fung et al.* [1984] was used to estimate longwave radiation based on the sea surface temperature from monthly-mean temperature [*Geshelin et al.*, 1999] and air temperature, dew point temperature, cloud cover and wind speed.

Usually, the wind field from the NARR dataset do not represent well the maximum sustainable wind of a storm. A more effective way to create hurricane winds in storm surge modelling [e.g. *Peng et al*., 2006a, b; *Weisberg and Zheng*, 2008] is to reconstruct the wind field by fitting the analytical cyclone model from *Holland* [1980].

The radial distribution of wind relative to the storm centre and the maximum wind speed are specified such that:

$$V_H = \sqrt{\frac{B(P_{amb} - MCP)}{\rho_a}\left(\frac{RMW}{r}\right)^B \exp\left(-\frac{RMW}{r}\right)^B} - \frac{rf}{2} \quad (3\text{-}1)$$

$$V_{\max} = \sqrt{\frac{B(P_{amb} - MCP)}{\rho_a e}} \quad (3\text{-}2)$$

where r is the radial distance from the hurricane centre, V_H is the axisymmetric 1-minute sustained wind speed as a function of the radius r, ρ_a is the air density $(=1.15kg/m^3), P_{amp}$ and MCP are the ambient and minimum central atmospheric pressures, respectively, e is the natural base logarithm, RMW is the radius of maximum winds, $V_{\max}$ is the maximum sustained wind speed, and B determines the shape of the storm wind filed, $1.0 < B < 2.5$. We use a constant value of 1.1 for B. A practical and approximate way of converting V_H to the 10-m winds is to multiply a constant factor [Phadke et al., 2003]. Instead, here we used another approximate approach, i.e., fitting the Holland model directly to 10-m wind data. The wind representation was determined from the NOAA Igor tracking report [*Pasch and Kimberlain*, 2011] and three-hourly forecasting data (www.nhc.noaa.gov/archive/2010/IGOR.shtml). The report provides storm centre location, pressure, maximum 10-m wind speed, and forecasting data including the 64 knot wind radius in four directions (NE, NW, SE, SW) every three hours. Based on the above equations (1) and (2), we calculated the maximum wind radius in each direction using the 64 knot wind radius data with the center location provided by the Igor summary [*Pasch and Kimberlain*, 2011]. Then, the averaged maximum wind radial

distance in four directions was treated as the *RMW* to construct the horizontal wind fields, neglecting asymmetry. The *RMW* and V_{max} are further interpolated linearly to provide values every one hour. Then 1-minute axisymmetric winds are generated every one hour. The axisymmetric wind is rotated for an inflow angle. The inflow angle was difficult to determine precisely. A common practice is to apply a constant inflow angle. *Tang et al*. [1997] used 35^o as the inflow angle suggesting that it was too large near the storm centre. *Zhang and Uhlhorn* [2012] estimated the averaged inflow angle to be 22.6 ± 2.2^o for the 10-m wind based on observations. In the current study, we selected 25^o as the inflow angle based on these two studies. The 1-minute sustained winds are also converted to 10-minute winds by multiplying a factor of 0.89 as a sensitivity case. Fig. 3-3 compares reconstructed 1-minute wind speeds from different B values with 1-minute observations at St. John's and Bonavista. The winds with B=1.1 have overall best agreement with observations.

The 1-minute (baseline) and 10-minute sustained winds from the hurricane model are further blended with the NARR winds: hurricane model winds within one RMW, NARR winds outside 4 RMW, and distance-based linear transition between the former and the latter between one and four RMWs.

Wind stress is computed every one hour by:

$$\vec{\tau}_s = C_d \rho_a \left|\vec{\mathbf{V}}_w\right| \vec{\mathbf{V}}_w$$

where ρ_a is the air density, $\vec{\mathbf{V}}_w$ is the blended wind velocity, and C_d, a drag coefficient dependent on wind speed, is given in the default setting of FVCOM:

$$C_d \times 10^3 = 1.2(\left|\vec{\mathbf{V}}_w\right| <= 11.0)$$

$$C_d \times 10^3 = (0.49 + 0.065\left|\vec{\mathbf{V}}_w\right|)(11 <= \left|\vec{\mathbf{V}}_w\right| <= 25)$$

$$C_d \times 10^3 = (0.49 + 0.065 \times 25)(\left|\vec{\mathbf{V}}_w\right| >= 25)$$

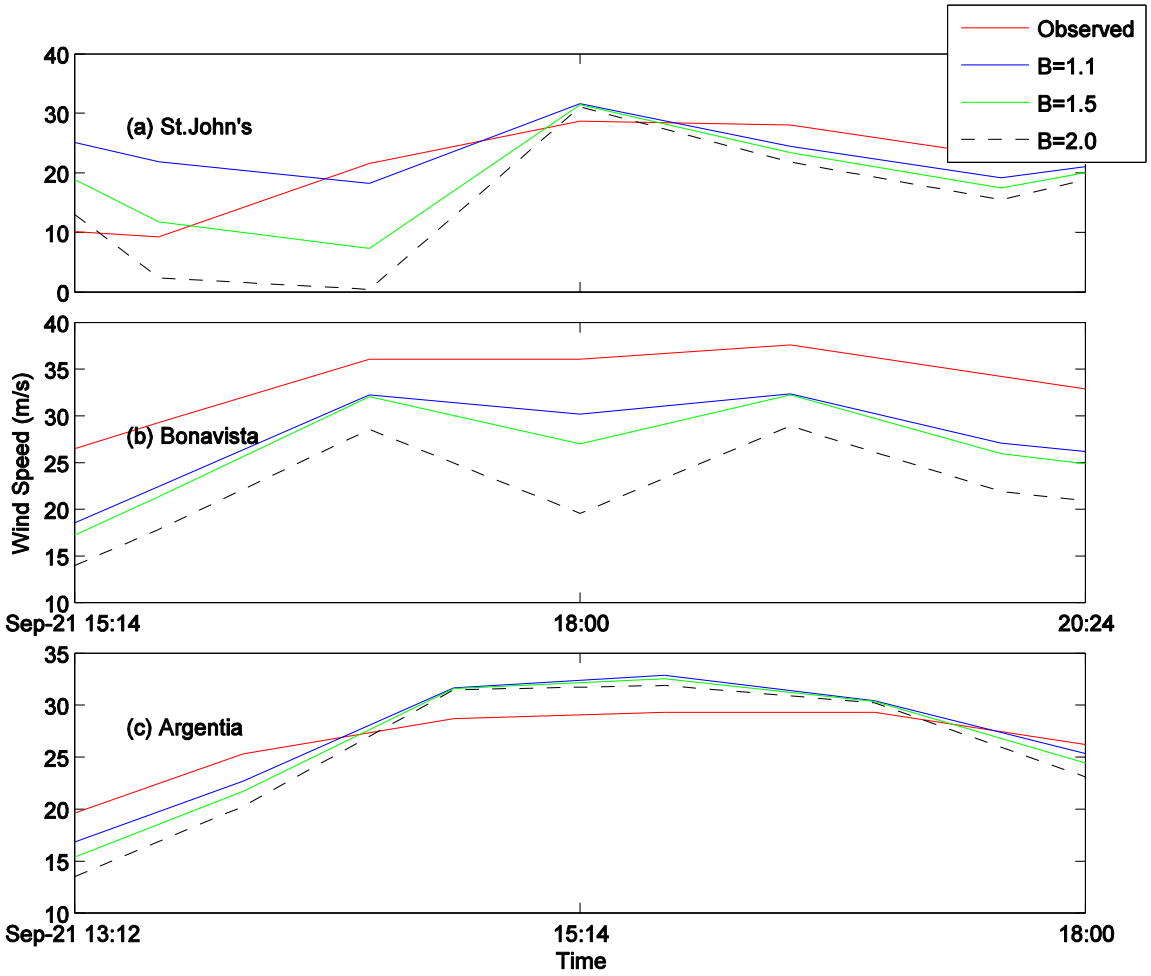

Fig. 3-3: Comparison of 1-minute sustained wind speeds reconstructed from the hurricane model using different B values with observations at St. John's, Bonavista and Argentia.

3.3.3 Initial and Boundary Conditions

The model sea level and velocity were initialized from zero. The initial temperature and salinity conditions were generated from the historical monthly-mean temperature and salinity data [*Geshelin et al.*, 1999] at standard *z*-levels. The model

reaches an approximate dynamic equilibrium after running for 15 days based on the experiments. The model was integrated for 15 days with the July climatological condition and restarted from 1 August to 15 October 2010. The results from 1 September to 15 October were analysed to examine the Igor influence over the upper ocean.

Tidal heights for the five major semi-diurnal (M_2, S_2 and N_2) and diurnal (K_1 and O_1) constituents based on *Han et al*. [2010] were specified along the open boundaries. Non-tidal sea level at the lateral open boundaries was obtained from the climatological monthly-mean solution of *Han et al*. [2008] and specified. The inverse barometric effect was adjusted at the open boundary [*Jones and Davies*, 2004; *Sheng et al*., 2006]. The temperature and salinity along the open boundaries were interpolated from *Geshelin et al.'s* [1999] $1/6^o$ by $1/6^o$ climatological, monthly-mean fields at each time step.

3.3.4. Model Validation

Besides commonly used correlation coefficient and root-mean-square difference, another quantitative index was used to evaluate the model sea level and sea surface temperature. This index was introduced by *Willmott* [1981] and used by others [e.g., *Liu et al*., 2009]. The index is defined as:

$$WS = 1 - MSE / < (|m - < o >| + |o - < o >|)^2 >$$

Where m and o represent the modelled and observed variables respectively and $< o >$ is the mean value of observed variable. The MSE includes the mean bias, standard deviation error and the cross-correlation error and represents in the following formula.

$MSE = < (m - o)^2 >$. WS=1 means the exact agreement, and the value closer to 1is in

better agreement.

3.4 Model Validation

3.4.1 Tidal and Non-tidal Sea Level

Harmonic constants of leading M_2, S_2, N_2, K_1 and O_1 constituents derived from the coastal tide gauges and bottom pressure gauges were obtained from *Han et al*. [2010]. Harmonic analysis including these five constituents and major over-tides (M_4, M_6, MS_4) was applied to the model solution from September 1 to October 15, 2010. For the five tidal constituents, the RMS error between observed data and model solution was 3.5 cm in amplitude and 8.3^o in phase compared with 2.4 cm and 14.2^o from *Han et al*. [2011]. The horizontal distributions (not shown) of five constituents are consistent with previous study and detailed description and figures could be found on *Han et al*. [2011]. Observed hourly sea levels were obtained from the Canadian Tides and Water Levels Data Archive (www.meds-sdmm.dfo-mpo.gc.ca/isdm-gdsi/twl-mne/index-eng.htm) at St. John's, Bonavista, Argentia, and St. Lawrence (Fig. 3-1) for 2010. Harmonic analysis with 35 tidal constituents (including the aforementioned 8 constituents) was applied to detide tide-gauge data [*Pawlowicz et al*., 2002]. The detided tide-gauge data were compared with the model solution.

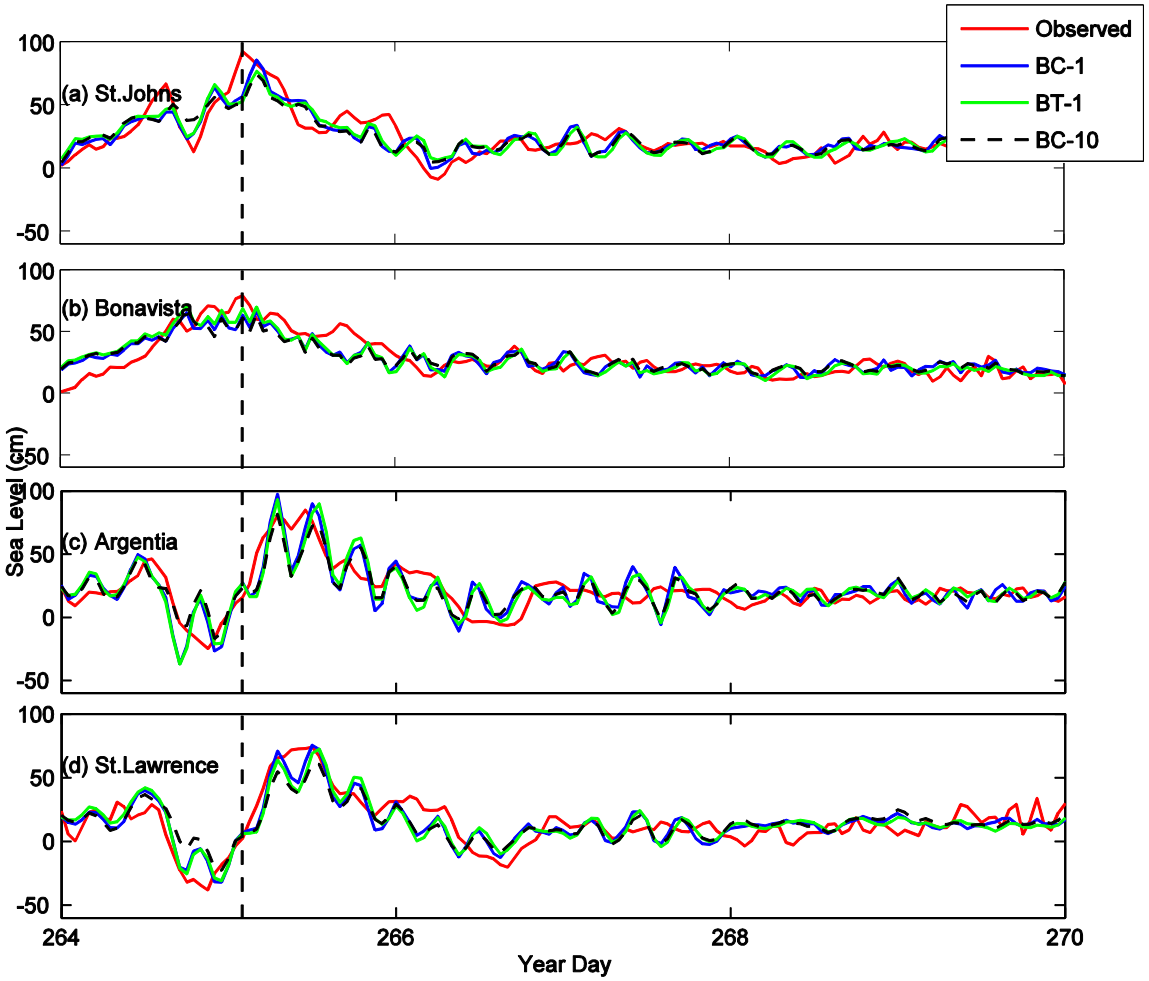

Fig. 3-4: Hourly sea level anomalies from tide-gauge observations (red), 3-D baroclinic baseline model (BC-1, blue), 3-D barotropic case (BT-1, green) and 10-minute sustained hurricane winds case (BC-10, black dash). Vertical black dash line indicates the time of highest peak in St. John's.

The results of hourly non-tidal sea level were shown in Fig. 3-4 (blue and red line), with the model mean sea level adjusted to match the observed relative to the chart datum over the period from day 264 to day 270. The inverse barometer effect was included. Simulated results agree well with observed water levels in these stations with a correlation coefficient above 0.9, including both storm-induced and other variability. During Hurricane Igor, sea level at these four stations, with the exception of Bonavista, showed two peaks. The first peak at St. John's was on year day 264, 15:30pm when the

storm centre made landfall near Cape Race (see Fig. 3-1), while the second one at this station was on year day 265, 02:30am when the storm centre travelled further north, about 530 km northeast from St. John's (Fig. 3-4). The second peak at St. Lawrence was 6-8 hours later.

The averaged RMS differences between the observed and simulated hourly values were averaged to be around 10 cm at the four tide-gauge stations,. which nevertheless was relatively small compared to an average surge magnitude of 80 cm (Table 3-1). The averaged Willmott Score stayed as high as 0.90. The differences for the peak amplitude and timing were shown in Table 2. On average, the absolute amplitude difference was 8 cm (less than 10% of the average surge magnitude) and the time lags were 1.3 hour. Even though the model slightly over- or under-estimated the peak surge, it did capture the local surge's evolution and well reproduced the low frequency sea level before and after the storm very well.

Table 3-1: validation statistics between model and observed non-tidal sea level anomalies (cm). BC-1 is baseline 3-D baroclinic model, BT is 3-D barotropic case, and BC-10 is 10 min sustainable wind case.

Tide-gauge Station	RMS Difference (cm)			Willmott Score (WS)		
	BC-1	BC-10	BT-1	BC-1	BC-10	BT-1
St. John's	9.5	10.5	10.2	0.91	0.88	0.90
Bonavista	9.1	9.9	9.2	0.90	0.87	0.90
Argentia	12.4	11.7	13.0	0.87	0.86	0.86
St. Lawrence	10.6	12.2	11.3	0.91	0.86	0.90
Mean Absolute	10.4	11.1	10.9	0.90	0.87	0.89

Table 3-2: Storm surge peak statistics (model minus observations) for the highest peak. BC-1 is baseline 3-D baroclinic model, BT is 3-D barotropic case, and BC-10 is 10 min sustainable wind case.

Tide-gauge Station	Observed Peak surge (cm)	Peak Difference (cm)			Peak Lag (hour)		
		BC-1	BC-10	BT-1	BC-1	BC-10	BT-1
St. John's	94	-6	-18	-15	2	2	2
Bonavista	79	-12	-10	-8	2	2	2
Argentia	85	12	-3	8	2	2	2
St. Lawrence	75	2	-13	-2	0	0	1
Mean Absolute	83	8	11	8	1.5	1.5	1.8

The model results at Argentia and St. Lawrence also show strong oscillations at a period of about 5 h (Fig. 3-4). Placentia Bay has a longitudinal length of 130 km and an average depth of 125 m [*Ma et al*., 2012]. By treating it as horizontally triangular the natural oscillation period is estimated to be 5.4 h [detailed formula can be found in the Handbook of Coastal and Ocean Engineering (edited by Y. C. Kim), World scientific Publ., Singapoure, 2009]. Thus the strong short-period oscillations are probably associated with storm-induced seiche. It is possible that tide gauges did not capture the seiche well because of their locations.

On year day 265, 02:40am, Jason-2 had a pass across the Grand Banks when the sea level was close to the second peak at St. John's. Simulated sea level anomalies along the track were interpolated and compared with satellite observations from *Han et al.* [2012b] (Fig. 3-5). Over the central Grand Banks ($42^o\,\mathrm{N} - 45.5^o\,\mathrm{N}$), computed sea level captured the observation well. A sea level dip was found between 44.5^o N to 45.5^o N both in the observation and the model results. However, a large difference between the observed and simulated sea level anomalies exist inshore (Fig. 3-5b) due to the model delay of the peak at St. John's (Table 3-2). After two hours, the model inshore elevation

anomaly reached 0.6 m.

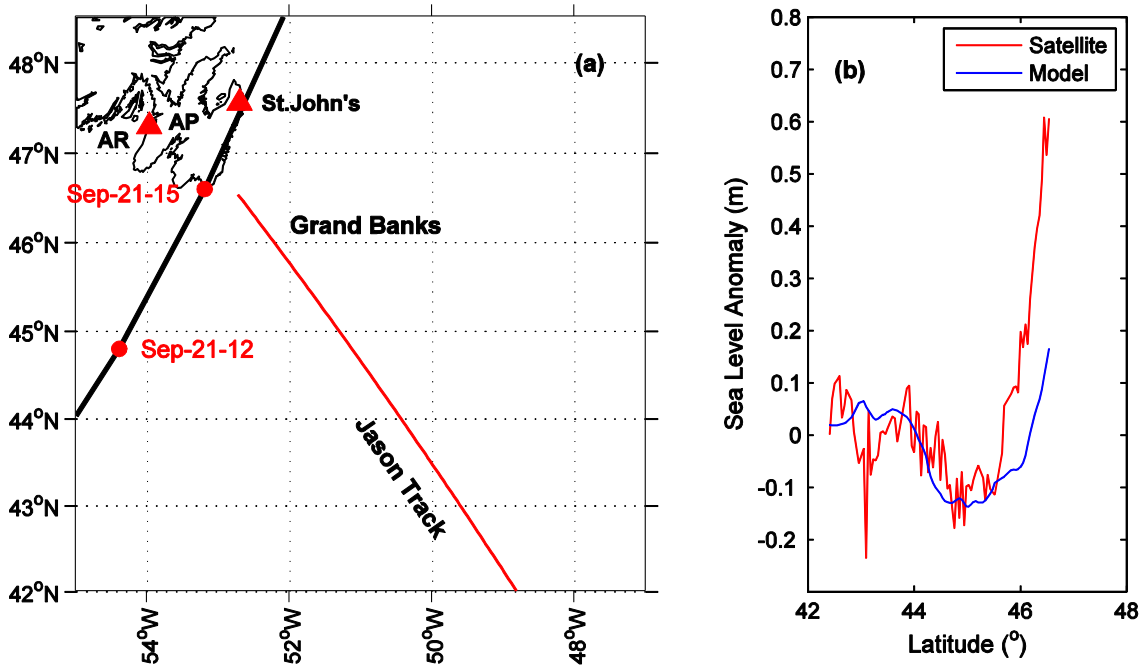

Fig. 3-5: (a) Jason-2 satellite ground track (Red) and (b) sea level anomalies between model and satellite observations. Black thick line in (a) is the storm track. AP stands for Avalon Peninsula. Red triangles depict the location of tide gauge stations.

3.4.2 Sea Surface Temperature

The simulated sea surface temperatures in the baseline run were compared with buoy measurements (Fig. 3-6 blue and red line, respectively). One buoy (C44251) was deployed inshore and the other two were located along the shelf edge in the southern part of the Grand Banks (Fig. 3-1). When the storm passed over, the sea surface temperature dropped by around $6\,^{o}C$. The simulated temperature changes from the baseline case agree well with those observed. The MY-2.5 case does less well than the other two cases in simulating the observed SST cooling in the three stations. The correlation coefficients from day 264 to 270 between observed and baseline run were all above 0.9. The averaged RMS error between the observed and simulated temperature stayed around $1.6\,^{o}C$. The

averaged Willmott Score was 0.83, indicating good agreement for both mean temperature and variability. The hurricane induced averaged temperature drop from the model was comparable to the observed temperature drop within 1 ^{o}C . By comparing the temperature before and after the storm, we found that the surface temperature did not return to the original level after the storm (Fig. 3-6). In general, the net heat flux at the surface becomes weak for this region in late September. Therefore it is unlikely for the sea surface temperature to recover following passage of the storm. *Sheng et al*. [2006] simulated sea surface cooling of 3.5 ^{o}C over the Scotian Shelf during Hurricane Juan. *Wada* [2005] reproduced sea surface cooling of 4 ^{o}C south of Japan during Typhoon Rex.

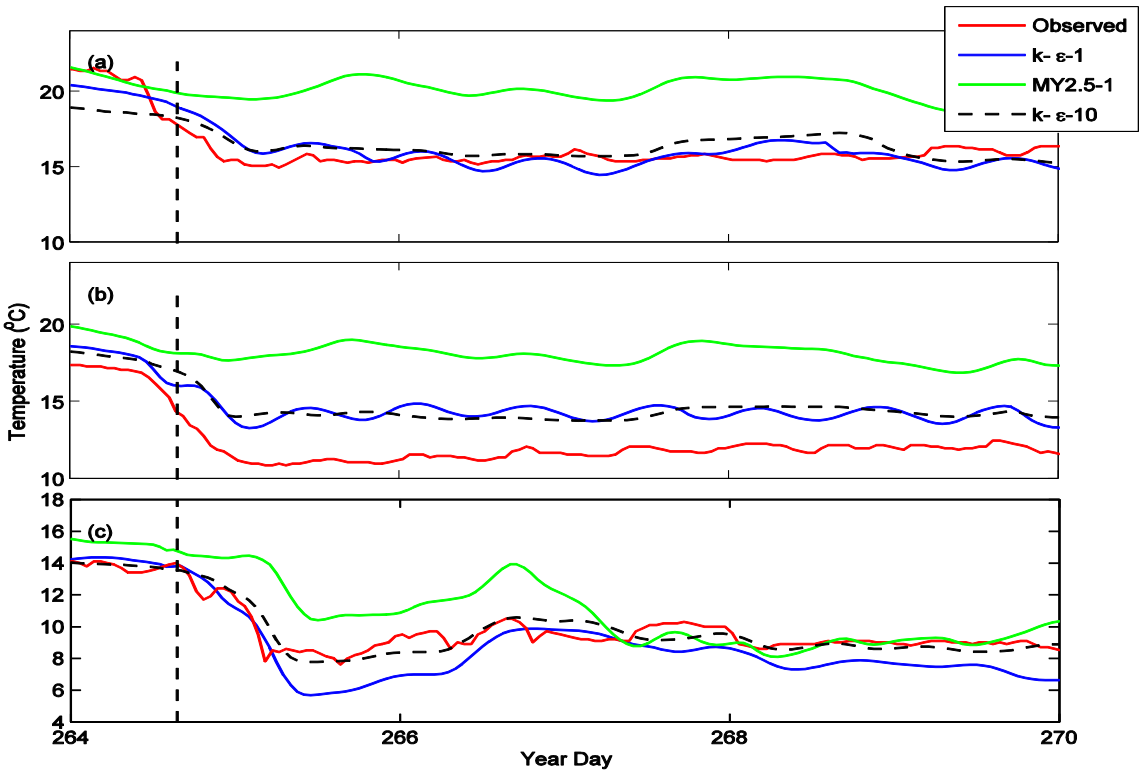

Fig. 3-6. Hourly sea surface temperature from observation (red), baseline model with k-ε turbulence closure (blue), sensitivity case with MY2.5 (green), and sensitivity case with 10-minute sustained hurricane winds (black dash) at C44140 (a), C44138 (b) and C44251(c). Vertical black dash line indicates the landfall time.

Table 3-3: Sea surface temperature comparison between model and observations at buoy locations.

Buoy Number	RMS Difference (^{o}C)			Willmott Score (WS)			Temperature Decrease (^{o}C)			
							Obs	Model		
	$k-\varepsilon$ -1	$k-\varepsilon$ -10	MY 2.5-1	$k-\varepsilon$ -1	$k-\varepsilon$ -10	MY 2.5-1		$k-\varepsilon$ -1	$k-\varepsilon$ -10	MY2.5-1
C44140	0.9	1.1	4.2	0.92	0.81	0.35	6.3	4.2	2.7	1.8
C44138	2.4	2.4	6.0	0.67	0.66	0.29	6.3	5.2	4.0	1.8
C44251	1.4	0.6	2.0	0.89	0.97	0.78	5.2	7.5	5.6	2.9
Mean Absolute	1.6	1.4	4.1	0.83	0.81	0.47	5.9	5.6	4.1	2.2

3.4.3 Horizontal Temperature Distribution and Mixed Layer Depth

Fig. 3-7 shows the eight-day averaged horizontal sea surface temperature distribution from the baseline case and from satellite remote sensing data [pathfinder.nodc.noaa.gov; *Casey et al.*, 2010]. As indicated, Fig. 3-7 (a, b) were the averaged sea surface temperature from 14 September to 21 September and from 22 September to 29 September. The satellite sea surface temperature was shown for the same time period. Before the storm, the satellite surface temperature showed an evident north-south gradient over the Grand Banks. The temperature was high, up to 20 ^{o}C in the south and low to 12 ^{o}C in the north. After the passage of the storm, the satellite surface temperature dropped significantly, by around 6 ^{o}C over the Grand Banks but held a similar north-south gradient. Compared with the satellite temperature, similar spatial patterns before and after storm were clearly found from the model solutions. A large

discrepancy between model results and satellite observations exist over the southern Grand Banks after the storm passed by. The model temperature is 14 °C while the satellite temperature is 11 °C. The averaged mixed layer depth (the criterion is based on density difference to surface is 0.125) around coastal buoy (C44251), calculated based on the model results (Fig. 3-8), showed that the mixed layer deepened substantially following the passage of the storm, increasing from 17 m before the storm to around 27 m afterwards.

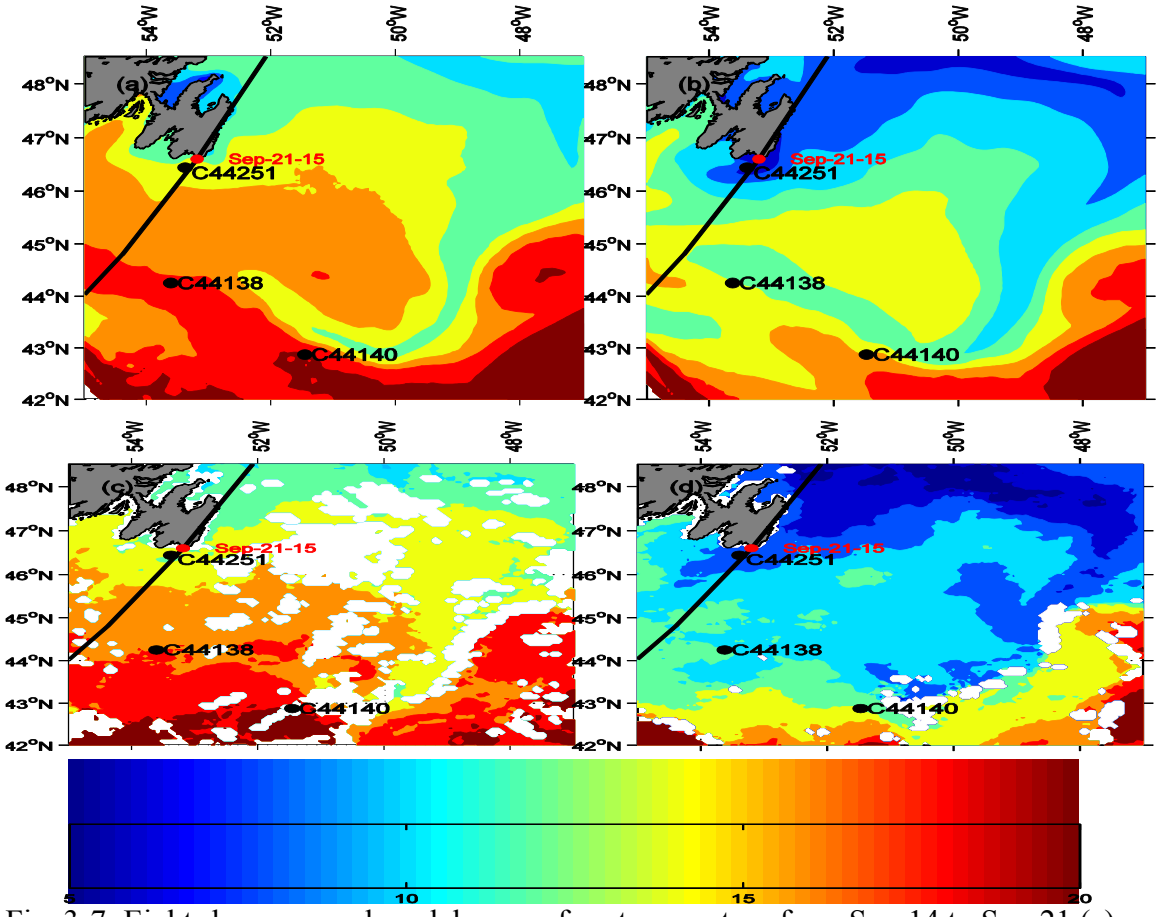

Fig. 3-7: Eight-day averaged model sea surface temperature from Sep-14 to Sep-21 (a) and Sep-22 to Sep-29 (b) and satellite sea surface temperature Sep-14 to Sep-21 (c) and Sep-22 to Sep-29 (d). Black line is the Igor track and the black dots are the buoy locations.

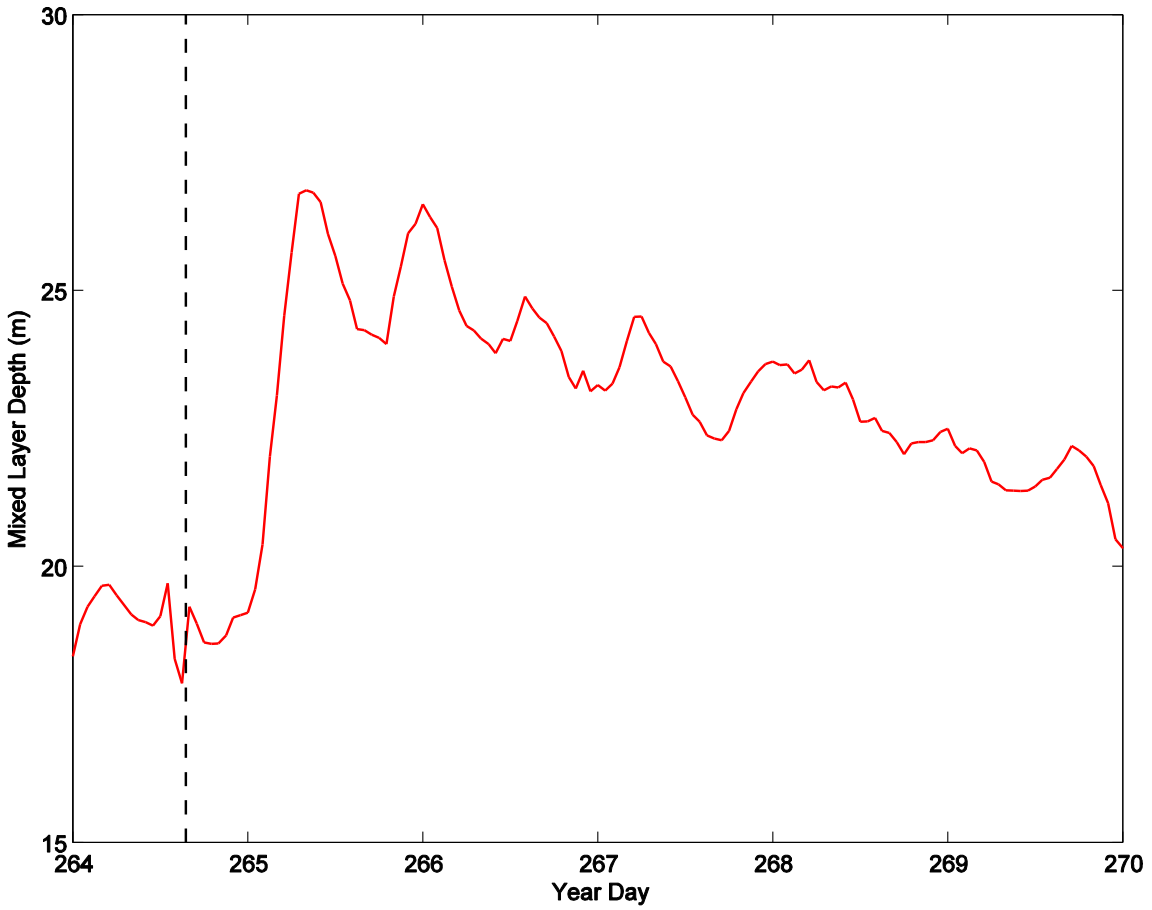

Fig. 3-8: Model mixed-layer depth averaged over an area (from 53 to 54 ^{o}W and from 46 to 46.5 ^{o}N) near the inshore buoy location. Black dash line indicates the landfall time.

3.4.4 Surface Current

Surface currents were compared with observations at a station located in the mouth of Placentia Bay where observed surface currents (0.5 m below the sea surface) are available. Half-hourly data were extracted from the Smart Bay Project (www.smartbay.ca). Data from August 1 to December 31, 2012 were de-tided for the 5 major constituents and 30 other minor constituents [*Pawlowicz et al*., 2002] and smoothed with a 3-hour low pass filter (Fig. 3-9). In general, model calculated currents compare reasonably well with buoy observations especially during Hurricane Igor. From year day

264 to 266, surface current significantly increased to around 0.6 m/s and the direction changed suddenly from positive to negative (positive is eastward and northward). The peak currents were reached at year day 264, 19:55 when the storm center moved to the northeast of Trinity Bay. Significant inertial oscillations were generated at a period of about 17 h. Detailed statistics were calculated between the observed and model currents. The RMS differences between the model and observation are 15 cm/s and 15 cm/s in the eastward and northward components, respectively. Therefore, the model simulated the variability of surface current reasonably, especially during Hurricane Igor.

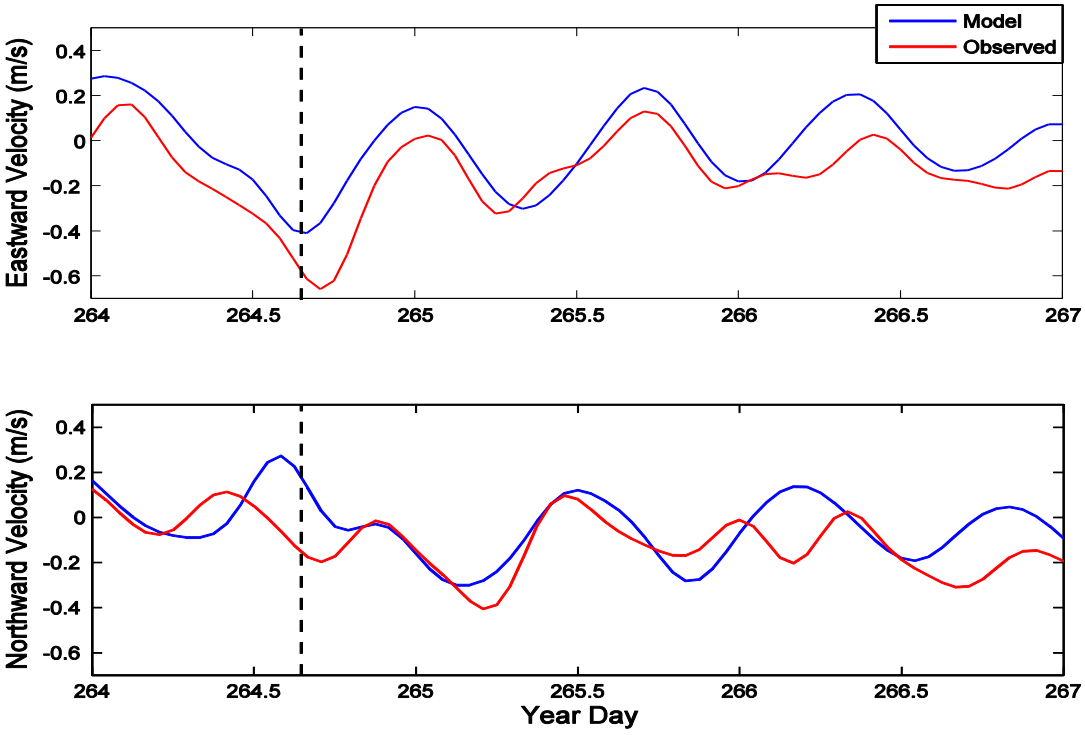

Fig. 3-9: Hourly surface currents at a location (see Fig. 3-1) in the outer Placentia Bay. Blue line is the model surface current while red line is the observed. Black dash line indicates the landfall time.

3.5 Discussion

3.5.1 Sensitivity simulations without stratification, with Mellor-Yamada turbulence closure, or with 10-minute sustained wind forcing

Weisberg and Zheng [2008] found the importance of using a 3-D barotropic model instead of a 2-D depth-averaged one for storm surge in Tampa Bay, Florida. They attributed the 20% underestimation of surge in the 2-D model to the overestimation of bottom stress. Here we extend their work to examine the difference between our baseline 3-D baroclinic model and an alternative 3-D barotropic (BT-3D) while keeping wind forcing and sea level open boundary conditions the same. The results are shown in Fig. 3-4, with detailed statistics in Table 3-1 and 3-2. The 3-D barotropic model is essentially as good as the baroclinic model in terms of the RMS difference and Willmott Score (Table 3-1). The statistics for the peak storm surge shows slightly lower skills of the 3-D baroclinic model. The barotropic model underestimate the observed surge to a greater degree than the baroclinic model, especially at St John's. This difference may be attributable to the increased bottom current (Fig. 3-10) and thus bottom stress in the barotropic model. The storm surge, as a temporal and spatial integral of the surface slope, depends strongly on the bottom stress and thus bottom current [*Weisberg and Zheng*, 2008].

The default turbulence closure for the vertical eddy viscosity/diffusivity in the FVCOM is the 2.5-level Mellor-Yamada turbulence model (MY2.5). *Han et al.* [2011] reported that the heat flux could not penetrate deep enough when the MY-2.5 was used in an FVCOM simulation of the seasonal circulation over the Grand Banks. As a result, the

model mixed layer depth was too shallow in summer. Thus, we used a second-order k-ε model in GOTM for our baseline simulation. Here we compare the model SST during Hurricane Igor from the k-ε and MY2.5 turbulence closures, respectively. Table 3-3 and Fig. 3-6 clearly show that the model SST change from the k-ε closure agrees well with observations, but those from the MY2.5 closure do not.

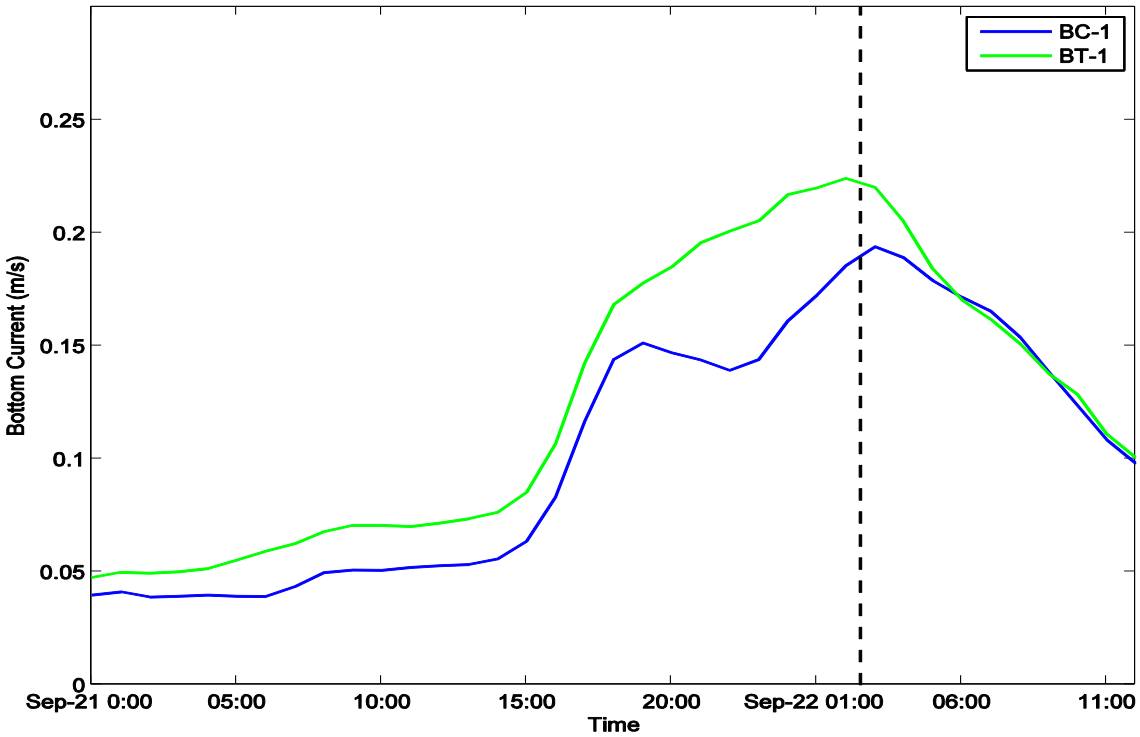

Fig. 3-10: Bottom current speed from the baseline baroclinic model (BC-1) and the sensitivity barotropic case (BT-1), averaged over an area from 52 to 53 °W and from 47 to 49 °N in the vicinity of St. John's.

Like in some previous studies [*Morey et al*., 2006; *Weisberg and zheng*, 2008], we used 1-minute sustained hurricane winds as the forcing for the baseline simulation as shown in the preceding section. As a comparison the results from a sensitivity run forced by the 10-minute sustained hurricane winds were also provided here. Overall, the sensitivity case has larger RMS differences and lower Willmott Score than the baseline

case (Table 3-1) against tide-gauge sea level variations. It underestimates the peak storm surge at all tide-gauge stations (Fig. 3-4, Table 3-2). The sensitivity case has essentially the same RMS differences and the Willmott Score against buoy-observed SST (Table 3-3). The sensitivity case agrees better with observed SST decrease at the nearshore buoy location, but underestimates sea surface cooling at the two offshore buoy locations (Table 3-3, Fig. 3-6).

3.5.2 Sea Level and Continental Shelf Wave

Fig. 3-11a showed the surface circulation pattern and sea level distribution at 12:00pm on Sep-21(year day 264), when the storm centre was located at the shelf edge, south of Newfoundland. The winds at this time pushed the water from the southern Grand Banks to the coast. Combined with the inverse barometric effect, a surge was formed at St. John's, Argentia and St. Lawrence when the storm centre moved close to the Avalon Peninsula (Fig. 3-1) and made landfall. As the storm centre passed the Avalon Peninsula and moved offshore, the coastal sea level along the southern coast receded and the winds pushed the water away from the coast towards the outer Grand Banks (Fig. 3-11b). These changes are also seen in the hourly tide gauge data (Fig. 3-4). As the storm travelled farther north, at 02:00-03:00 on Sep-22 (year day 265) (Fig. 3-9 c and d), the direct storm effects over the Grand Banks became weaker. However, we still observed a significant second surge peak at St. John's at 02:40 on Sep-22, and at St. Lawrence several hours later.

Both model solution and observation data revealed a stronger second peak at St. John's. In contrast there was only one peak at Bonavista. The source for the second peak can be traced to the higher sea level in Trinity and Conception Bay (Fig. 3-11d). This sea level

setup propagated equator-ward along the coast, and caused the second peak surge at St. John's, Argentia and St. Lawrence. To quantify the effect of sea level setup within the two bays, a numerical experiment without them was carried out to examine their impacts on the storm surge magnitude. To do so, the two bay areas were covered with land. The model results without the two bays showed that the second peak at St. John's decreased by 5 cm, but still stronger than the peak at Bonavista. This experiment suggests that the existence of the two bays had some effects on the surge magnitude at St. John's. However, the dominant reason to generate the stronger second peak at St. John's is attributed to inshore Ekman setup when the storm centre was located northeast of St. John's.

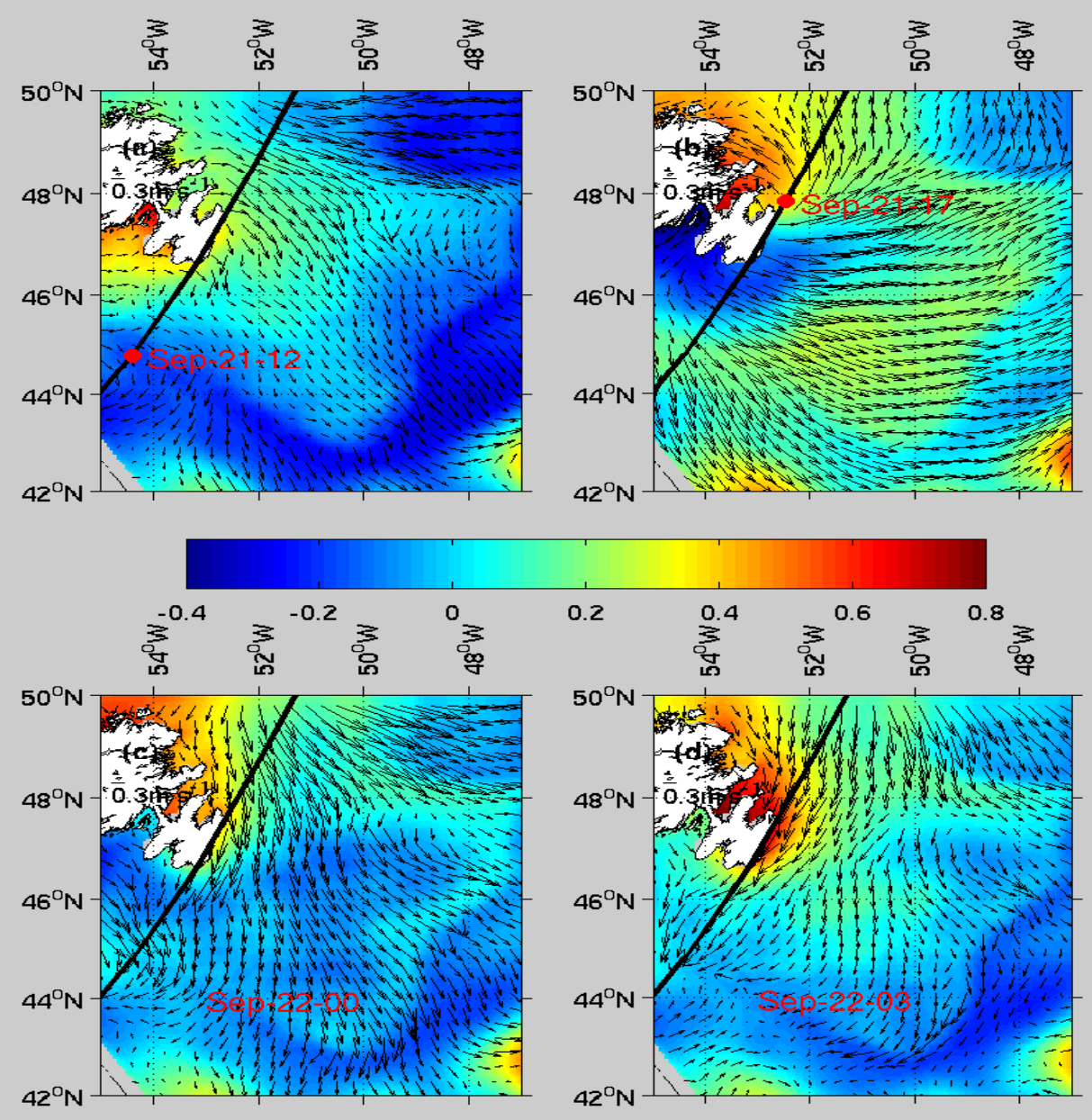

Fig. 3-11: Model surface circulation and sea level distribution at (a) 12:00 on Sep-21 (day 264); (b) 17:00 on Sep-21; (c) 02:00 on Sep-22 (day 265) and (d) 03:00 on Sep-22. Black thick line is the Hurricane Igor track. Red spots are the storm center at the corresponding time.

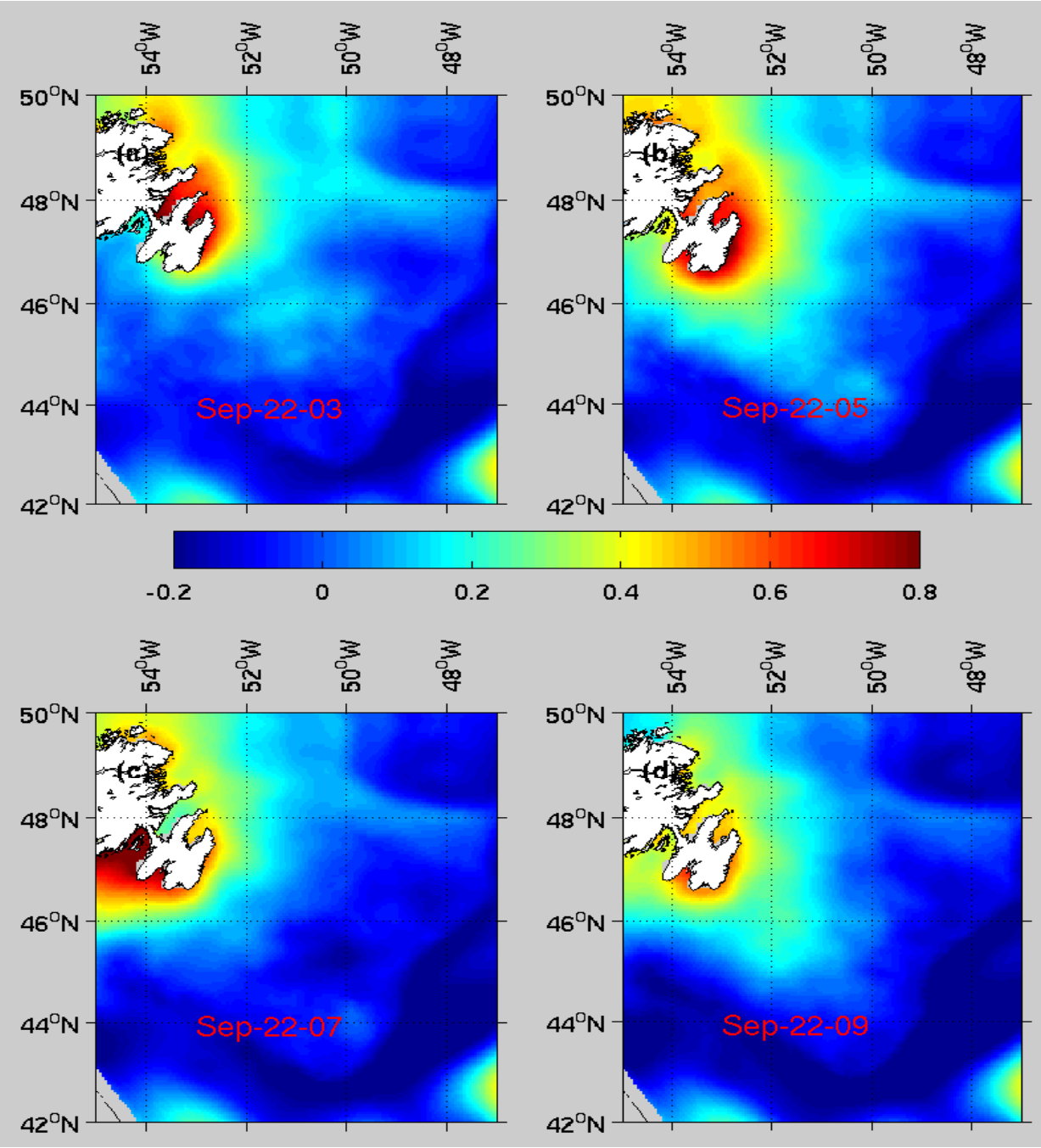

Fig. 3-12: Temporal evolution of the sea surface elevation (SSE) from the model after the second peak at St. John's at (a) 03:00, (b) 05:00, (c) 07:00 and (d) 09:00 on September 22 (day 265).

Another important feature associated with the storm is the generation and propagation of coastally-trapped waves. For example, *Morey et al.* [2006] attributed an

anomalously high storm surge along the Florida coast of Apalachee Bay during Hurricane Dennis to a topographic Rossby wave. *Han et al.*, [2012b] suggested the generation of a continental shelf wave when Hurricane Igor passed over the Grand Banks. The propagation of a shelf waves excited by the storm can also be seen from the storm-induced sea surface elevation (Fig. 3-12a). The surface elevation anomaly (Fig. 3-12a) showed a relatively high sea level anomaly in Trinity Bay and Conception Bay at 03:00 on Sep-22 (year day 265). The model showed that this anomaly propagated southward and arrived at St. John's around at 05:00 on Sep-22 (Fig.3-12b). However, the tide-gauge observation at St. John's indicated this high anomaly around, 02:30 on Sep-22. This demonstrated the delay of two hours in the calculated sea level. At about, 09:00 on Sep-22, the high anomaly left the Placentia Bay to farther west.

To further quantify the storm induced shelf wave we analysed the observed and simulated sea levels at Bonavista, St. John's and St. Lawrence. The time period is from 01:30 September 23 to 01:30 September 27, 2010, the same as that used in *Han et al.* [2012b]. Observed post-storm sea level indicates that the dominant period of oscillation is 48 hours or 0.5 cycle per day (cpd) at St. John's. A similar oscillation was also found at St. Lawrence, but not at Bonavista. Sea level at St. Lawrence lags that at St. John's by 7-8 hours. The propagation speed of sea level is estimated to be 14-16 m/s (Fig. 3-13a), consistent with previous results for the Canadian Atlantic shelves based on the numerical model and sea level observations [*Tang et al.*, 1998; *Sheng et al*., 2006; *Thiebaut and Vennell*, 2010; *Han et al*., 2012b]. Han et al. [2012b] estimated the first-mode shelf-wave speed to be ~10 m/s from St. John's to Argentia. In contrast, the barotropic Kelvin wave speed is estimated to be about 30 m/s by assuming an averaged water depth of 100 m

along the eastern Newfoundland coast. Therefore we argue the post-storm sea level propagation is associated with the first-mode continental shelf wave. Compared with the observations, our model results show similar wave characteristics both in the time lag as well as the wave propagation speed and dominant frequency (Fig. 3-14). Some difference was observed at St. Lawrence where the model frequency was 0.7 cpd.

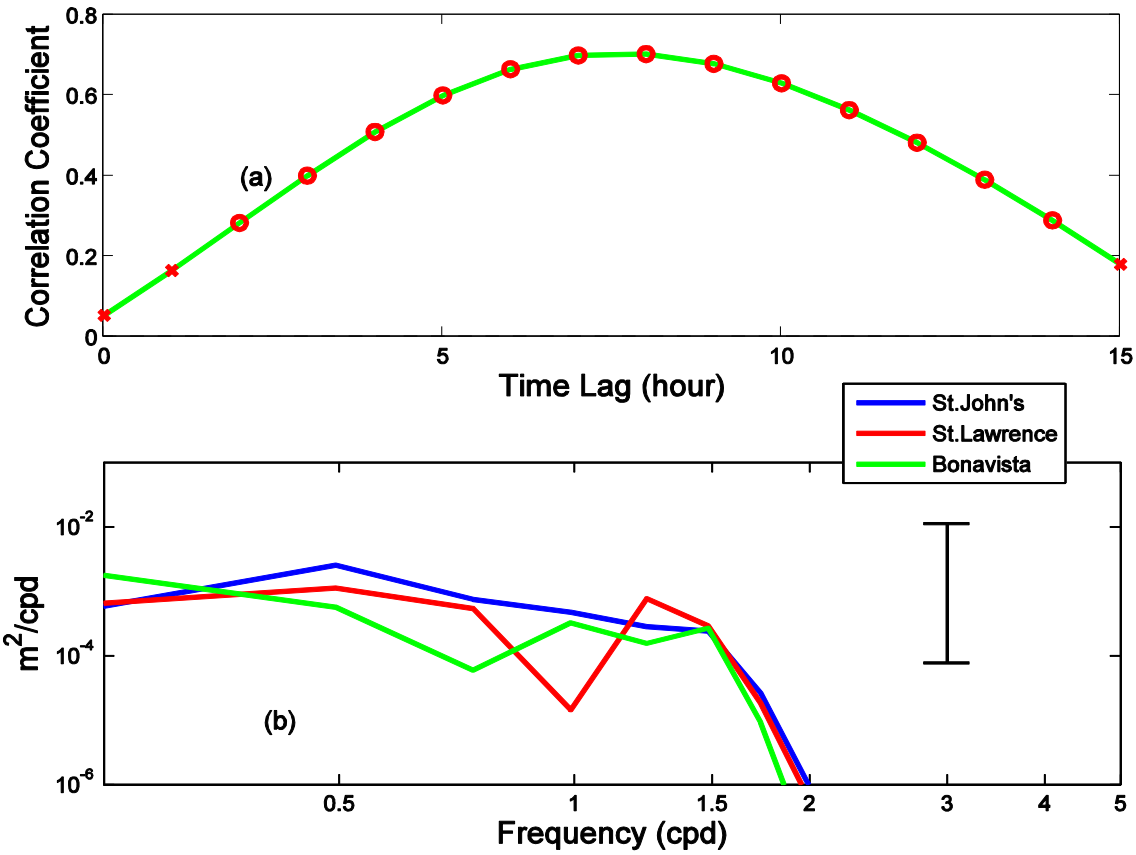

Fig. 3-13: (a) Lagged correlation coefficients (open circles: significantly different from zero at the 99% confidence level; cross: insignificant) between the tide-gauge sea level anomalies at St. John's and St. Lawrence, with the latter lagging the former. (b) Power spectral density of the tide-gauge sea level anomalies at St. John's, Bonavista and St. Lawrence.

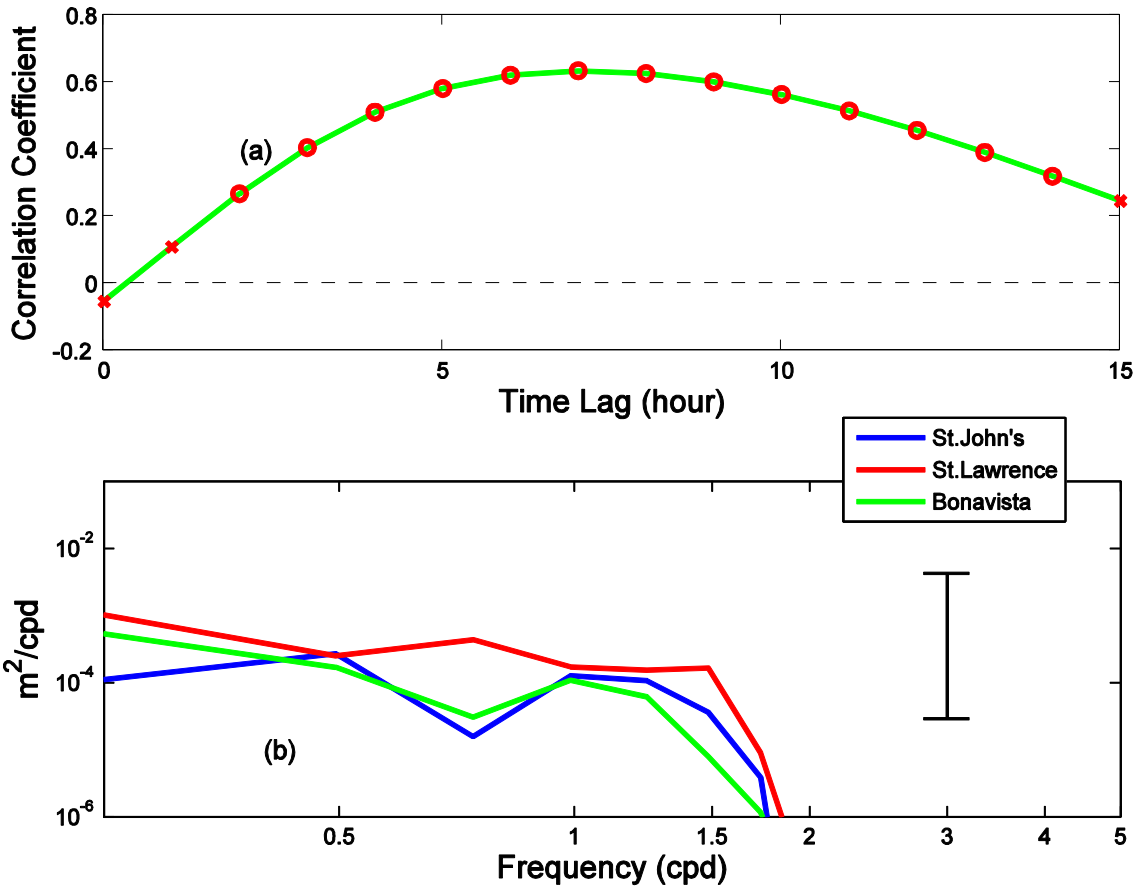

Fig. 3-14: (a) Lagged correlation coefficients (open circles: significantly different from zero at the 99% confidence level; cross: insignificant) between the model sea level anomalies at St. John's and St. Lawrence, with the latter lagging the former. (b) Power spectral density of the model sea level anomalies at St. John's, Bonavista and St. Lawrence.

Overall, the simulated sea level agrees well with observations in the sub-inertial band. After separating the high- and low-frequency signals of sea level at St. John's bounded by the inertial frequency, we found that the correlation coefficient between observed and model results was 0.8 for the sub-inertial band; but insignificant for the other band. Similarly, Bonavista and St. Lawrence stations had high correlation in the sub-inertial frequency. Thus, the model and observed sea level difference is mainly in the high-frequency band above the inertial frequency, which is in part associated with

uncertainty in representing the storm high frequency wind forcing.

By analysing the time series of model depth-averaged current at a location off St. Lawrence (Fig. 3-1), the storm-induced free-wave oscillations were also examined. The magnitude of the depth-averaged horizontal current speed at this location reached 20 cm/s during the storm period (Fig. 3-15). The oscillation had a dominant period of about 0.7 cpd (Fig. 3-15b), consistent with that of the sea level oscillation at the same location (Fig. 3-13d).

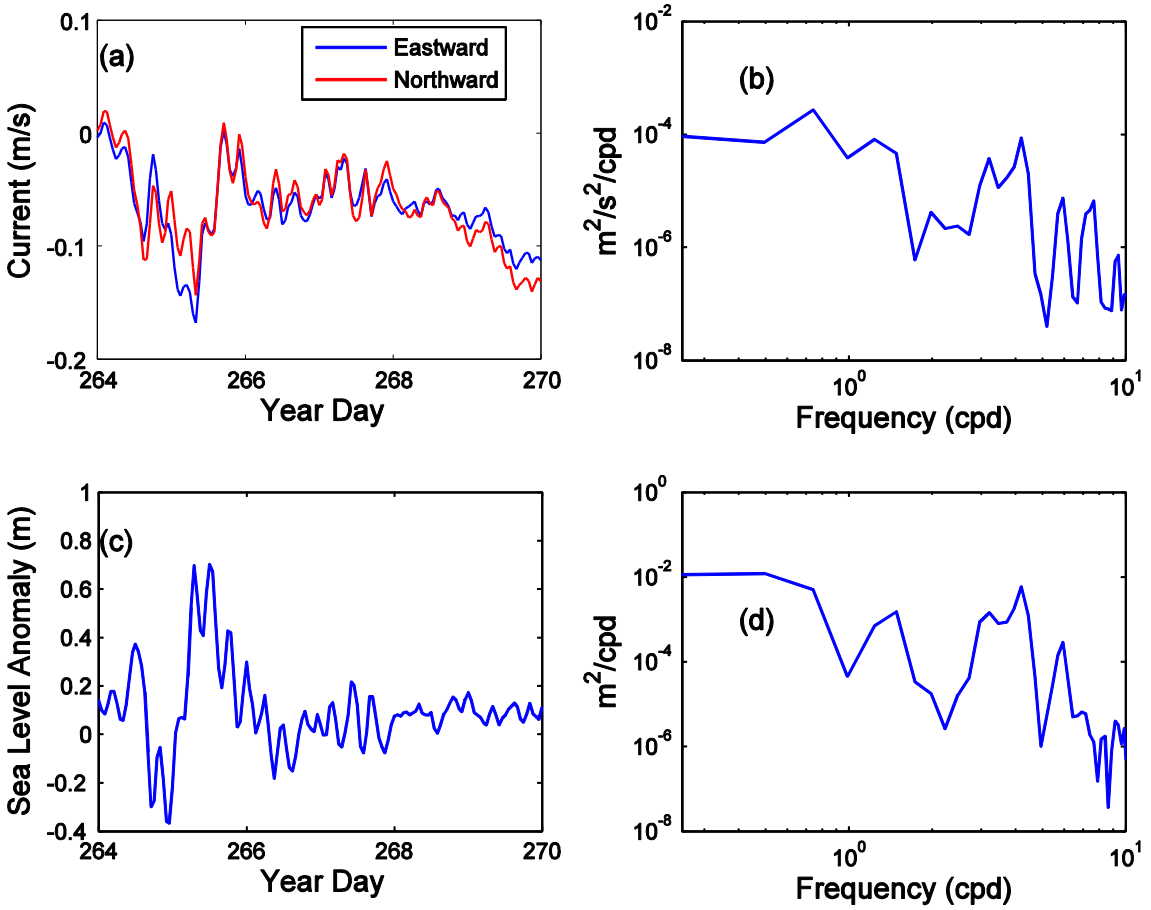

Fig. 3-15: (a) Vertically averaged current at a location indicated in Fig. 1 and (b) its power spectral density of the total current speed. (c) Sea level anomaly and (d) Power spectral density.

3.5.3 Entrainment and Upwelling

Price [1981] and *Wada* [2005] suggest the sea surface cooling during the hurricane is primarily caused by entrainment and upwelling. These papers also introduce two non-dimensional numbers: the Burger Number and the Rossby number, to demonstrate the evolution of storm effects on surface cooling. Here, we follow their definition for the Burger number (B):

$$B = \frac{g' h_l}{4 f^2 R_{\max}^2} \tag{3-3}$$

where g' is the reduced gravity and h_l is the mixed layer depth after cooling. The Burger number represents the scale of turbulent mixing. We first determine the mixed-layer depth. The difference between the mixed–layer density and that in the rest of water column is used to calculate the reduced gravity. Instead of the Rossby number, we introduce an Ekman Pumping Index (E):

$$E = \frac{curl(\vec{\tau})}{\rho_o U_H f} \tag{3-4}$$

where U_H is the storm translation speed. We calculated the Burger number and the Ekman Pumping Index from the model results at the inshore buoy location (C44251, Fig. 3-1).

When the storm centre was approaching to Newfoundland in the morning of Sep. 21, the ocean was well stratified, with a large Burger number (Fig. 3-16a). One to two hours before landfall, the Ekman upwelling effect started to pump colder water from subsurface. The turbulent mixing also picked up. Thus the density difference between the mixed layer and the lower water column decreased and the Burger number began to fall. At 15:00, the turbulent mixing and upwelling effects reached sea surface and SST started

to fall. The Ekman upwelling weakened at 16:00 (Fig. 3-16b). The SST fell by about $2^{o}C$ from 15:00 to 17:00. While the Burger number continued to fall, the SST fall paused for 2-3 hours. Afterwards, SST fell again together with the Burger number. The SST adjustment ended at 03:00 on September 22, while the Burger number did not end until five hours later.

Although the Burger number and Ekman pumping index show when turbulent entrainment and Ekman upwelling take place, they do not provide information on their relative importance. The two processes both contribute to sea surface cooling but their influences on the mixed-layer depth are opposite. The former deepens it and the latter uplifts it. We have calculated the Ekman pumping velocity and cumulative distance for an area around the buoy location (Fig. 3-16c and d). The net cumulative distance is estimated to be 5 m. With the simulated mixed-layer deepening of about 8 m, the turbulent entrainment deepened the mixed-layer by 13 m. Therefore, the turbulent entrainment is the dominant process over the Ekman upwelling in inducing the sea surface cooling, consistent with Sheng et al. (2006).

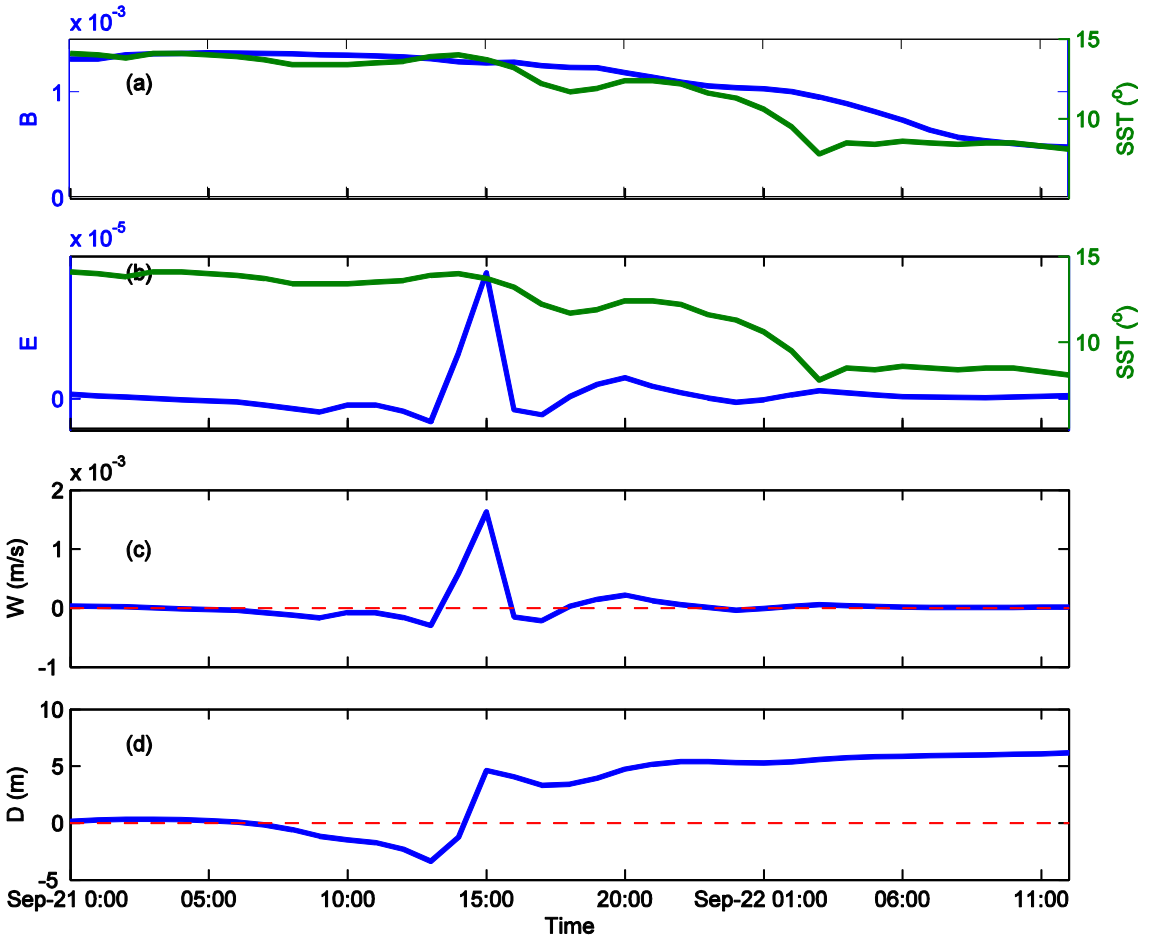

Fig. 3-16: Time series of (a) the Burger Number B, (b) the Ekman Pumping Index E, (c) Ekman upwelling velocity W and (d) Cumulative upwelling distance D. The right axis in (a) and (b) indicates the sea surface temperature (SST). Location of C44251 can be seen in Fig. 3-1.

3.6 Conclusion

A 3-D, baroclinic, finite-volume ocean model was developed to study the upper ocean responses to Hurricane Igor over the Grand Banks of Newfoundland. Reconstructed hurricane winds were applied to force this ocean model to explore the dynamics of mid-latitude coastal waters.

The 3-D baroclinic ocean model reproduced the sea surface elevation before and

after the storm reasonably well. Especially, the two surges generated by the passage of Hurricane Igor were well captured. Both the model and observations showed two surges at St. John's, Argentia and St. Lawrence. The first surge was attributed to the direct local wind forcing and the second one was the result of the equator-ward propagating continental shelf wave generated by the storm. Compared with hourly observations, the model sea surface elevation had an RMS error of 10 cm on average from day 264 to 270. The model tends to underestimate storm surge magnitude at St. John's and Bonavista, but overestimate them at Argentia and St. Lawrence. For the highest surges, the average model-observation magnitude difference was 8 cm, with a model time lag within 1.3 hour. Sea level at the three stations was separated into high- and low-frequency components bounded by the inertial frequency for further analysis, which indicates poor and good agreement with observations for the former and latter, respectively. In the future, by applying the observed hourly and high-resolution wind data in the hurricane model [*Rego and Li*, 2010], we should improve the reconstructed local winds so that the ocean model could generate more accurate high-frequency sea level.

The model surface temperatures were compared with observations at three buoy stations over the Grand Banks. Both model and observation showed a significant decrease about $6^{o}C$ in the sea surface temperature. The RMS difference between the model and observation from day 264 to day 270 was about $1.6^{o}C$. Furthermore, the calculated horizontal distribution of the sea surface temperature was compared with satellite observations. The model reproduced well the southward increase of temperature observed before the storm and the sharp decrease afterwards.

The model near sea surface current was compared with observations at a point located in the outer Placentia Bay. The correlation coefficient between the model and observations was 0.7. The model was able to generate the observed variability of surface currents. In particular when the storm passed over Newfoundland, the calculated surface currents well captured the strong southwestward flow of 0.7 m/s.

The storm induced shelf wave was examined by analysing the sea level at tide-gauge stations and currents at a point far away from the storm centre to prevent direct storm wind effects. Both observation and model results showed a propagation speed of 14-16 m/s and 0.5-0.7 CPD, consistent with the continental shelf-wave estimation from *Han et al.*, [2012b]. We further analyzed the vertically averaged currents in the outer Placentia Bay. The results highly support those from sea level data. The storm excited waves propagate equatorward along the Newfoundland coast. These waves can not only be observed from the sea surface elevation field but also from the horizontal currents.

An examination of Burger number and Ekman pumping parameters indicates that the entrainment due to turbulent mixing is the dominant process to cause the salient drop in SST. Upwelling associated with the wind stress curl plays a small supplementary role only.

The present study provides new insights into simulating ocean's response to hurricanes. It is found that a 3-D baroclinic model simulates storm surge slightly better than an alternative 3-D barotropic model. The difference may be attributed to smaller bottom current and thus friction in the 3-D baroclinic model. It is shown that sea surface cooling is well simulated with a k-ε turbulence closure, but is significantly underestimated with the commonly used MY2.5 closure.

3.7Acknowledgement

We thank Dr. Changsheng Chen for providing the FVCOM code and three anonymous reviewers for their useful comments.

3.8 Reference

Casey, K.S., T.B. Brandon, P. Cornillon and R. Evans (2010), The Past, Present and Future of the AVHRR Pathfinder SST Program, in Oceanography from Space: Revisited, eds. V. Barale, J.F.R. Gower, and L. Alberotanza, Springer, DOI: 10.1007/978-90-481-8681-5_16.

Chen, C., H. Liu and R.C. Beardsley (2003), An unstructured grid, finite volume primitive equation coastal ocean model: application to coastal ocean and estuaries. *J. Atmos. Ocean. Technol*, 20, 159–186.

deYoung, B., and C. Tang (1990), Storm-forced baroclinic near-inertial currents on the Grand Bank, *Journal of Physical Oceanography*, 20: 1725-1741.

Fairall, C.W., E.F. Bradley, D.P. Rogers, J.B. Edson and G.S. Young (1996), Bulk parameterization of air-sea fluxes for COARE, *J. Geophys. Res*, 101: 3747–3764.

Foreman, M., P. Czajko, D.J. Stucchi and M. Guo (2009), A finite volume model simulation for the Broughton Archipelago, Canada, *Ocean Modelling*, 30: 29–47.

Fung, I.Y., D.E. Harrison and A.A. Lacis (1984), On the variability of the net long-wave radiation at the ocean surface. Rev, *Geophys. Space Phys*, 22 (2): 177–193.

Geshelin, Y., J. Sheng and R.J. Greatbatch (1999), Monthly mean climatologies of temperature and salinity in the western North Atlantic. *Can. Tech. Rep. Hydrogr. Ocean Sci. Report*, No. 153. Ocean Sci. Div. of Fish. and Ocean Can., Dartmouth, NS, Canada.

Han, G., Z. Lu, Z. Wang, J. Helbig, N. Chen and B. deYoung (2008), Seasonal variability of the Labrador Current and shelf circulation off Newfoundland, *J. Geophys. Res*, 113, C10013, doi: 10.1029/2007JC004376.

Han, G., S. Paturi, B. deYoung, S. Yi, and C.K. Shum. (2010). A 3-D data assimilative tide model of Northwest Atlantic. *Atmosphere-Ocean*. 48, 39-57.

Han, G., Z. Ma, B. deYoung, M. Foreman and N. Chen (2011). Simulation of three-dimensional circulation and hydrography over the Grand Banks of Newfoundland, *Ocean Modelling*, 40: 199–210, doi:10.1016/j. ocemod.2011.08.009.

Han G., Z. Ma and N. Chen (2012a), Hurricane Igor impacts on the stratification and phytoplankton bloom over the Grand Banks, *Journal of Marine System*, 100-101, 19-25.

Han G., Z. Ma, D. Chen, B. deYoung and N. Chen (2012b), Observing storm surges from space: Hurricane Igor off Newfoundland, *Scientific Report*, DOI: 10.1038/srep01010.

Holland, G. J. (1980), An analytic model of the wind and pressure profiles in hurricanes, Mon, *Weather Rev*., 108, 212–1218.

Jones, J.E., and A.M. Davies (2004), On the sensitivity of computed surges to open-boundary formulation, *Ocean Dynamics*, 54 (2), 142–162.

Li, J., J. Scinocca, J. Lazare, M. Mcfarlane, N. Mcfarlane, K. Von Salzen and L. Solheim (2006), Ocean surface albedo and its impact on radiation balance in climate model, *J. Clim*, 19: 6314–6333.

Liu, Y., P. MacCready, B.M. Hickey, E. P. Dever, P.M.Kosro, and N.S. Banas. (2009). Evaluation of a coastal ocean circulation model for the Columbia River plume in summer 2004. *J. Geophys. Res.* 114, C00B04, doi: 10.1029/2008JC004929.

Ma Z., G. Han and B. deYoung. (2012). Modelling temperature, currents and stratification in Placentia Bay. Atmosphere-Ocean. 50. DOI:10.1080/07055900.2012.677413.

Monahan, E.G. and G. MacNiocaill (1986), Oceanic whitecaps and their role in air-sea exchange processes, *Springer-Verlag New York, LLC*.

Mellor, G.L., T. Ezer and L.Y. Oey (1993), The pressure gradient conundrum of sigma coordinate ocean models, *J. Atmos. Ocean. Tech*, 11: 1126–1134.

Morey, S.L., S. Baig, M.A. Bourassa, D.S. Dukhovskoy and J.J. O'Brien (2006), Remote forcing contribution to storm-induced sea level rise during Hurricane Dennis. *Geophysical Research Letters*, 33, L19603, doi: 10.1029/2006GL027021.

Pawlowicz.R, B. Beardsley and S. Lentz. (2002). Classical tidal harmonic analysis including error estimates in MATLAB using T_TIDE. *Computers and Geosciences*. 28:929-937.

Phadke, A. C., C. D. Martino, K.F. Cheung, and S. H. Houston. (2003). Modelling of tropical cyclone winds and waves for emergency management. *Ocean Engineering*. 30, 553-578.

Pepin, P. and J.A. Helbig (1997), Distribution and drift of Atlantic cod (Gadus morhua) eggs and larvae on the northeast Newfoundland shelf, *Can. J. Fish. Aquat. Sci*, 54, 670–685.

Peng, M., L. Xie and J. Pietrafesa (2006a), A numerical study on hurricane induced storm surge and inundation in Charleston, South Carolina, *J. Geophys. Res*, 111, C08017. doi:10.1029/2004JC002755.

Peng, M., L. Xie and J. Pietrafesa (2006b), Tropical cyclone induced asymmetry of sea level surge and fall and its presentation in a storm surge model with parametric wind fields, *Ocean Model*,14, 81–101.

Price, F. (1981), Upper ocean response to a hurricane, *J.Phys.Oceanogr*., 11, 153-175.

Resio, D.T. and J.J. Westerink (2008), Modeling the physics of storm surges, *Physics Today*, 61 (9), 33–38.

Rego, J.L. and C. Li (2010), Storm surge propagation in Galveston Bay during Hurricane Ike, *Journal of Marine System*, 82, 265-279.

Pasch, R.J. and T.B. Kimberlain (2011), Tropical Cyclone Report Hurricane Igor (AL112010).

Shen, J., W. Gong and H.V. Wang (2006), Water level response to 1999 Hurricane Floyd in the Chesapeake Bay, *Cont. Shelf Res*, 26, 2484–2502.

Sheng, J., X. Zhai and R. Greatbatch (2006), Numerical study of storm –induced circulation on the Scotian Shelf during Hurricane Juan using a nested-grid ocean model, *Progress in Oceanography* , 70, 233-254.

Tang, C.L., Q. Gui and B.M. Detracey (1998), Barotropic response of the Labrador/Newfoundland Shelf to a moving storm, *J. Phys. Oceanogr*, 28, 1152-1172.

Thiebaut.S and R. Vennell (2010), Observation of a fast continental shelf wave generated by a storm impacting Newfoundland using wavelet and cross-wavelet analyses, *J. Phys. Oceanogr*, 40, 417-428.

Wada, A. (2005). Numerical simulations of sea surface cooling by a mixed layer model during the passage of Typhoon Rex. *J. Oceanogr*. 61. 41-57.

Weisberg, R.H. and L. Zheng (2006a), Hurricane storm surge simulation for Tampa Bay, *Estuaries Coasts*. 29 (6), 899–913.

Weisberg, R.H. and L. Zheng (2006b), A simulation of the Hurricane Charley storm surge and its breach of North Captiva Island, *Fla. Sci.* 69, 152–165.

Weisberg, R.H. and L. Zheng (2008), Hurricane Storm surge simulations comparing three-dimensional with two-dimensional formulations based on an Ivan-like storm over the Tampa Bay, Florida region, *J. Geophys. Res*., 113, C12001, doi:

10.1029/2008JC005115.

Westerink, J.J., R.A. Luettich, J.C. Feyen, J.H. Atkinson, C. Dawson, H.J. Roberts, M.D. Powell, J.P. Dunion, E.J. Kubatko and H. Pourtaheri (2008), A basin- to channel-scale unstructured grid hurricane storm surge model applied to Southern Louisiana, *Mon. Weather Rev*, 136, 833–864.

Willmott, C.J. (1981). On the validation of models. *Phys. Geogr*., 2, 184-194.

Xie, L., L. Pietrafesa and M. Peng (2004), Incorporation of a mass-conserving inundation scheme into a three dimensional storm surgemodel, *J. Coast. Res*, 20 (4), 1209–1223.

Xie, L., S. Bao, L. Pietrafesa, K. Foley and M. Fuentes (2006), A real-time hurricane surface wind forecasting model: formulation and verification, *Mon.Weather Rev*, 134, 1355–1370.

Zhang, J.A. and E. W. Uhlhorn (2012). Hurricane sea surface inflow angle and an observation-based parametric model. *Mon.Weather Rev,*140, 3587-3605.

Connecting Text

The second article addressed the second objective. It mainly focused on the Placentia Bay, Newfoundland to further investigate the oceanic response to two different hurricanes (Hurricane Igor in 2010 and Hurricane Leslie in 2012). Resolution including the inner bay was refined to 50 m. Hurricane Igor (2010) and Hurricane Leslie (2012) were selected as two hurricanes with different tracks, maximum sustainable wind and landfall points. This article also discussed the significantly influence by local atmospheric forcing during Hurricane Igor and Hurricane Leslie. Baroclinicity was also demonstrated in this article as an important portion in producing the hurricane-induced near-inertial oscillation.

This article has been written with the intention of being submitted to *Ocean Modelling*.

4. Modelling the response of Placentia Bay to hurricanes Igor and Leslie

Zhimin Ma[1], Guoqi Han[2] and Brad de Young[1]

[1] Department of Physics and Physical Oceanography, Memorial University of Newfoundland, St. John's, Newfoundland, Canada.

[2] Biological and Physical Oceanography Section, Fisheries and Oceans Canada, Northwest Atlantic Fisheries Centre, St. John's, Newfoundland, Canada.

4.1 Abstract

A three-dimensional, baroclinic, finite-volume coast ocean model (FVCOM) is used to examine the hurricane induced responses in Placentia Bay, Newfoundland. Two hurricanes chosen are Hurricane Igor (2010) and Hurricane Leslie (2012), both of which made landfall within 100 km of the mouth of the bay. The model results agree reasonably well with field observations on sea level, near-surface currents and sea surface temperature (SST). Two hurricanes feature significant different tracks, radius and maximum sustainable wind, causing the opposite shifts in inner bay circulation. Hurricane Igor overwhelms the mean inflow into the inner bay and shifts the currents to outflow. Hurricane Leslie reinforces the inflow into the head of bay. The peak storm surge is significantly influenced by local atmospheric forcing during Leslie, but predominately due to remote forcing during Igor. Baroclinicity is important for the hurricane-induced inertial oscillation in the near-surface currents. The barotropic simulation results in a significant underestimate of the near-surface currents, including the inertial oscillation.

4.2 Introduction

Placentia Bay is located in the southern Newfoundland, bordered by the Burin Peninsula to the west and the Avalon Peninsula to the east. It supports important fisheries, especially for Atlantic Cod, which has received considerable interest recently because of its ecological sensitivity and economic importance (Bradbury et al., 2000). In summer, Placentia Bay features coastal upwelling on the western side of the bay due to the westerly upwelling favourable wind. *In situ* observations in the Placentia Bay region by

Hart et al. (1999) and Shillinger et al. (2000) revealed the mean circulation together with seasonal current variability and hydrographic changes. The circulation of the outer bay is cyclonic (Hart et al., 1999), a result confirmed by many modelling studies (Greenberg and Petrie, 1988; Tang et al., 1996; Han, 2005; Han et al., 2008; Han et al., 2010; Han et al., 2011; Ma et al., 2012). Ma et al. (2012) applied a robust prognostic high resolution model on Placentia Bay. They reproduced the mean circulation and modelled the spring-summer seasonal hydrographic variability in 1999. Smart Bay, a project funded by Marine Institute of Memorial University, deployed three mooring stations over Placentia Bay to provide the real-time near surface current, temperature data. Occasionally hit by tropical storms during late summer, the oceanic response of the Grand Banks (which is outside Placentia Bay) to a moving hurricane is characterized by a rise in sea level, a decrease in sea surface temperature and a surface phytoplankton bloom (Han et al., 2012a). However, it is unclear what and how different responses are during different storms in Placentia Bay.

In recent years, Placentia Bay was hit by two hurricanes, Hurricane Igor in 2010, considered to be the most intense hurricane to Newfoundland in recent years (Pasch and Kimberlain, 2011), and Leslie in 2012. Both hurricanes made landfall in southern Newfoundland (Table 4-1). Hurricanes tracks were almost parallel to each other and 45^{o} northeast towards the coast (Fig. 4-1). Igor made landfall to the east of Placentia Bay, classified as an eastern-type storm based on the landfall location, while Leslie's landfall was on the western side of Placentia Bay as a western-type storm. The storm translation speed intensifies winds on the right side of storm, resulting in asymmetry. Leslie had its right side facing Placentia Bay and the landfall point is at the mouth of bay (Table 4-1).

The eastern-type storm like Igor had the bay on its left side. The different tracks and landfall locations could lead to significantly different oceanic responses over Placentia Bay. Observed tide gauge records revealed different sea level responses along the coast. The sea level response observed at Argentia during Leslie is surprisingly stronger than that during Igor, 116 cm compared with 86 cm; even though Igor was more intense than Leslie (Table 4-1). Han et al. (2012b) analysed the water level peaks during Igor, suggesting a non-local effect to the sea level rise. These authors also attributed the sea level rise at St. John's and Argentia to continental shelf wave propagation. Therefore, our first goal is to apply the numerical method, examining the different oceanic response to hurricane Igor and Leslie, and further investigating the effect of local and non-local forcing on storm surges. de Young et al., (1993) also demonstrated the non-local effect of Kelvin wave propagation into Conception Bay from neighbouring Trinity Bay, Newfoundland. They also point out the strong coupled baroclinic and topographic response of Newfoundland coastal bays to winds. Thus, the second part of this work will focus on the baroclinic oceanic response to the wind during hurricane event.

Table 4-1: Some comparative aspects of Hurricane Igor and Leslie.

Name	Hurricane Igor	Hurricane Leslie
Date under Effect	September 21-22, 2010	September 11-12, 2012
Landfall location	Burin Penninsula, Newfoundland(East)	Cape Race, Newfoundland (South)
Maximum Sustainable Wind	40km/h	35 km/h
Minimum Centre Pressure	950 mb	968 mb
Storm surge at Argentia	0.86 m	1.16 m
Storm surge at St. Lawrence	0.77 m	0.96 m
Distant from Landfall point to mouth of Placentia Bay	Around 100 km	0 km

In this paper, we will describe the first application of a three-dimensional (3-D), coastal ocean model (FVCOM, Chen et al., 2004) to Placentia Bay forced by Hurricane Igor and Leslie. We will first establish and validate the model against independent observational data including mooring and tide-gauge data, to demonstrate the ability of the model in capturing the bay characteristics of the oceanic response. We will conduct case studies to examine the local and non-local influences and the baroclinic response to the hurricanes. The paper is arranged as follows. In section 4.3, we will describe the model setup, boundary conditions, forcing data and initial conditions. In section 4.4, we will evaluate model against observations. In section 4.5, we will first examine the inner

bay circulation during Hurricane Igor and Leslie. Then cases are developed to investigate the local forcing and baroclinic influence on reproducing the oceanic response to hurricanes. Finally, in section 4.6, we will present the summary and conclusions.

4.3 Model Configuration

4.3.1FVCOM model (Version 3.1)

Combining horizontal grid flexibility and computational efficiency, the FVCOM model used in this study integrates independent variables through individual unit control volumes. It is solved numerically by flux through the volume boundaries to guarantee the horizontal conservation of mass and momentum. A time splitting method is used for computational efficiency including an internal mode and an external mode constrained by the Courant-Friedriches-Levy (CFL) condition. A sigma coordinate is chosen to better resolve the topography. Barometric pressure term is applied in momentum equation. The current study use Mellor-Yamada turbulence scheme. Previous work (Weisberg and Zheng, 2006; Resio and Westerink, 2008; Rego and Li, 2010; Han et al., 2011; Ma et al., 2012; Ma et al., 2015) successfully demonstrates the advantage of FVCOM in simulating the physical environment around coastal shelf and bay areas.

4.3.2 Model domain

The model domain is from 53 ^{o}W to 56 ^{o}W and 45.5 ^{o}N to 47.8 ^{o}N (Fig. 4-1). The geometry of the domain features some coastal ocean banks, such as Green Bank and Whale Bank which is a part of the Grand Banks and St. Pierre Bank, which forms two channels with Green Bank and the Burin Peninsula. The shoreline of the bay has many inlets, and is surrounded by relatively steep cliffs. Three large islands are located in the

upper Placentia Bay (Fig. 4-1). The centre of the outer bay is 200 m deep, while much of the remainder of the outer bay is typically 100 m deep. The average depth of the Bay is around 125 m (Ma et al., 2012) although there are several 400 m deep channels that run along the longitudinal axis of the inner bay. The model bathymetry is mainly derived from the multi-beam bathymetry of the Canadian Hydrographic Service. To minimize the pressure gradient errors (Mellor et al., 1993), the bathymetry was smoothed using the same method as in Ma et al. (2012). The governing equations of the model are solved on an unstructured triangular grid whose spacing is largest (3-5 km) along the open boundary and smallest (50 m) along the inner bay coastline (Fig. 4-2). There are 31 unequally spaced levels in the vertical, with a minimum spacing of within 0.2 m near sea surface and seabed in order to resolve the shear current and thermodynamic process near surface and bottom. The model equations are solved using an integration step of 0.5 s for the external mode and an internal to external mode ratio of 10.

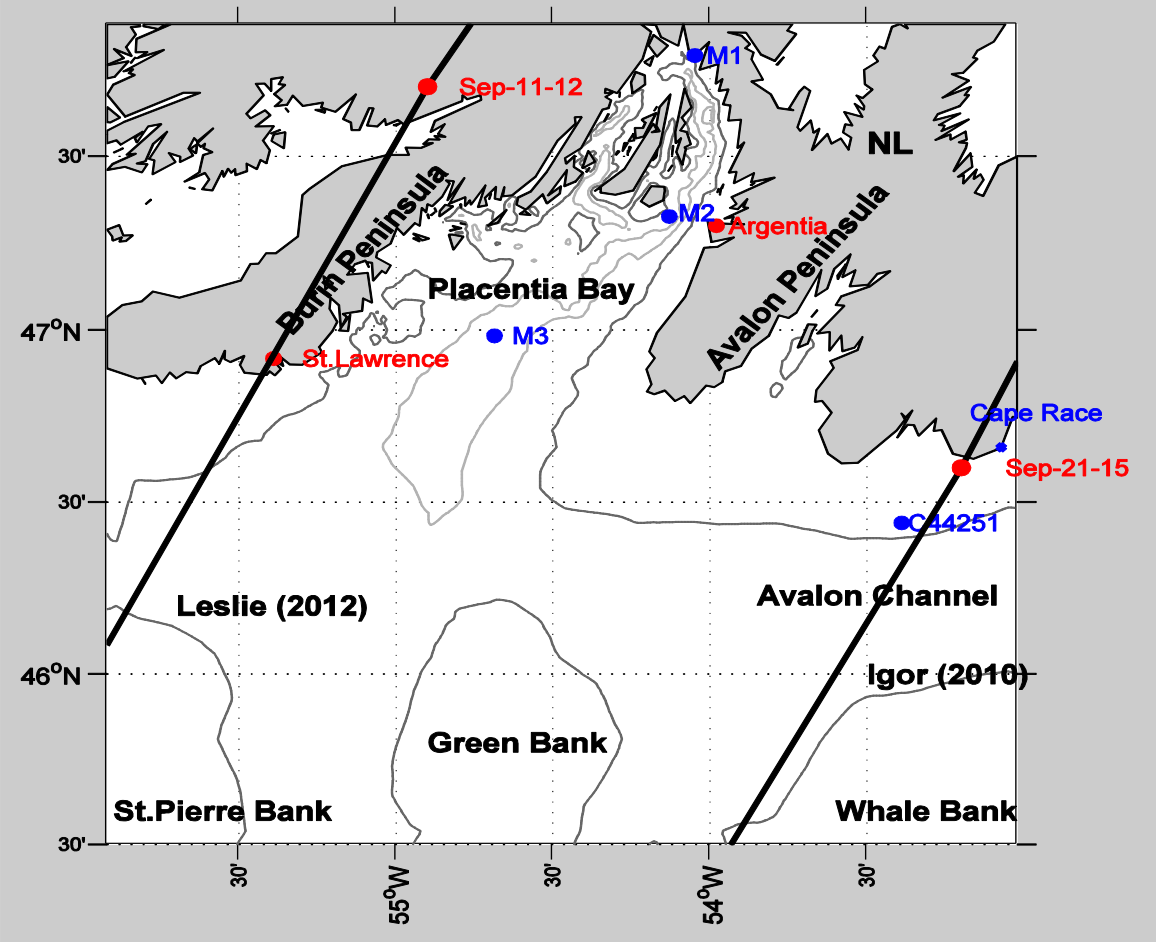

Fig. 4-1: Map showing model domain including 100 and 200 m depth contours (gray lines). Black thick lines are the tracks for Hurricane Igor and Hurricane Leslie. The red dots are tide-gauge stations, and the blue dots indicate mooring stations for surface temperature and currents.

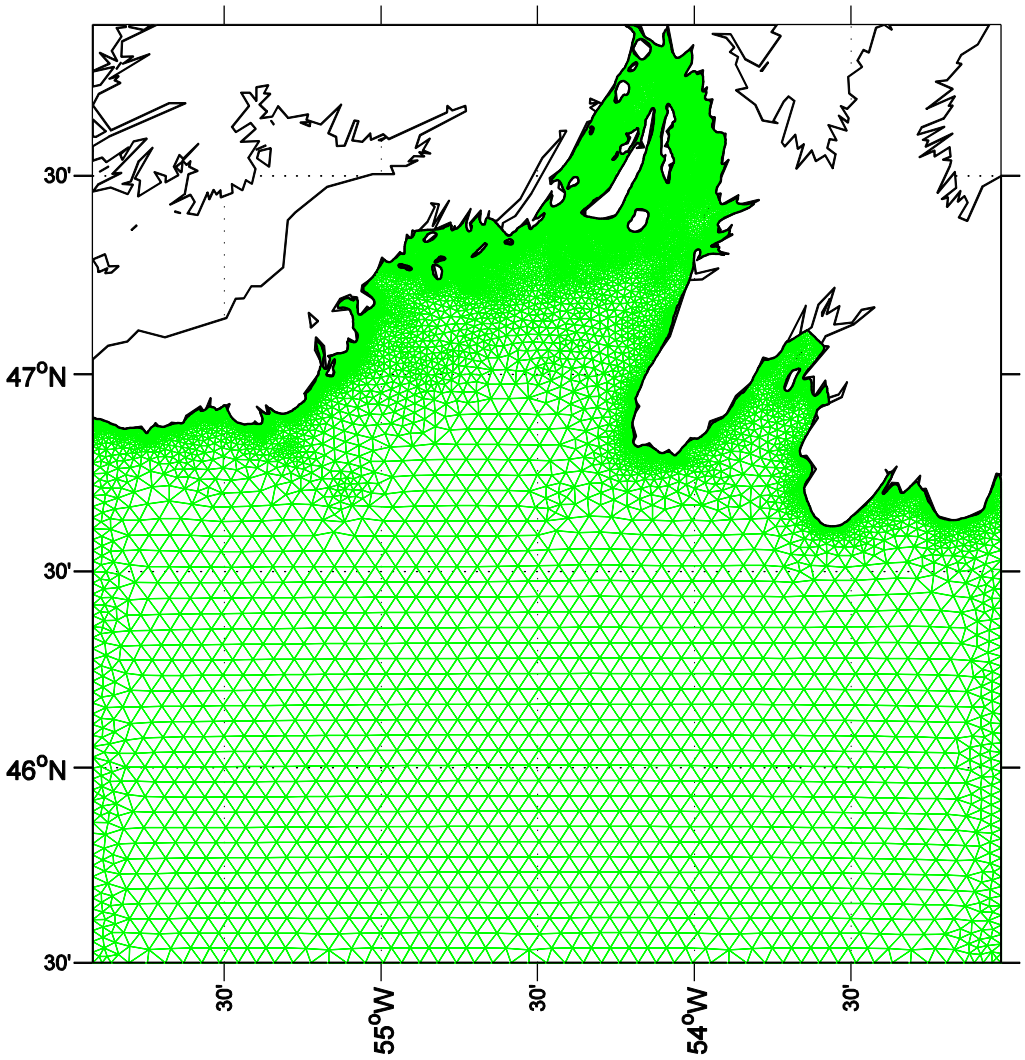

Fig. 4-2: The horizontal grid used in the numerical model. The grid spacing range from 50 m around inner Bay to 5 km over the outer Bay.

4.3.3 Model Forcing and Initial Conditions

The model is forced by winds, air pressure and heat fluxes at the sea surface, tidal and non-tidal sea levels and temperature and salinity at the lateral open boundaries. Wind and air pressure fields from Ma et al. (2015) are interpolated onto the model grids. These fields are blended from 3 hour North American Regional Reanalysis (NARR)

atmospheric forcing (www.esrl.noaa.gov/psd) and Holland hurricane model (Holland, 1980). The blending method is described in Ma et al. (2015). To improve the accuracy of the wind and air pressure fields, a distance-weighted correction scheme (Shen et al., 2006) based on the observational atmospheric data is applied on these atmospheric fields. The correction method applies the observed wind speed, direction and air pressure inside the Bay area (See Fig. 4-1 for locations of M1, M2, M3, C44251, Argentia and St. Lawrence, data are from Environment Canada and Fisheries and Canada) to assimilate the blending fields. Heat flux data including net showrtwave, net longwave, latent and sensible flux are extracted from NARR dataset (www.esrl.noaa.gov/psd, Mesinger et al., 2006) over the entire computational domain. The NARR project is an extension of the NCEP Global Reanalysis that is run over North America. The NARR model uses NCEP Eta Model (32 km/45 layer) together with the Regional Data Assimilation System (RDAS). This dataset has output 8 times daily. Net heat flux are calculated from the four flux components and mapped to the triangular nodes, as the same way with short wave radiation.

Five leading semidiurnal and diurnal constituents (M_2, S_2, N_2, K_1, O_1) and non-tidal sea levels at the lateral open boundaries are obtained from a large-scale Newfoundland Shelf model (Ma et al., 2015) and specified along the open boundary. The temperature and salinity along the open boundaries were specified in the same way. The Newfoundland Shelf model demonstrated a good quality of tidal and non-tidal elevation compared with observations over the Newfoundland Shelf. The model reasonably reproduced the inshore Labrador Current transport in year 2010 and 2012. Results from the Newfoundland Shelf model are interpolated to provide the hourly offshore variability.

However, to maintain conservation, this condition is used only when the boundary flux is directed into the domain.

The sea level and velocity were initialized with the results of the large-scale Newfoundland Shelf model (Ma et al., 2015) throughout the computational domain to reduce the spin-up time. The initial temperature and salinity condition was also generated from Ma et al. (2015).

The present model considers the fresh water input from the Piper Holes River in the upper bay. The river discharge rate was 29 m^3/s in 2010 and 19 m^3/s in 2012, but reached above five times of the average discharges when the storms hit the bay.

The model was run from August 15 to September 30 in 2010 and 2012. Model results from September 1 to 30 are compared with observations and used in analysis. Based on previous work with this model (Ma et al., 2012), 15 days is long enough to spin up the model for realistic forcing of Placentia Bay.

4.4 Validation

To evaluate the model solutions qualitatively and quantitatively, we compare the model solutions with various measurements. In addition to the correlation coefficient and the root-mean-square (RMS) difference, we examine the velocity difference ratio (VDR) defined as the ratio of the sum of the squared magnitudes of the vector velocity differences to the sum of the squared magnitudes of the observed velocities, that is,

$$\mathrm{VDR} = \sum |V_m - V_o|^2 \,/\, \sum |V_o|^2 \qquad (4\text{-}1)$$

where V_m is the horizontal model velocity and V_o is the horizontal observational velocity, Lower VDR values indicate better agreement, with $\mathrm{VDR} = 0$ indicating the exact agreement.

Another measure is the speed difference ratio (SDR) defined as the ratio of the sum of the squared speed difference to the sum of the squared magnitudes of the observed velocities, that is,

$$\mathrm{SDR} = \sum (|V_m| - |V_o|)^2 / \sum |V_o|^2 \qquad (4\text{-}2)$$

The third index is the correlation coefficient (R) between the model and observational components.

4.4.1Evaluation of Tidal Elevation

The horizontal distribution of M_2 shows an increasing trend in amplitude towards the head of bay. For K_1, the amplitude decreases towards the western side of bay, consistent with previous model and observation results (Han et al., 2010; Ma et al., 2012). Horizontal tidal distribution in detail can be found in Ma et al. (2012). The tidal elevation (for location of Argentia and D, see Ma et al. 2012, Fig. 4-1) is compared to observations. The detailed statistics are calculated in Table 4-2. The RMS difference of amplitude is within 2.5 cm, indicating good agreement in magnitude of tidal elevation and its distributions. The RMS difference of phase is within 6^{o} except K_1. The statistics from Ma et al. (2012) is also listed in Table 4-2. The current solution clearly shows the improvement in reproducing the diurnal tidal constituents.

Table 4-2: Summary and statistics for observed and computed semi-diurnal and diurnal tidal elevations at two coastal tide-gauge stations. Observational locations were shown in Ma et al. (2012), Fig. 4-1. Both model results are listed for comparison.

	M_2		S_2		N_2		K_1		O_1	
	Ma et al.(2012)	Current Study	Ma et al.(2012)	Current Study	Ma et al.(2012)	Current Study	Ma et al.(2012)	Current Study	Ma et al.(2012)	Current Study
RMS amplitude(cm)	2.6	2.5	2.3	1.2	1.4	1.4	2.8	1.0	4.2	1.8
RMS Phase(^{o})	1.9	4.9	4.6	5.8	5.4	2.3	24.4	12.4	3.6	2.4

4.4.2Validation of Non-tidal Water Levels

Hourly model water level at Argentia and St. Lawrence station (see locations in Fig. 4-1) are compared with tide-gauge observations. Observed water levels are detided with the T-Tide toolbox (Pawlowicz et al., 2002). Harmonic analysis including five main tidal constituents (M_2, S_2, N_2, K_1, O_1) and major over-tides (M_4, M_6, MS_4) was applied to the model solutions. The inverse barometer effect is applied directly through the model momentum equations. It should be noted the observation in 2012 is not available from September 8 to 10.

The model-data comparison is shown in Fig. 4-3 after matching model mean sea level to tide-gauge datum. Simulated Igor responses agree well with observed water

levels at tide-gauge stations, especially with the water levels retreating after the storm landfall and the subsequent high storm surge (Fig. 4-3a and b). Water levels showed the first response around September-21 at 13:00 pm when the storm centre approached landfall near Cape Race (Southeast corner of the Newfoundland, Fig. 4-1). Around 21 hours later, another increase in sea level developed on September 22 at 10:00am as the storm centre travelled farther north to the central Labrador Sea. The second peak is probably associated with continental shelf wave propagation (Han et al., 2012b). Unlike Igor, the water levels associated with Leslie reached their peaks just before the storm made landfall on September 11 at 10:45am. Sea level at the tide-gauge stations started increasing on September 10, continuously rising until landfall (Fig. 4-3c and d). After peaking, sea level started to decrease and fluctuated for four cycles in one day with a period of about 5 hours. This fluctuation, presented as a bay seiche, existed in both model and observations, but its amplitudes is overestimated by the model. If we treat the bay as a triangular and the length is 130 km and with an averaged depth of 125 m (Ma et al., 2012), the fundamental seiche period is 5.4 h. The difference in amplitude may be attributed to poorly resolving the harbour area where the tide-gauge is located. In reality, the large seiche amplitude may be prohibited from propagating into harbour area. The sea level surge response to Leslie was in part attributed to the Ekman transport induced by intensified wind and low air pressure (see Section 4.2 for details).

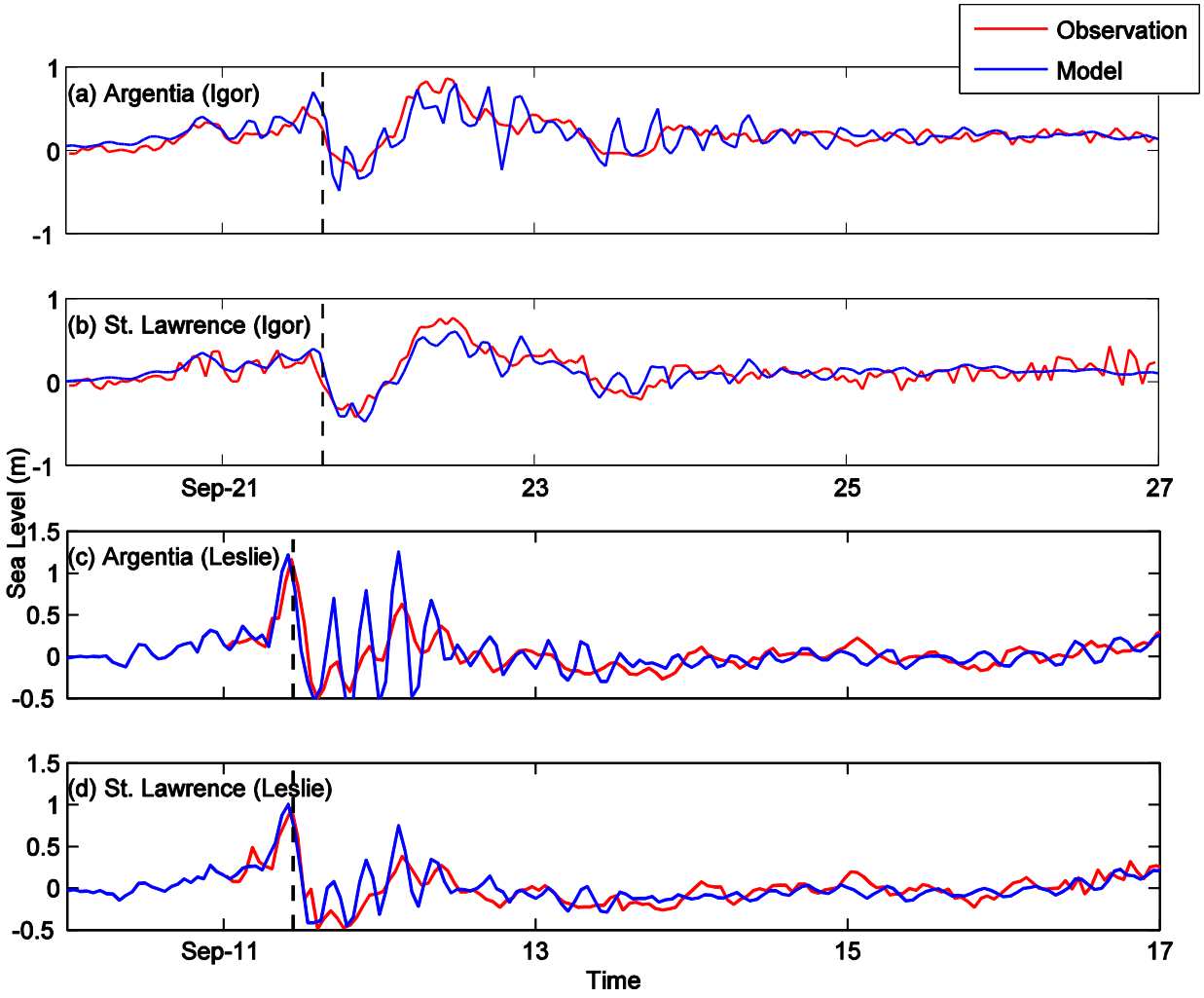

Fig. 4-3: Time series of sea level anomalies at (a) Argentia and (b) St. Lawrence under Hurricane Igor and at (c) Argentia and (d) St. Lawrence under Hurricane Leslie. Black dashed line indicates the landfall time at September-21, 15:00, 2010 and September-11, 10:45, 2012.

Quantitative comparisons are also calculated between the model results and observations (Table 4-3). By using the RMS difference and correlation, statistics are estimated to determine the model's ability to reproduce the sea level under hurricane forcing. The averaged RMS difference and correlation between the observed and modelled sea level is 0.15 m and 0.74, demonstrating reasonable agreement in terms of magnitude and variability. To evaluate the performance of the model in producing the

hurricanes induced sea level rising, the sea level surge difference and its time lag are calculated. On average, the amplitude difference is 0.09 m and the time lags are 0.6 hour. Even though the model underestimated the peak surge at St. Lawrence under Igor, it did well capture the local evolution of the storm surge.

Table 4-3: Statistics for observed and modelled sea level anomalies at Argentia and St. Lawrence. See Fig. 4-1 for location. (Model-Observation)

	Argentia		St. Lawrence	
	Hurricane Igor	Hurricane Leslie	Hurricane Igor	Hurricane Leslie
RMS difference (m)	0.15	0.21	0.11	0.14
Correlation	0.69	0.67	0.82	0.76
Surge difference (m)	-0.06	0.06	-0.17	0.05
Surge time lag (hour)	1	-0.5	0.5	-0.5

4.4.3Evaluation of Non-tidal Surface Current

Model currents are validated with the moored buoy data from the Smart Bay Project (http://www.smartatlantic.ca/PlacentiaBay/). Current data at 0.5 m below surface were recorded by every 0.5 hour at three different locations since 2006 (See locations M1, M2 and M3 in Fig. 4-1). M1 is located at the head of bay and M3 is near the mouth of bay (Fig. 4-1). M2 is in the eastern deep channel connecting from the outer bay to the inner bay, and is also close to Argentia. Currents at these different sites are likely to have quite different dynamical characteristics (Fig. 4-4 and Fig. 4-5). The surface current at M1 is relatively weak due to its location near the head of bay and its reduced influence from outside of the bay, especially during hurricanes (Fig. 4-5 a and b). At M3, currents

fluctuate at a frequency of 15 hours as Igor and Leslie passed by, suggesting a wind induced near inertial oscillation. Igor and Leslie lead to an opposite near-surface response at M3 at the time of storm landfall, with strong southwestward currents under Igor but northeastward currents under Leslie. Model and observed data during the simulation time have mean velocity of 0.21 m/s at M2 under Hurricane Igor. Currents at M2 also show large shifts in magnitude and direction during Igor, from weak northeastward to strong southwestward and then back to weak northeastward, due to the surface Ekman flow (Fig. 4-4). The maximum southwestward current reaches 0.6 m/s. During Leslie, the near surface currents at M2 were intensified to be northeastward. The model did reasonably at capturing the observational variability and magnitude, especially during the hurricane, though with the overestimation of near inertial oscillation at M3 under Igor. The spatial difference of near-surface currents at these three locations depends largely on the coastal geometry and the Rossby number, with strong inertial oscillation at M3 compared with weak magnitude at M1 and M2.

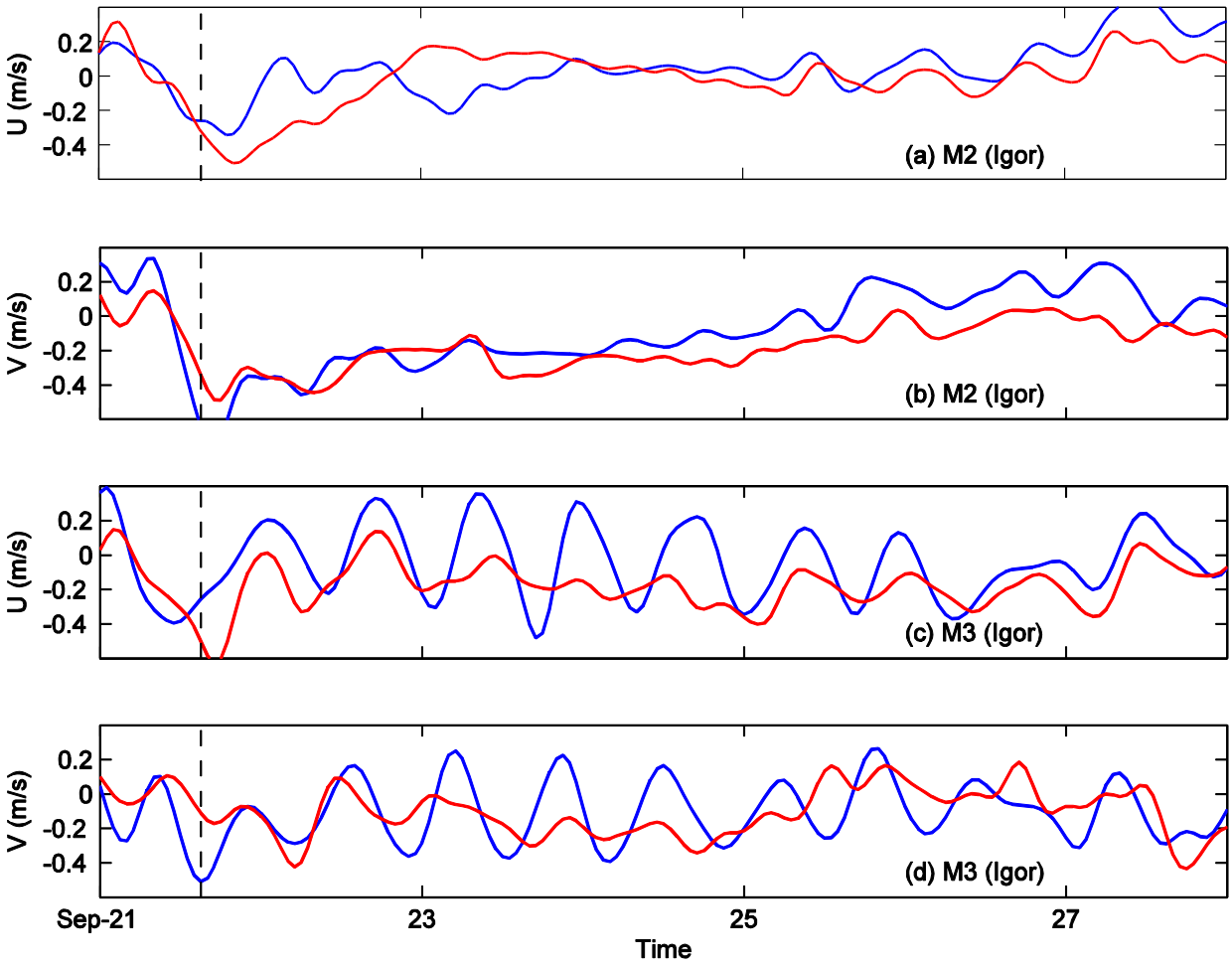

Fig. 4-4: Time series of observed (red) and modelled (blue) (a) eastward (U) and (b) northward (V) surface currents at M2 and (c) U and (d) V for M3 under Hurricane Igor. Black dashed line indicates the time of Sepember-21, 15:00 when Igor made landfall on Newfoundland Island.

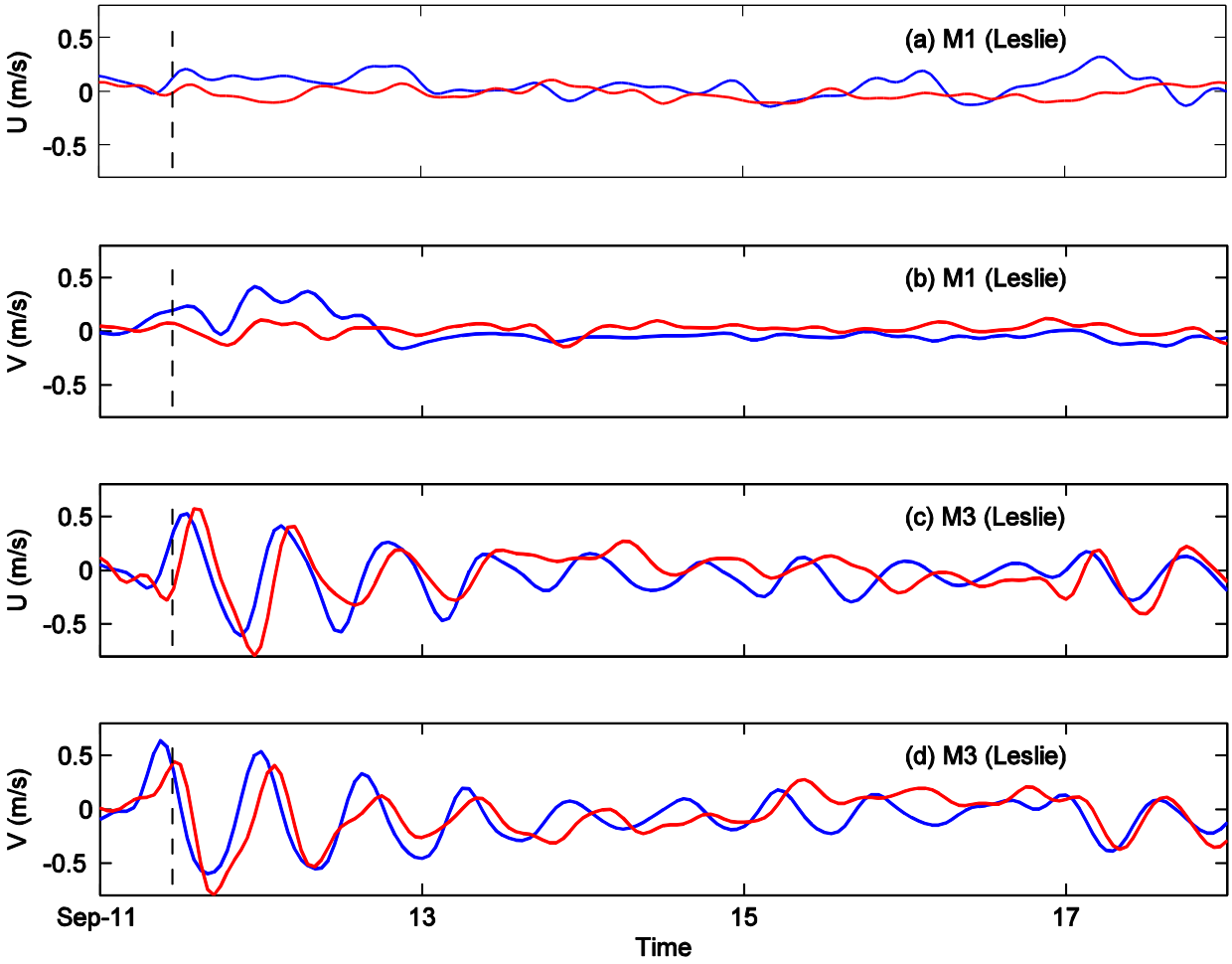

Fig. 4-5: Time series of observed (red) and modelled (blue) (a) eastward (U) and (b) northward (V) surface currents at M1, (c) U and (d) V at M2, (e) U and (f) V at M3 under Hurricane Leslie. Black dashed line indicates the time of Sepember-11, 10:45 when Leslie made landfall on southern of Newfoundland Island.

Quantitative statistics are calculated between the model and observed results (Table 4-4). Data were unavailable at M1 during Hurricane Igor and at M2 during Leslie. The averaged correlation coefficients for each direction component are 0.4, with somewhat better comparison during Leslie. The SDR values are generally smaller than 0.5 except for M1, indicating the well captured magnitude and variability for observed surface current. The VDR values, accounting for both speed and direction, are generally greater

than SDR. All VDR estimates except for M1 indicate fair agreement between model and observations. The poor VDR value at M1 is primarily due to the weak current magnitude.

Table 4-4: Current statistics: Eastward (U) and Northward (V) VDR and SDR at near surface for M1, M2 and M3. See Fig. 4-1 for the locations of M1, M2 and M3.

	Hurricane Igor				Hurricane Leslie			
	VDR	SDR	Correlation		VDR	SDR	Correlation	
			U	V			U	V
M1	-	-	-	-	3.2	1.0	0.25	0.12
M2	0.8	0.3	0.68	0.57	-	-	-	-
M3	1.0	0.3	0.44	0.18	0.9	0.3	0.35	0.35

4.4.4Comparison of Sea Surface Temperature (SST)

Fig. 6 presents the time series of surface temperature at M2, M3 and C44251 based on observations and model results for Hurricanes Igor and Leslie. The observed sea surface temperature at C44251 shows a sharp drop of 6^{o}C during Igor (Fig. 4-6b), in response to the strong vertical mixing. Inside the bay at M3, the model sea surface temperature has a 3^{o}C decrease from September 21 to 23 (Fig. 4-6a), comparable to observation but with underestimated magnitude. Unlike Igor, the response to Hurricane Leslie shows rapid changes in surface temperature, with a 1^{o}C drop in sea surface temperature at M2 and M3 as the storm passes by (Fig,. 4-6c, d). Simulated surface temperature under Leslie reproduced well the observed temperature drop timing, but

overestimated the change. The over- and under-estimation of magnitude are perhaps associated with limitation in heat flux input data over Placentia Bay.

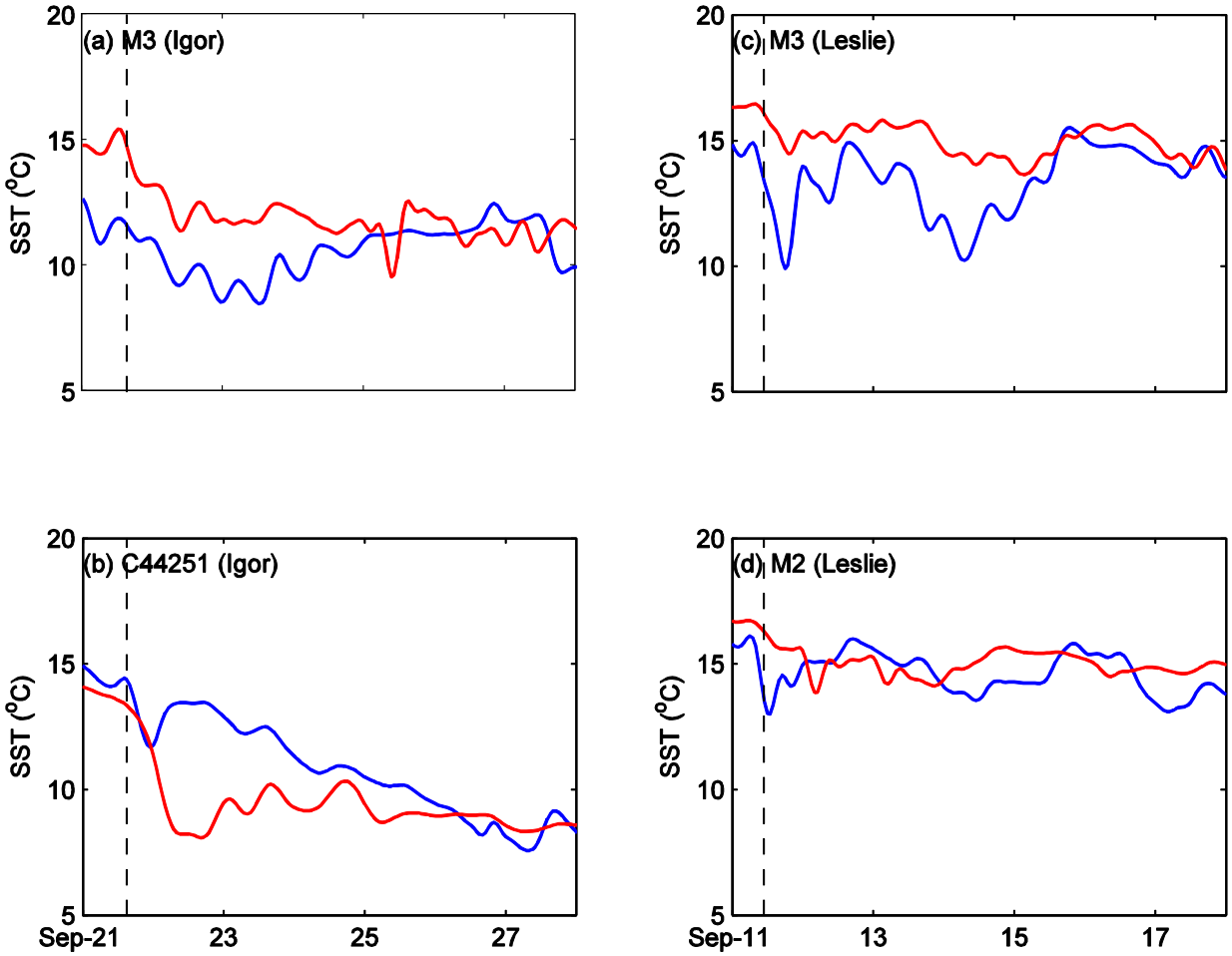

Fig. 4-6: Time series of observed (red) and modelled (blue) sea surface temperature (SST) at (a) M3 and (b) C44251 under Hurricane Igor; and SST at (c) M3 and (d) M2 under Hurricane Leslie. Black dashed line indicates the landfall time at September-21, 15:00, 2010 and September-11, 10:45, 2012.

The RMS difference and correlation are calculated to quantify the model performance (Table 4-5). The RMS differences are within 2°C in the middle bay and outer bay, except at M3 where the model underestimates the pre-hurricane ocean

temperature by about $2^{o}C$, indicating reasonable comparison between the model and observation.

Table 4-5: Statistics for the comparison between modelled and observed surface temperature (SST) at M2 and M3. See Fig. 4-1 for the locations.

	Hurricane Igor		Hurricane Leslie	
	M3 SST	C44251 SST	M2 SST	M3 SST
RMS difference(^{o}C)	3.9	1.8	1.9	3.0
Correlation	0.65	0.87	0.56	0.5

4.5 Discussion

4.5.1 Spatial Pattern of Inner Bay Velocity Fields

The time sequences of sub-tidal 0-30 m depth-averaged flows related to Hurricane Igor are shown in Fig. 7. On September 21, 10:00 am, around 5 hours before the landfall of Igor (Fig. 4-7, a), the upper ocean current has an inflow through the eastern side of the steep channel into the inner bay, due to the inshore Labrador Current flowing along the coast. Three eddies are generated in the east channel, inner bay, and west channel. These eddies may contribute to fish egg and larvae retention during late summer (Bradbury et al., 2000). After Igor made landfall (Fig. 4-5, b), the hurricane wind overcomes the Labrador Current inflow, pushes the surface current toward the southwest and intensifies the currents to 0.4 m/s. As Igor moves northeastward onto the Labrador Shelf, the direct hurricane influence diminishes and the upper ocean current relaxes (Fig. 4-7, c and d).

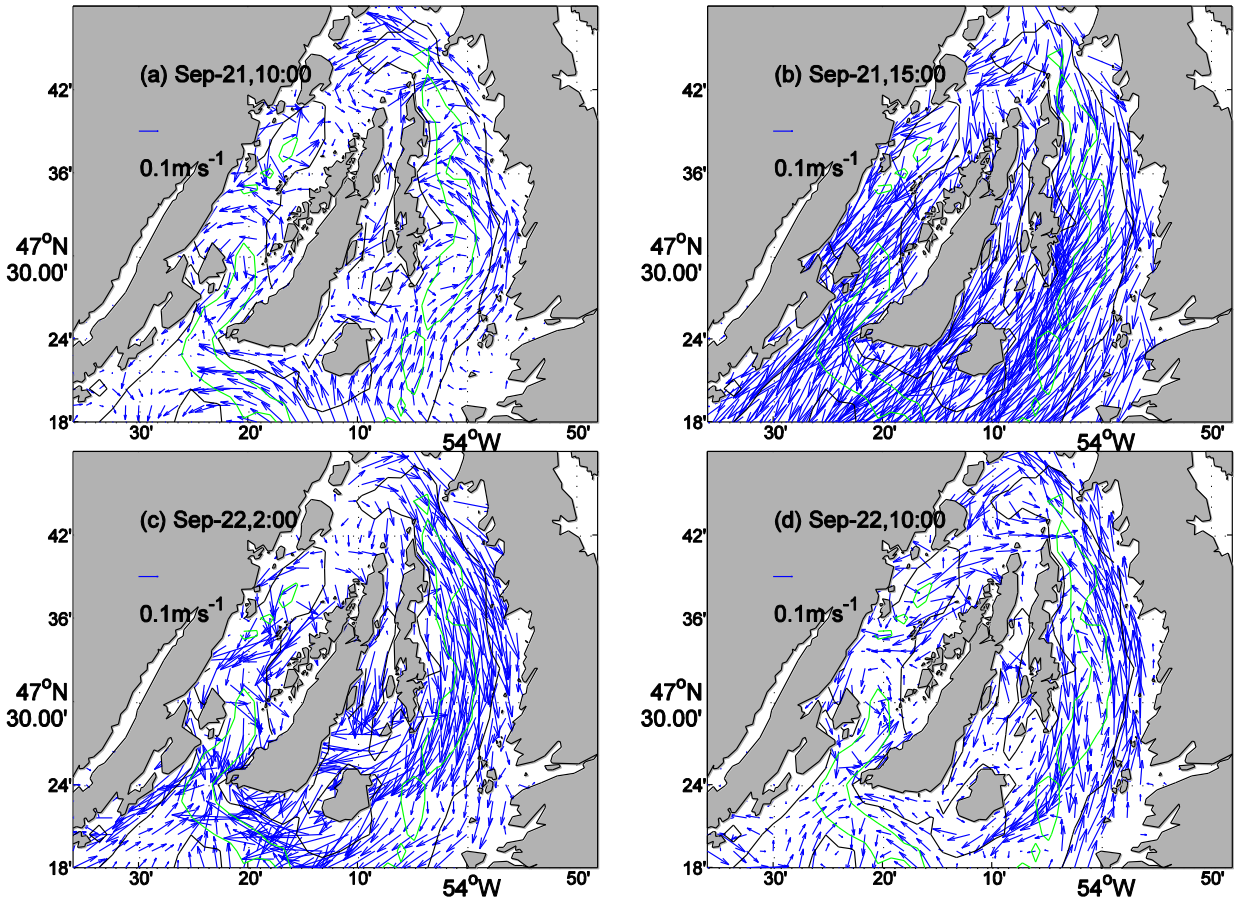

Fig. 4-7: Vertically averaged current in the top 30 m during Hurricane Igor at (a) 10:00 and (b) 15:00 on September-21, and at (c) 2:00 and 10:00 on September-22 in 2010.

Fig. 4-8 shows the 0-30m averaged current during Hurricane Leslie. As Leslie approaches, the inner bay circulation features the inflow and eddies (Fig. 4-8, a) at the same location as for Igor case. Six hours later when Leslie made landfall on the western side of Placentia Bay, currents become significantly strong, with combined wind induced Ekman inflow and inshore Labrador Current inflow. As Leslie travels farther north, the inflow is weaker and the inner bay circulation is counter-clockwise (Fig. 4-8 c and d).

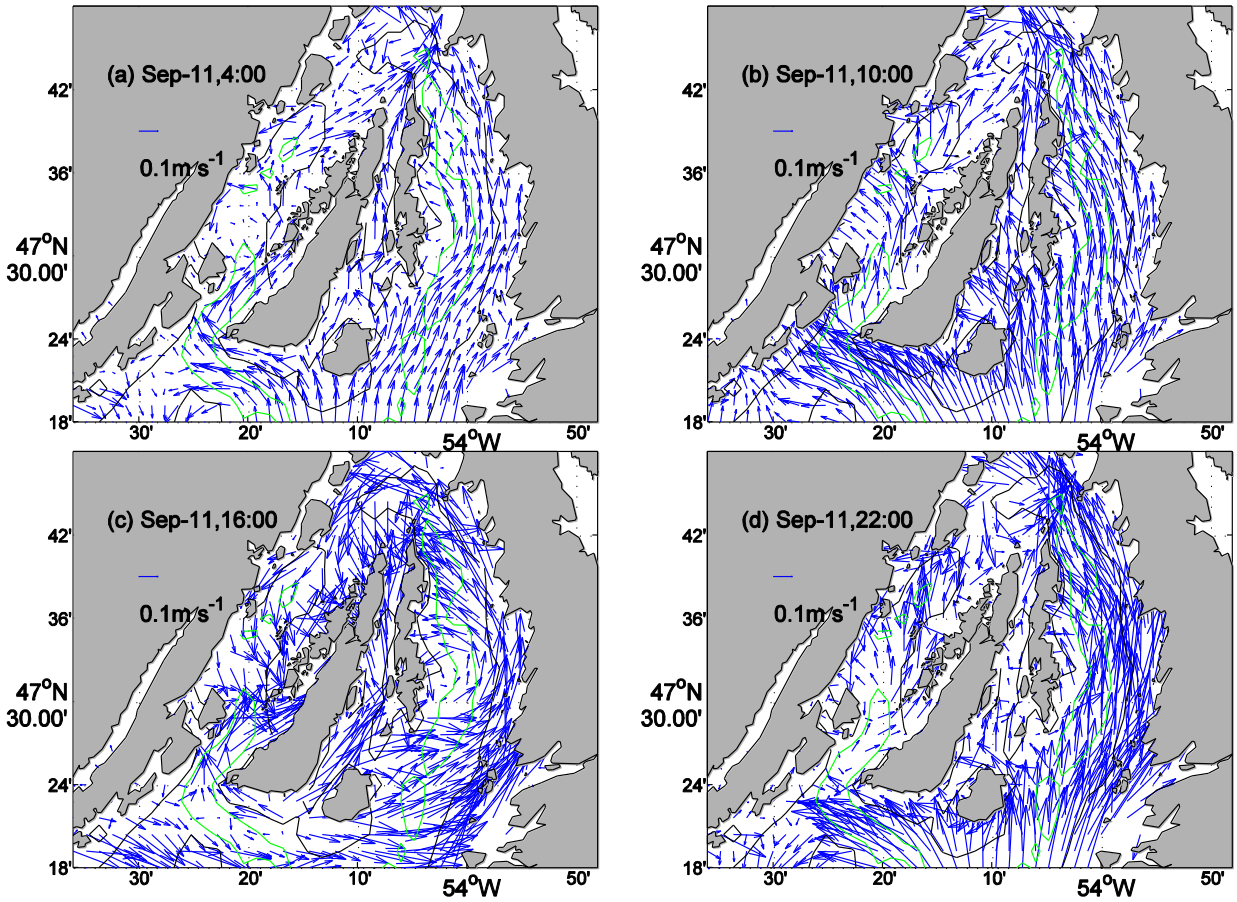

Fig. 4-8: Vertically averaged current in the top 30 m during Hurricane Leslie at (a) 10:00 and (b) 15:00 on September-21, and at (c) 2:00 and 10:00 on September-22 in 2012.

At the first stage before landfall of the storm, the upper ocean current shows a similar response in both cases. Counter-clockwise eddies appear in the upper bay. As the hurricanes pass, surface currents in the upper 30m are intensified, with outflow and inflow for Igor and Leslie, respectively. Igor cancels the inflow and generates a strong outflow from the inner bay. Leslie intensifies the inflow and stimulates a clear anti-clockwise circulation inside of bay. The different oceanic response is primarily attributed to the hurricane tracks and differing landfall positions. Igor passes Placentia Bay on its eastern side making landfall 100 km away from Placentia Bay (Fig. 4-1). The Ekman

flow from Igor is mostly outflow and pushed away from the eastern coast. Leslie is on the western side and the landfall point is at the right side of bay. During the early stages of Leslie, the strong southeast wind reinforces the inflow in the upper bay. After Leslie moves farther north, the wind turns from the southeast to southwest, contributing to the reversed direction of the Ekman flow with the southward surface current on the western channel of the inner bay.

4.5.2 Sea Level Response to local hurricane wind

Han et al. (2012) stated the observed sea level response to Igor peaked along the Placentia Bay coast as the storm center moves farther away. They argued the main surge during Igor is primarily associated with remote forcing, from a continental shelf wave. Unlike Igor, the sea level response to Leslie increased to the surge point before the storm made landfall. Therefore, this storm surge was formed primarily from local forcing. Here, we have conducted sensitivity runs to quantify the importance of the local atmospheric forcing effect to the main surge. Table 6 shows the percentage of water level changes at Argentia and St. Lawrence under Hurricane Igor and Leslie. During Igor, the water level without the local forcing increases by about 10%, indicating the dominant role of the remote forcing in reproducing the storm surge. While during Leslie, sea level surge decreases substantially, with more than half of the original magnitude, showing the importance of local atmospheric forcing.

Table 4-6: Statistics showing the decreasing of sea level surges at tide-gauge stations in case without local forcing.

	Hurricane Igor		Hurricane Leslie	
Tide gauge station	Argentia	St. Lawrence	Argentia	St. Lawrence
Simulated Sea level surge (m)	0.81	0.61	1.21	1.00
storm surge change in percentage (%) without local forcing	15	7	-45	-58

4.5.3 The Importance of Stratification on Near-Surface Velocity

To examine the influence of stratification on the response to hurricane forcing, a homogeneous barotropic case (hereafter referred to as BT) was developed for the domain of Placentia Bay. The case is initialized with the same velocity fields as for the baseline baroclinic case (referred to BC). In BT, the model is run with spatially uniform temperature and salinity over the domain. Same atmospheric forcing is applied at the surface.

Fig. 4-9 shows the 0-30m averaged current from BT at the exact same time as in BC (Fig. 4-7). By September 21, 10:00am, the cyclonic inner-bay circulation has already been formed, in corresponding to geostrophic pressure gradient. Compared with the BC case (Fig. 4-7), a swirl loop current at the head of bay disappeared, suggesting the importance of baroclinic instability in forming the small-scale counter-clockwise rotation. After Igor made landfall and the wind intensified on September 21, 19:00pm (Fig. 4-9 b), the wind-driven current overcame the inshore Labrador Current over the upper layer and

carried the water out of the inner bay. After the storm passed and the strong wind died down, the barotropic circulation returned to a state of dynamic rest very quickly, primarily due to the fast speed of the barotropic wave (Fig. 4-9 c and d). For Leslie, Fig. 4-10a shows the overall cyclonic circulation in Placentia Bay before storm. Leslie intensified the inflow into the head of bay (Fig. 4-10b). The BC and BT cases clearly show the near-surface currents are stronger for the baroclinic case, especially during hurricanes.

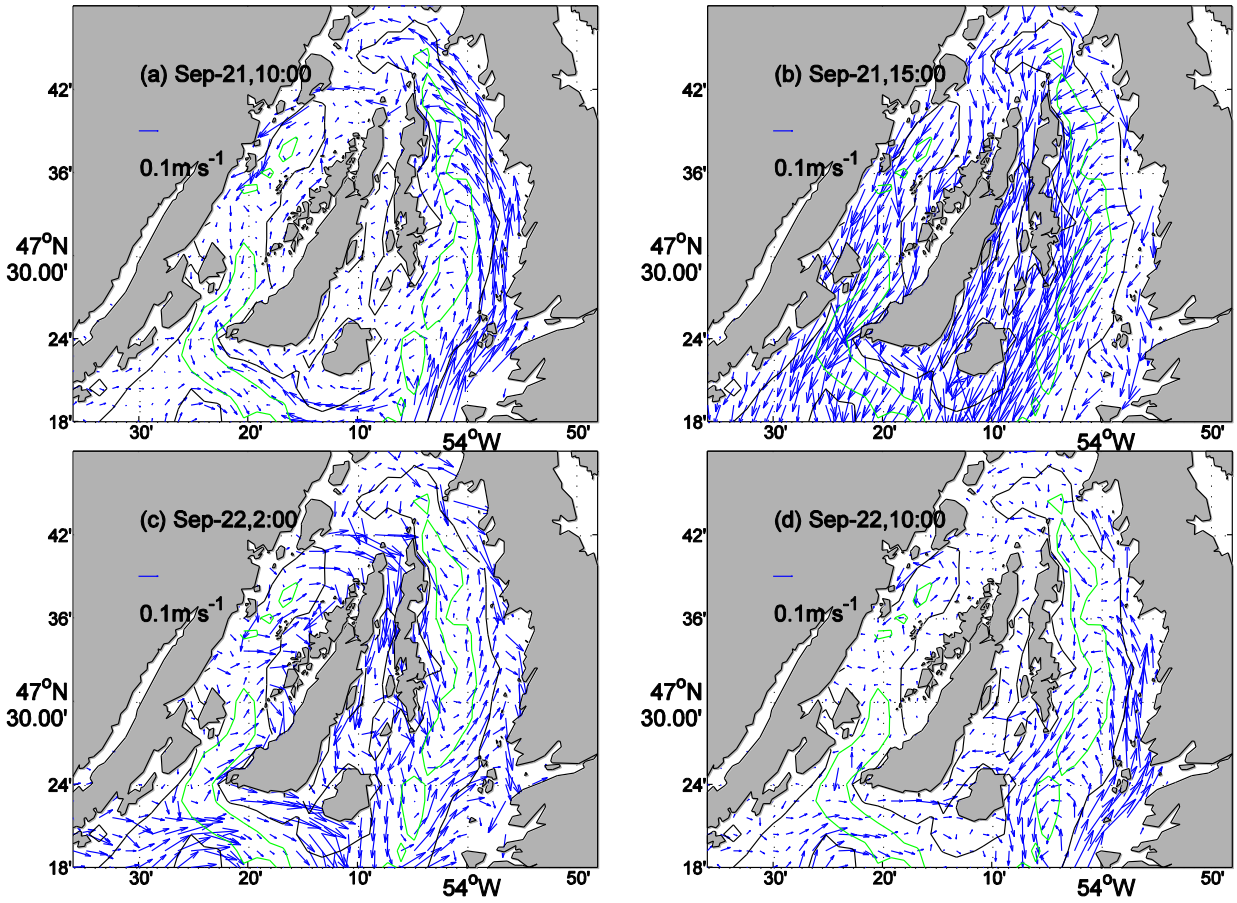

Fig. 4-9: Vertically averaged current in the top 30 m during Hurricane Igor calculated from BT case at (a) 10:00 and (b) 15:00 on September-21, and at (c) 2:00 and 10:00 on September-22 in 2010.

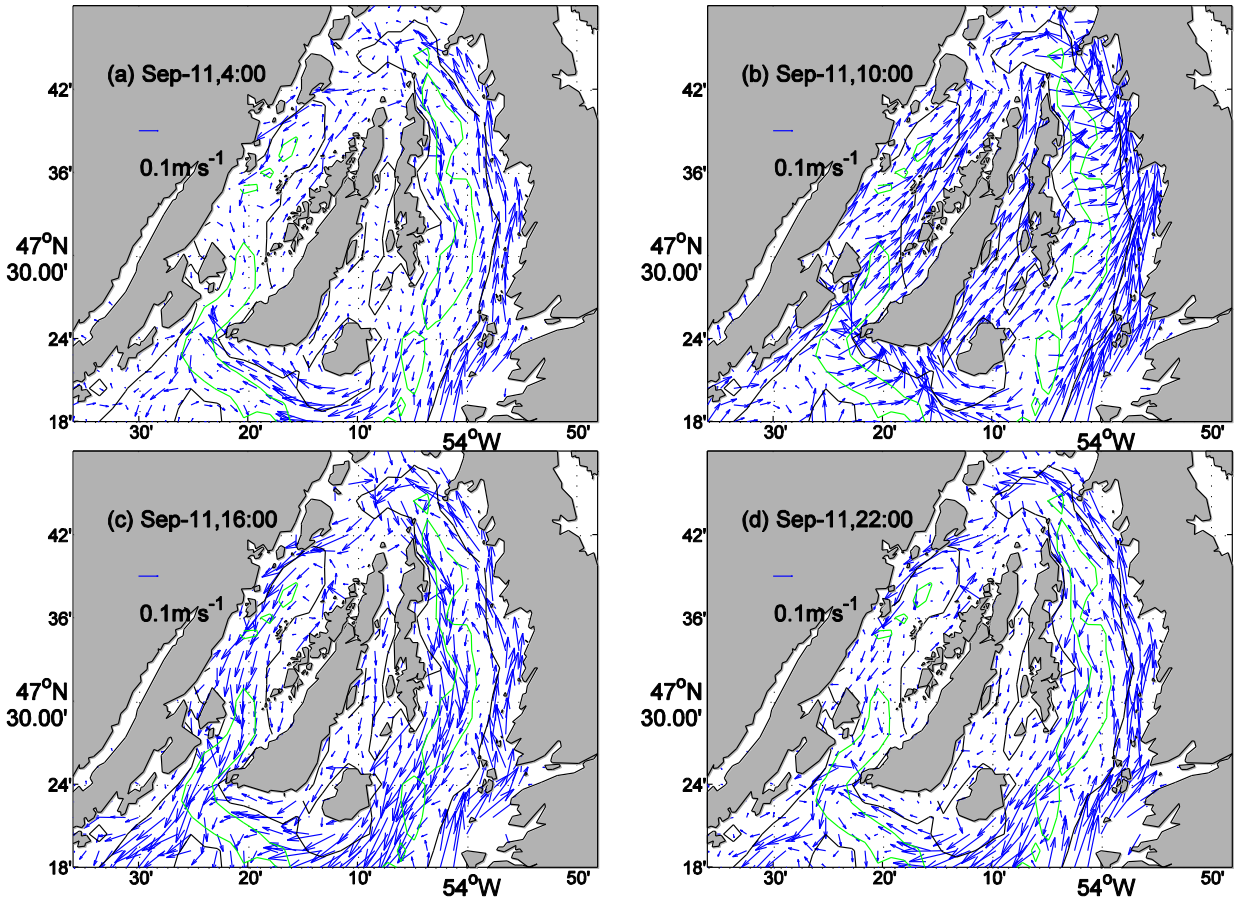

Fig. 4-10: Vertically averaged current in the top 30 m during Hurricane Leslie calculated from BT case at (a) 10:00 and (b) 15:00 on September-21, and at (c) 2:00 and 10:00 on September-22 in 2012.

To further examine the baroclinic influence, especially during the storm event, we select M2 and M3 near-surface currents as example (Fig. 4-11). Obviously, surface currents for the case BT are significantly underestimated in terms of both magnitude and variability, especially during Leslie. During Igor (Fig. 4-11 a-d), the currents changed drastically at the beginning stage of storm, especially at M3. The maximum currents during the storm are well captured in the BC case. During Leslie (Fig. 4-11 e-h), strong hurricane wind intensifies the near-surface currents in both cases. Currents in the BC case,

however, are much stronger than those for the BT case, especially for the hurricane-induced inertial oscillation from 12-15 September at M3. The BC case well simulates the current variations during Leslie. The above comparison of the near-surface current from Igor and Leslie indicates the stratification is a key dynamic factor in reproducing the inertial oscillation, while there remain issues to be resolved for improved quantitative agreement during Igor. Due to the overestimation of near-surface current during Igor, we do see some better comparisons in BT case. A latter experiment shows the improvement of the surface current at M3 in Igor by using the $k-\varepsilon$ turbulence scheme. This mechanism is consistent with Csanady (1972), Krajcar and Orlic (1995) and Chen and Xie (1997).

To demonstrate the baroclinic effect on the vertical structure of currents, we examine the vertical profiles from the BC and BT cases at M2 and M3 (Fig. 4-12). Again, we clearly see the model current from the BT case is significantly weaker than that from the BC case during the hurricanes. The BC model shows strong increase of the current gradient in the vertical in response to the hurricane forcing; while the BT model does not.

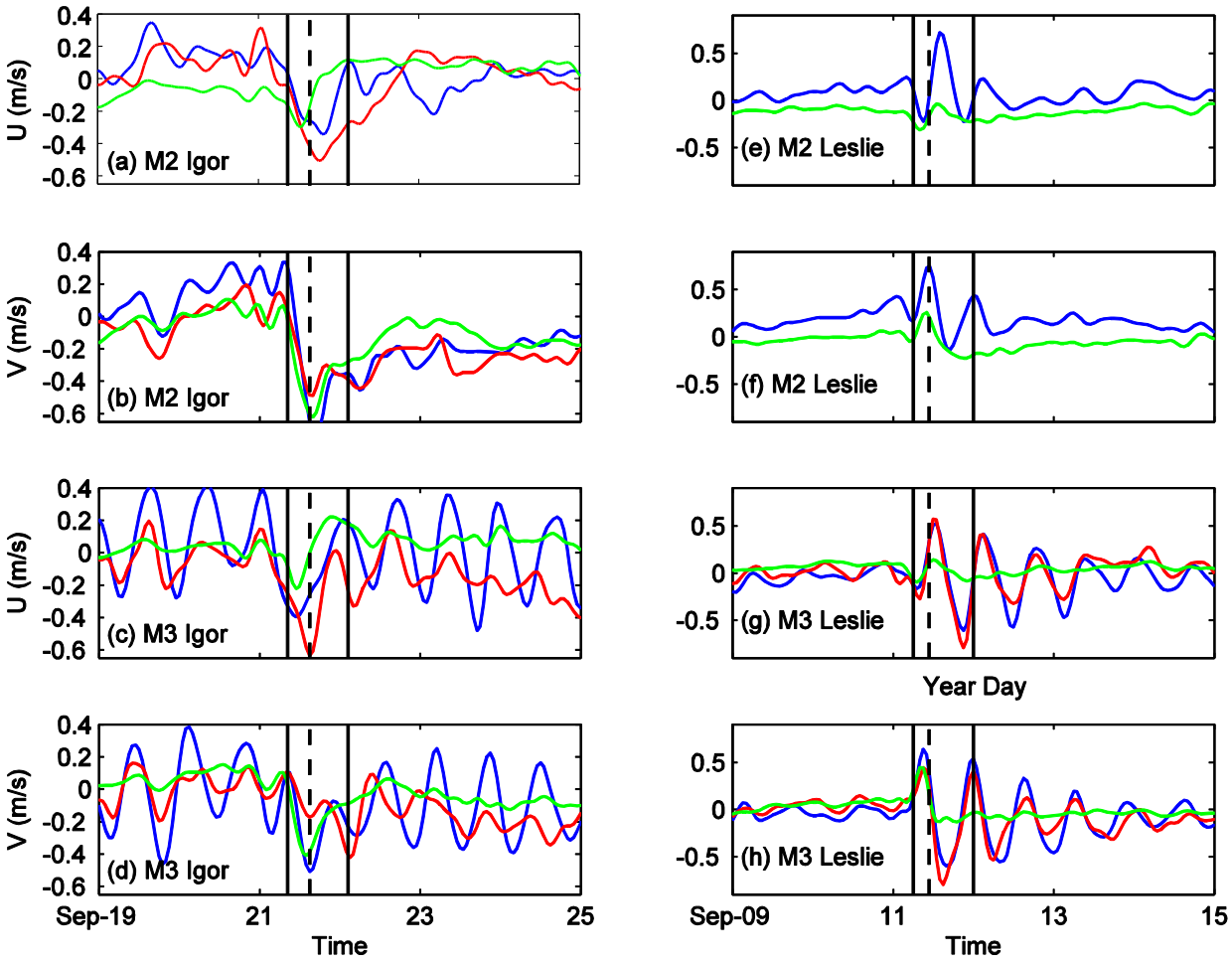

Fig. 4-11: Time series of near surface currents for case-BC (blue) and case-BT (green) compared to the observed near surface currents (Red). Black dashed line indicates the landfall time at September-21, 15:00, 2010 and September-11, 10:45, 2012 for Igor and Leslie, respectively. The time between two black thick lines is from storm approaching to leaving.

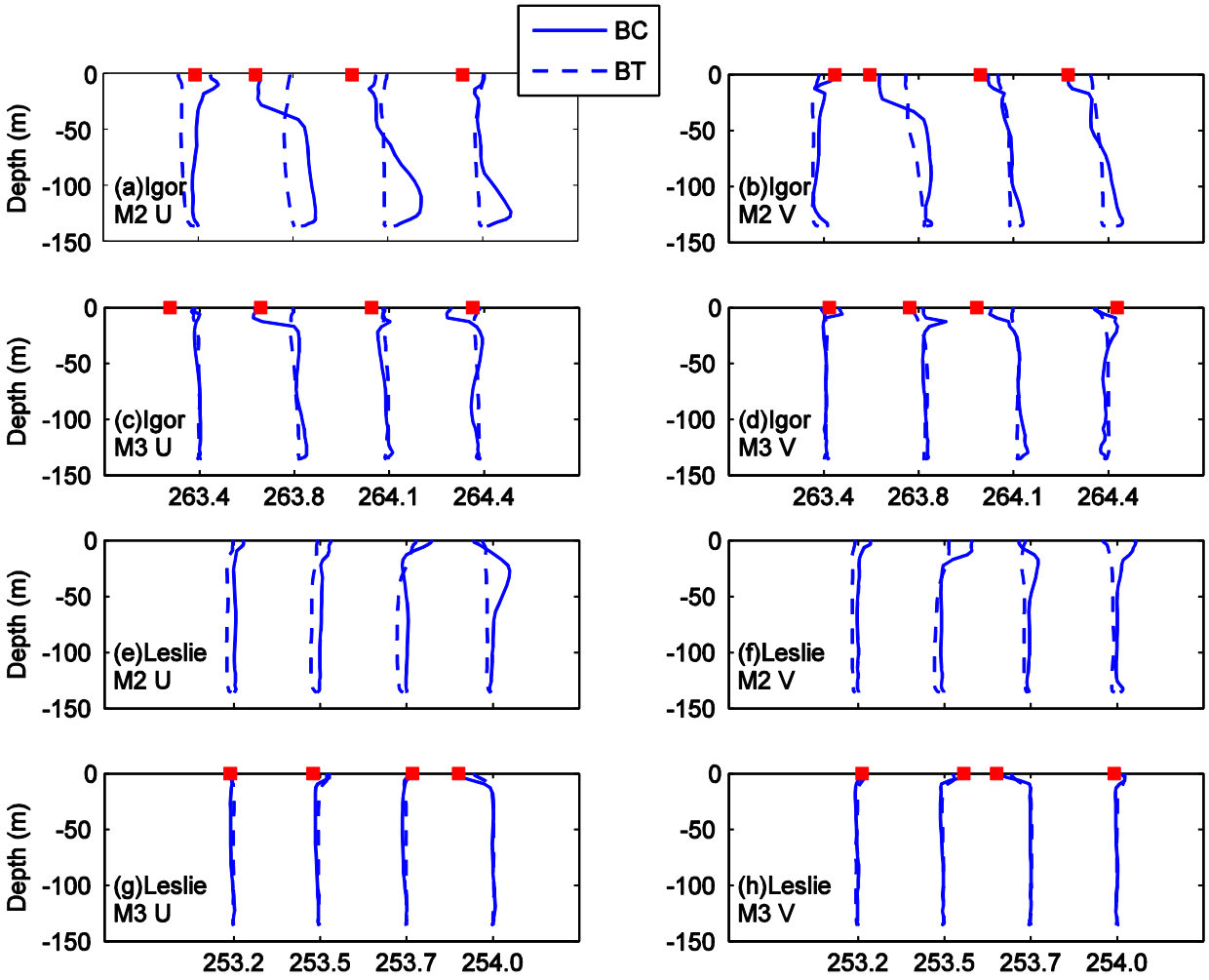

Fig. 4-12: Vertical profiles of currents at M2 and M3 under Hurricane Igor and Leslie. U is the eastward component and V is the northward component. Red squares indicate the observed near surface currents.

4.6 Conclusion and Summary

A three-dimensional finite-volume ocean model was applied to study the upper-layer responses to two hurricanes in Placentia Bay, Newfoundland. The hurricanes chosen for the study are Hurricane Igor (2010) and Hurricane Leslie (2012). Hurricane Igor was the more powerful storm, making landfall on the eastern side of bay while Hurricane Leslie made landfall at the western side. The two hurricanes feature different tracks,

strength, and translation speed, resulting in quite different oceanic responses on sea level and upper-layer circulation.

The finite-volume ocean model reproduced the water level rise before and after hurricanes. Especially, the surges generated by the passage of Hurricane Igor were well captured. The model sea level showed a good agreement with observations for Hurricane Leslie, in spite of over-estimation of the storm-induced inertial oscillation. The model near-surface current was compared with observations at three different locations in Placentia Bay, two of which are located in the inner bay. The statistics indicate reasonable agreement with observation, with 0.5 for an average Speed Difference Ratio. Especially during hurricane events, simulated currents well capture the observed currents, in terms of magnitude and variability.

The model reproduced the general cyclonic circulation in Placentia Bay before the two hurricanes. The upper 30 m circulation responding to the two hurricanes had opposite patterns. Upper-layer currents during Igor had strong outflow out of the inner bay while during Leslie strong inflow was observed. Cases without local wind and air pressure were examined. The results showed the local atmospheric forcing contributed to the peak storm surges by over 50% during Leslie, but insignificantly during Igor, indicating that the local forcing may have much more influence in western-type storms than in eastern-type storms, depending on the distance from the landfall point to the bay. The remote coastally trapped wave contributes more to sea level rise for the Igor-like case.

An examination of the circulation with and without stratification revealed the importance of baroclinicity for the hurricane response in Placentia Bay. The near surface currents during the two hurricanes were significantly decreased after removing the

stratification. Thus, the local baroclinic effect was essential in reproducing the hurricane-induced current intensification and inertial oscillation in Placentia Bay. The recovery time is much longer for the baroclinic case, due to the reduced propagation speed of the baroclinic wave. This also suggests that the baroclinic wave and its propagation are an important process in generating the storm-induced surface current. Vertical structures of the model currents at the mooring stations show substantially different vertical energy distribution between the baroclinic and barotropic cases.

This paper provides the first local examination of oceanic response to hurricanes over Placentia Bay. Physically, this article demonstrates the importance of stratification in simulation of wind induced events. The present study also suggests that the sea level response to Igor-like storm over Placentia Bay could be estimated from upstream tide-gauge stations like St. John's. The direct response to local wind and air pressure is important in storm surge during Leslie-like hurricanes. The results will be of interest to local communities for coastal management and marine safety and for applications to fisheries oceanography.

4.7Acknowledgement

We thank Dr. Changsheng Chen for providing the FVCOM code. The tide-gauge data and offshore buoy data are from the Integrated Science Data Management, Fisheries and Oceans Canada. The buoy data inside Placentia Bay are from the Smart Bay Project. The NCEP Reanalysis data is provided by the NOAA/OAR/ESRL PSD, Boulder, Colorado, USA, from their Web site at http://www.esrl.noaa.gov/psd/.

4.8 Reference:

Bradbury, I.R.; Snelgrove, P.V.R., Fraser, S., 2000. Transport and development of eggs and larvae of Atlantic cod, Gadus morhua, in relation to spawning time and location in coastal Newfoundland. Can. J. Fish. Aquat. Sci. 57: 1761–1772.

Csanady,G.T., 1972. Response of large stratified lakes to wind. J. Phys.Oceanogr. 2, 3-13.

Chen, C., Cowles, G., Beardsley, R. C., 2004. An unstructured grid, finite-volume coastal ocean model: FVCOM User Manual. SMAST/UMASSD Technical Report-04-0601. 183.

Chen, C., Xie, L., 1997. A numerical study of wind-induced, near-inertial oscillations over the Texas-Louisiana shelf. J. Geophys. Res. 102, 15583-15593.

deYoung, B., Otterson, T., Greatbatch, R.J., 1993. The local and nonlocal response of Conception Bay to wind forcing. J. Phys. Oceanogr. 23, 2636-2649.

Greenberg, D. A., Petrie, B. D., 1988. The mean barotropic circulation on the Newfoundland shelf and slope. J. Geophys. Res. 93, 15541-15550.

Han, G. 2005. Wind-driven barotropic circulation off Newfoundland and Labrador. Cont. Shelf Res. 25, 2084-2106.

Han, G., Lu, Z., Wang, Z., Helbig, J., Chen, N., deYoung, B., 2008. Seasonal variability of the Labrador Current and shelf circulation off Newfoundland. J. Geophys. Res. 113, 1-23.

Han, G., Paturi, S., de Young, B., Yi, S., Shum, C.-K., 2010. A 3-D data-assimilative tide model of Northwest Atlantic. Atmosphere-Ocean. 48, 39-57

Han, G., Ma, Z., de Young, B., Foreman, M., Chen, N., 2011. Simulation of three-dimensional circulation and hydrography over the Grand Banks of Newfoundland, Ocean Modelling. 40, 199-210.

Han G., Ma, Z., Chen, N., 2012a. Hurricane Igor impacts on the stratification and phytoplankton bloom over the Grand Banks. J. Mar. Syst. 100-101, 19-25.

Han, G, Ma, Z., Chen, D., deYoung, B., Chen, N., 2012b. Observing storm surges from space: Hurricane Igor off Newfoundland. Sci. Rep. 2, 1010; DOI:10.1038/srep010101.

Hart, D.J., deYoung, B., Foley, J., 1999. Observations of currents, temperature and salinity in Placentia Bay, Newfoundland. Physics and Physical Oceanography Data Report 1998–9, Memorial University of Newfoundland, St. John's: Newfoundland.

Holland, G. J. 1980. An analytic model of the wind and pressure profiles in hurricanes. Mon, Weather Rev. 108, 212–1218.

Krajcar, V., Orlic, M., 1995. Seasonal variability of inertial oscillations in the Northern Adriatic. Cont. Shelf. Res. 15,1221-1233.

Ma, Z., Han, G., deYoung, B., 2012. Modelling temperature, currents and stratification in Placentia Bay. J. Atmos. Ocean. 50: 244-260.

Ma, Z., Han, G., deYoung, B., 2015. Oceanic responses to hurricane Igor over the Grand Banks: a modelling study. J. Geophys. Res. Oceans. 120:doi:10.1002/2014JC010322.

Mellor, G.L., Ezer, T., Oey, L.Y., 1993. The pressure gradient conundrum of sigma coordinate ocean models. J. Atmos. Ocean. Tech. 11: 1126–1134

Mesinger, F., Dimego, G., Kalnay, E., Shafran, P., Ebisuzaki,W., Jovic,D., Wollen,J., Mitchell, K., Rogers, E., Fan, M., Ek,Y., Grumbine, R., Higgins, W., Li, H., Lin, Y., Manikin,G., Parrish,D., Shi,W., 2006. North American Regional Reanalysis. Bull. Amer. Mereor. Soc. 87, 343-360.

Pasch, R.J., Kimberlain, T.B, 2011. Tropical Cyclone Report Hurricane Igor (AL112010)

Rego, J.L., Li. C., 2010. Storm surge propagation in Galveston Bay during Hurricane Ike. J. Mar. Syst. 82, 265-279

Pawlowicz, R., Beardsley,B., Lentz, S., 2002. Classical tidal harmonic analysis including error estimates in MATLAB using T_TIDE. Computers and Geosciences 28, 929-937.

Resio, D.T., Westerink, J.J., 2008. Modeling the physics of storm surges. Physics Today. 61 (9), 33–38.

Schillinger, D.J., Simmons,P., deYoung, B., 2000. Analysis of the mean circulation in Placentia Bay: spring and summer 1999. Physics and physical oceanography data report 2000-1, Memorial University of Newfoundland: St. Johns, Newfoundland.

Shen, J., Gong, W., Wang, H., 2006. Water level response to 1999 Hurricane Floyd in the Chesapeake Bay. Cont. Shelf Res. 26, 2484-2502.

Tang, C. L., Gui, Q., Peterson, I. K., 1996. Modelling the mean circulation of the Labrador sea and adjacent shelves. J. Phys. Oceanogr. 26, 1989-2010.

Weisberg, R. H., Zheng, L., 2006. Circulation of Tampa Bay driven by buoyancy, tides and winds, as simulated using a Finite Volume Coastal Ocean Model. J. Geophys. Res. 111, C1005, doi:10.1029/2005JC003067.

Connecting Text

This third article described the application of three-dimensional finite volume ocean model off the Easter Newfoundland including the Trinity Bay. The model was developed with high resolution mesh grid with 20 m in the Trinity Bay. The simulation period was from spring to late summer for 2000 and 2001. The model results along the eastern Newfoundland coast agreed reasonably well with observations of sea level and currents. Temperature variations at 2000 and 2001 were well simulated compared with ADCP observations and current meter data inside Trinity Bay. This article also described the model surface circulation patterns and temperature distributions in Trinity Bay in spring and summer. Summer circulation showed significant upwelling along the western side of the bay, together with the emergence of two eddies in the bay. The stratification along the Newfoundland coast was investigated in this article too.

This article has been written with the intention of being submitted to *Continental Shelf Research.*

5. **Modelling currents, hydrography and stratification off the Eastern Newfoundland**

Zhimin Ma[1], Guoqi Han[2] and Brad de Young[1]

[1] Department of Physics and Physical Oceanography, Memorial University of Newfoundland, St. John's, Newfoundland, Canada.

[2] Biological and Physical Oceanography Section, Fisheries and Oceans Canada, Northwest Atlantic Fisheries Centre, St. John's, Newfoundland, Canada.

5.1 Abstract

A three-dimensional finite-volume ocean model (FVCOM) is applied off Eastern Newfoundland to study the circulation and hydrographic variability in 2000 and 2001. The model is forced at lateral open boundaries with non-tidal sea level and at the surface with hourly wind stress and heat flux. The open boundary temperature, salinity and non-tidal sea levels are derived from a large-scale shelf model. The model results along the eastern Newfoundland coast agree reasonably well with observations of sea level and currents. The estimated transport associated with the inshore Labrador Current is consistent with calculation based on the observations in summer. Temperature variations at 2000 and 2001 are well simulated compared with ADCP observations and current meter data inside Trinity Bay. The model surface circulation patterns and temperature distributions in Trinity Bay in spring and summer reveal seasonal differences along the coast. Summer circulation shows significant upwelling along the western side of the bay, together with the emergence of two eddies in the bay. The generation of these eddies reveals the importance of nonlinear dynamics. The stratification along the Newfoundland coast shows the spatial differences and the seasonal and inter-annual change of stratification due to the wind stress and heat flux.

5.2 Introduction

The circulation and its dynamics along the coast can be quite complex and are therefore of interest because flow near the coast can be convergent or divergent due to the upwelling- or downwelling-favorable wind, shedding from topography and convection from coastal currents (Ferrer and Caballero, 2011; Afargan and Gildor, 2015). Other

processes such as internal tidal propagation, coastal upwelling can also be studied. Inside a coastal bay, the wind-induced vertical current shear and horizontal baroclinic gradient, together with the topography can generate complex dynamic circulation system, resulting in spatially different stratification evolution (Ma et al., 2012). Bounding the Newfoundland Shelf, the eastern Newfoundland coast together with its embayments is an area with highly dynamical circulation and significant topographic slope especially near the coast. There are three large embayments in eastern Newfoundland: Bonavista Bay, Trinity Bay and Conception Bay from the northern to the southern coast (Fig. 5-1). Trinity Bay and Conception Bay feature deep channels over 300 m deep at the centre of the bay with steep topographic change onshore. However, the water at the head of two bays is shallow around 20 m. Observations have been made at Station 27 and along the Bonavista and Flemish Cap transects for many decades by Fisheries and Oceans Canada to monitor the hydrographic change and Labrador Current transport variability (Fig. 5-1). *In situ* observations have also been made inside Trinity Bay and Conception Bay to gain the knowledge of the seasonal variation of hydrography (Tittensor et al., 2002 a and b; Schillinger et al., 2000 a and b; de Young and Sanderson, 1995). The mooring deployments in Trinity Bay started in 2001 by Memorial University of Newfoundland. The mooring data show persistent summer upwelling events in the bay, together with the eddy-like circulation (Tittensor et al., 2002 a and b). The early observational study of the physical environment in Conception Bay can be traced back to 1987 and the data indicated relative weak tide and weak mean flow (Aggett et al., 1987; de Young and Sanderson, 1995).

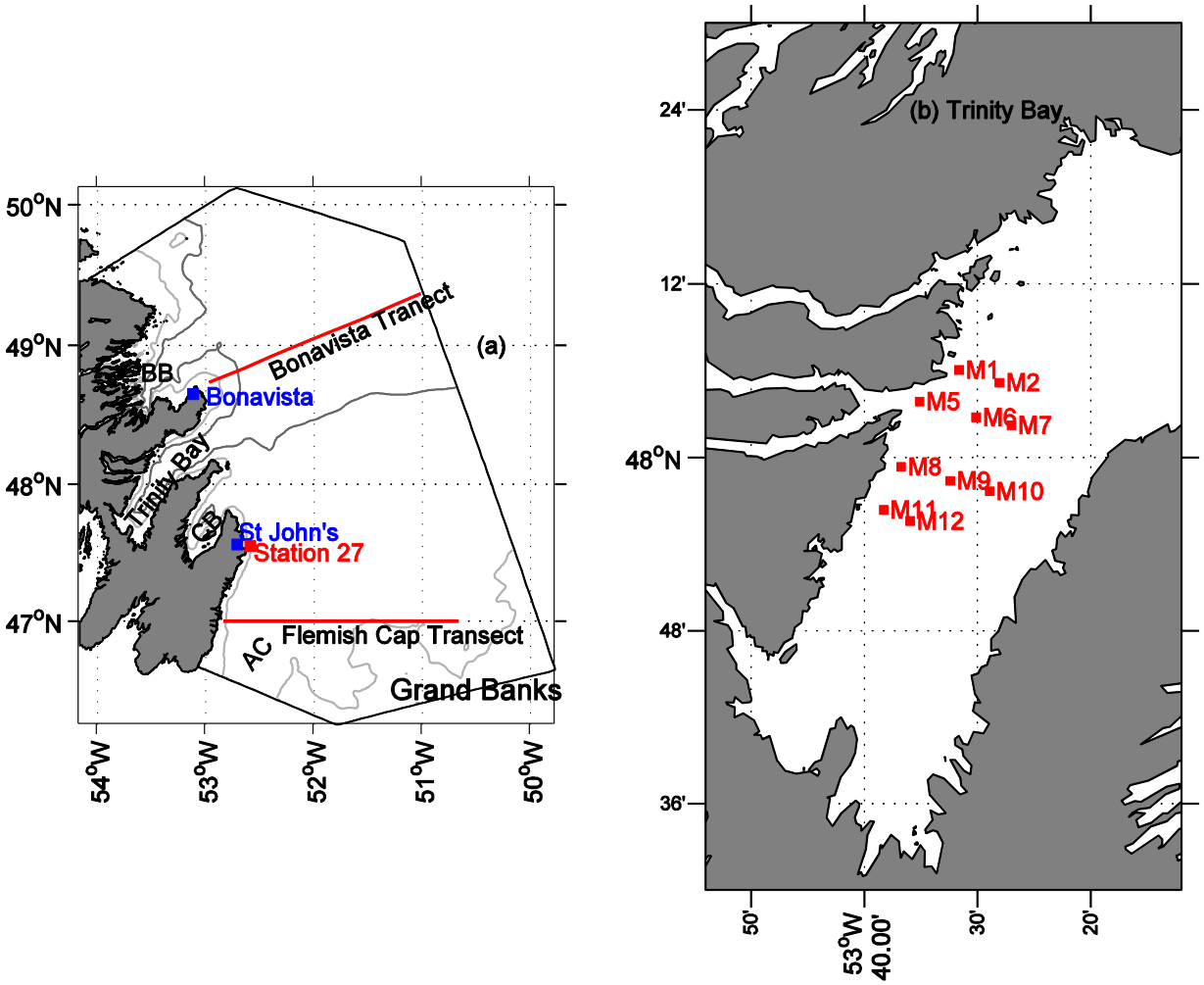

Fig. 5-1: (a) Map showing model domain including 100 and 200 m isobaths (grey line). AC is Avalon Channel. BB is the Bonavista Bay and CB is the Conception Bay. (b) Trinity Bay, with mooring stations in red squares.

Modeling studies off the eastern Newfoundland coast are mainly focusing on the dominant Labrador Current and its seasonal variability of volume transport (Greenberg and Petrie, 1988; Tang et al., 1996; Han, 2005; Han et al., 2008; Han et al., 2011). Over this area, the inshore Labrador Current flows past Bonavista Bay and has a current separation near the mouth of Trinity Bay (Han et al., 2011). One part of the inshore branch flows offshore joining the shelf-edge Labrador Current and the remaining current

follows the coast on its pathway through Avalon Channel. Davidson et al. (2001) used a simple numerical model for Trinity Bay with several sensitivity cases, and their idealized results show two anti-cyclonic gyres at the surface in Trinity Bay with the addition of nonlinear terms to the model. The circulation in Conception Bay was initialized with a simple ocean model by deYoung et al. (1993a). These authors developed a diagnostic circulation model for Conception Bay and concluded that the bay has no single dominant circulation patterns, indicating highly dynamical circulation, variable wind-forced currents. deYoung et al. (1993b) also investigated the wind-forced responses of Conception Bay using a reduced-gravity model, showing the influence of neighbouring Trinity Bay on the internal response of Conception Bay.

Previous model results and observations revealed the dominant inshore Labrador Current over the eastern Newfoundland coast, together with weak, eddy-like circulation inside Trinity Bay and Conception Bay. However, our knowledge of coastal upwelling and associated stratification evolution is limited in this area. The wind-driven coastal upwelling has been studied in other areas for decades due to its role in forcing biological productivity (Smith, 1995; Gan and Allen 2002; Lentz and Chapman, 2004; Ma et al., 2012; Chen et al., 2012). Thus, in this study, we will describe the application of a 3-D, prognostic finite-volume ocean model (FVCOM, Chen et al., 2004) to the eastern Newfoundland coast including three embayments. Our first goal is to validate the model results as the first time FVCOM application in this area. The main purpose is to examine the seasonal variability of temperature and circulation and to investigate the wind induced coastal upwelling and associated stratification change. The arrangement of the paper is as follows. In section 5.3, we will describe the model setup, boundary conditions, forcing

data and initial conditions. In section 5.4, we will evaluate model against observations over the east Newfoundland coast including Trinity Bay. In section 5.5, we will examine surface bay circulation and the upwelling along the coast, discussing its seasonal and spatial change and the evolution of the stratification. Finally, in section 5.6, we will present a summary and the conclusions.

5.3 Model Configuration

5.3.1 FVCOM model (Version 3.1)

Combining two advantages of horizontal grid flexibility and computational efficiency, the FVCOM model used in this study integrates independent variables through individual unit control volumes. The model is solved numerically by determining the flux through the volume boundaries to guarantee the horizontal conservation of mass and momentum. A time-splitting method is used for computational efficiency including an internal mode and an external mode constrained by its Courant-Friedriches-Levy (CFL) condition. For a more accurate estimation of sea level, currents, and salinity and temperature fluxes, all variables except currents are placed at nodes, while currents are placed at centroids. Previous work (Weisberg and Zheng, 2006; Resio and Westerink, 2008; Rego and Li, 2010; Han et al., 2011; Ma et al., 2012; Ma et al., 2015) has successfully demonstrated the advantage of FVCOM in simulating the physical environment around coastal shelf and embayments.

5.3.2 Model Domain

The model domain is from 46.2 ^{o}N to 50 ^{o}N and 50 ^{o}W to 54 ^{o}W (Fig. 5-1). The domain includes a portion of the Grand Banks on the southern end. Trinity Bay is a long (~100 km) and narrow (~30 km at the mouth) bay. The bay is wide compared with the internal Rossby radius (~1-10 km) but narrow relative to the external Rossby radius (~500 km) (deYoung et al., 1995). The model bathymetry is mainly derived from the multi-beam bathymetry of the Canadian Hydrographic Service. To minimize the pressure gradient errors (Mellor et al., 1993), the bathymetry has been smoothed with volume conserved method (Ma et al., 2012). The governing equations of the model are solved on an unstructured triangular grid whose spacing is largest (3-5 km) along the open boundary and smallest (50 m) along the coastline of the inner bay (Fig. 5-2). There are 31 unequally spaced levels in the vertical, with a minimum spacing of 0.1 m near the sea surface and seabed for 100 m water depth in order to resolve the near surface shear current and thermodynamic process near surface and bottom. The model equations are solved using an integration step of 0.1 s for the external mode and an internal to external mode ratio of 10.

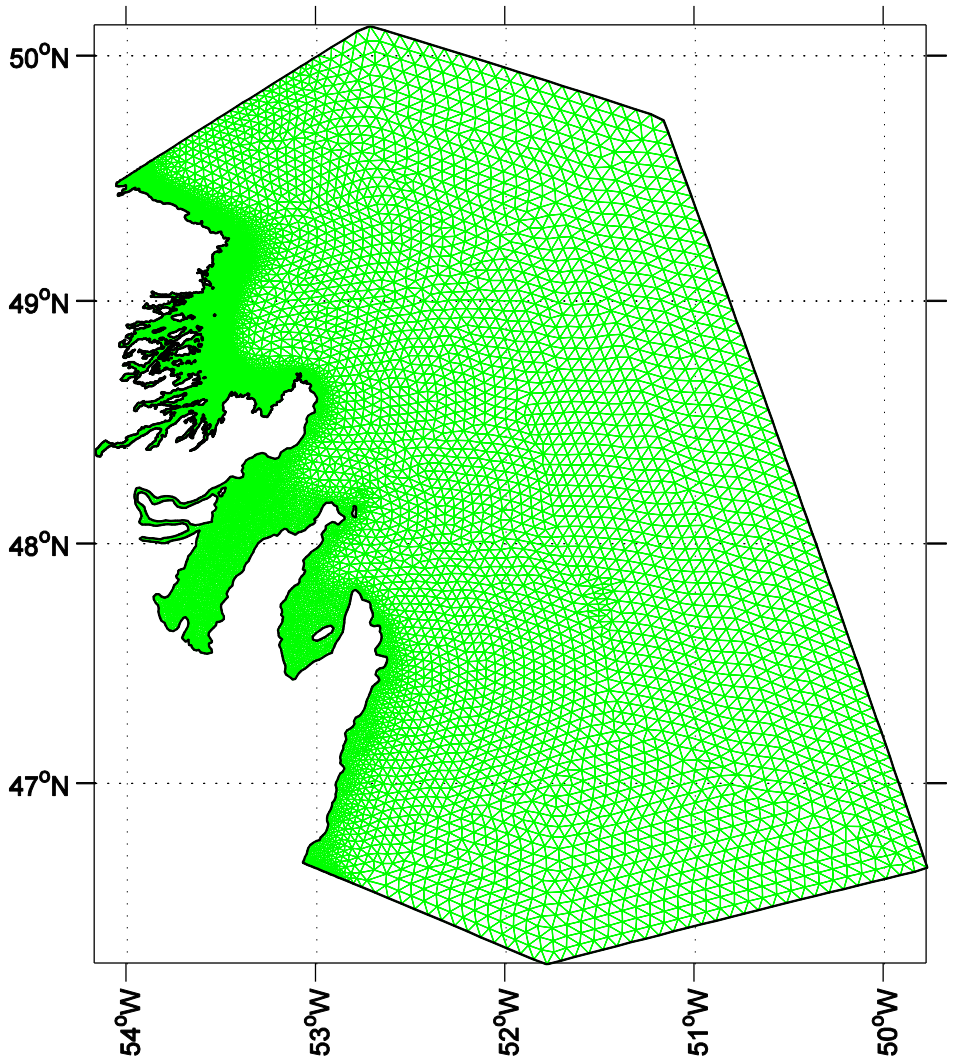

Fig. 5-2: The horizontal grid used in the numerical model. The grid spacing ranges from 50 m around coast to 5 km along the open boundary.

5.3.3 Model Forcing and Initial Conditions

The model is forced by hourly winds and heat fluxes at the sea surface and non-tidal sea levels, temperature and salinity at the lateral open boundaries. Surface salinity is restored to monthly climatology. We use wind speed and direction from local weather station at St.John's from Environment Canada. Heat fluxes, including shortwave

radiation, longwave radiation, latent heat flux and sensible heat flux, were calculated based on Environment Canada's meteorological data and the spatially variable sea surface temperature from a monthly-mean temperature climatology (Geshelin et al., 1999). The surface shortwave heat flux was calculated using the formulations of Curry and Webster (1998). A revised equation from Li et al. (2006) was used to calculate the albedo, including the white cap effect (Monahan and MacNiocaill, 1986); modified code from the Tropical Ocean and the Global Atmospheric Program (TOGA)-Coupled Ocean Atmospheric Response Experiment (COARE) (Fairall et al., 1996) was used to calculate the sensible and latent heat fluxes. The formulation of Fung et al. (1984) was used to estimate longwave radiation based on Geshelin et al.'s (1999) sea surface temperature and the observed air temperature, dewpoint temperature, cloud cover and wind speed. Then net heat flux was calculated from these four heat flux components.

Monthly non-tidal sea levels at the lateral open boundaries are obtained from a Newfoundland Shelf model (Han et al., 2011). The temperature and salinity along the open boundaries are also extracted from the same model. The shelf model output is interpolated hourly and specified along the open boundaries. The Newfoundland Shelf model reproduced the inshore Labrador transport well.

The sea level and velocity are initialized from the May climatology case for the computational domain to reduce the ramp-up time. The initial temperature and salinity condition are generated the same way.

The model is run from year day 120 to 255 in 2000 and 2001. The model results from day 142 to 255 are compared with observed results and used for this analysis. Ma et al. (2012) demonstrates that 20 days are enough for spin-up in such a small region.

5.4 Validation Metrics

To evaluate the model solutions quantitatively, we compare the model solutions with various measurements. In addition to the root-mean-square (RMS) difference, we examine the velocity difference ratio (VDR) defined as the ratio of the sum of the squared magnitudes of the vector velocity differences to the sum of the squared magnitudes of the observed velocities, that is,

$$VDR = \sum |V_m - V_o|^2 / \sum |V_o|^2 \tag{5-1}$$

where V_m is the horizontal model velocity and V_o is the horizontal observational velocity. Lower VDR values indicate better agreement, with $VDR = 0$ being exact agreement. Another is the speed difference ratio (SDR) defined as the ratio of the sum of the squared speed difference to the sum of the squared magnitudes of the observed velocities, that is,

$$SDR = \sum (|V_m| - |V_o|)^2 / \sum |V_o|^2 \tag{5-2}$$

The third index is γ^2 defined as followes:

$$\gamma^2 = \frac{\mathrm{VAR}(\zeta_o - \zeta_m)}{\mathrm{VAR}(\zeta_o)} \tag{5-3}$$

where VAR is the variance, ζ is the sea level; o and m represent the observation and model.

The fourth index is the correlation coefficient (R) between the model and observational components.

5.4.1 Validation of Non-tidal Water Levels, Currents and Transport

Hourly model water levels at the St. John's station (Fig. 5-1) are compared with tide-gauge observations. Observed water level data are detided with the T-tide toolbox (Pawlowicz et al., 2002). The comparisons of modelled hourly sea level anomaly (SLA) with mean sea level removed are shown in Fig. 5-3. The wind vectors at St. John's are also shown with the sea level variability. Simulated results agree well with observed water levels at St. John's not only for the seasonal variability but also for wind-induced high frequency fluctuations. Both modelled and observed sea level anomalies range between -0.2 and 0.2 m.

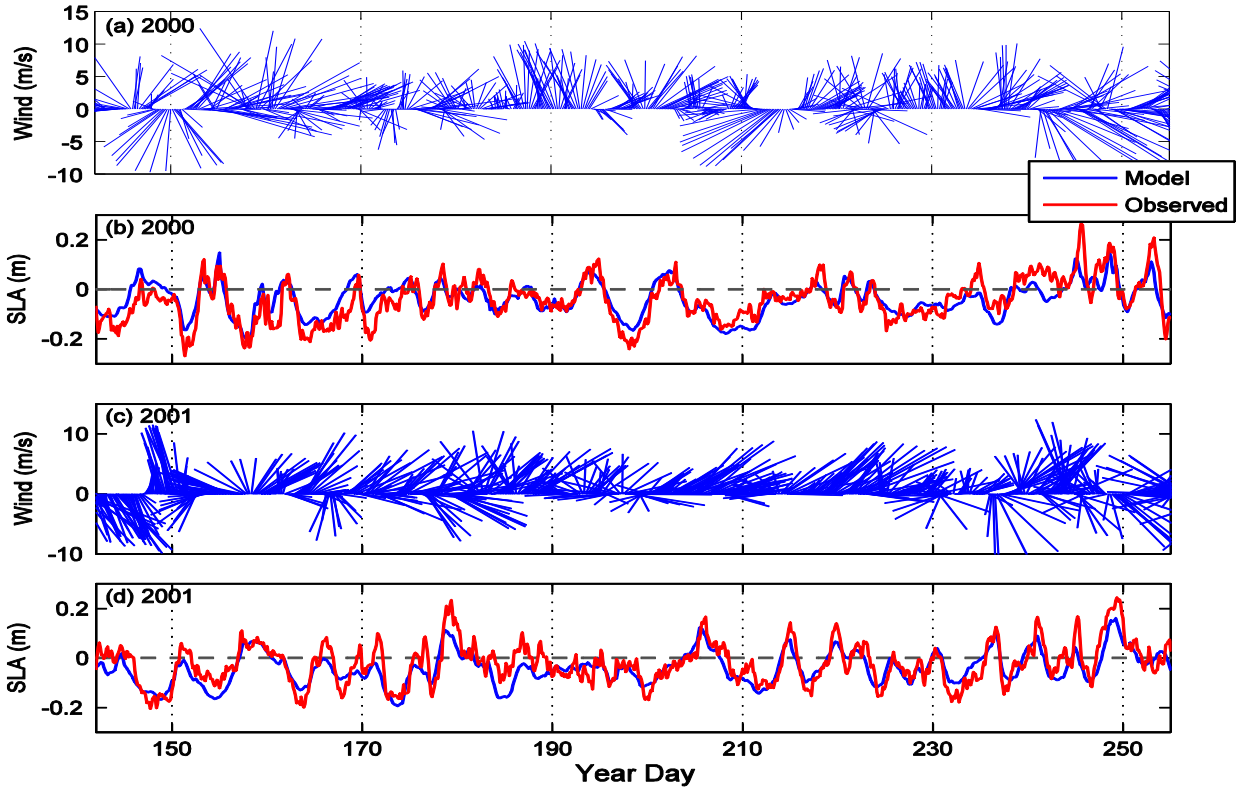

Fig. 5-3: Time series of (a) wind vectors at St. John's in 2000, (b) sea level anomalies at St. John's in 2000, (c) wind vectors at St. John's in 2001 and (d) sea level anomalies at St. John's in 2001. Black dashed line indicates the zero.

Quantitative comparisons are also made using the hourly time series data (Table 5-1). By using the RMS difference, correlation and γ^2, statistics are calculated to determine the model's ability in reproducing observed sea level. The averaged RMS difference and the correlation coefficient between the observed and modelled sea levels are 5.5 cm and 0.81 respectively, demonstrating good agreement for both magnitude and variability. For detailed evaluation of the model performance in producing observational variability, γ^2 is calculated. The index γ^2 is 0.38 and 0.28 in 2000 and 2001, indicating a good overall comparison that is better in 2001.

Table 5-1: Statistics from the comparison between the observed and model non-tidal sea level anomalies at the St. John's station in 2000 and 2001. See Fig. 5-1 for location. RMSD: root-mean-square difference.

	2000	2001
RMSD(cm)	5.6	5.3
Correlation	0.82	0.79
Observed RMS (cm)	9.1	10.0
γ^2	0.38	0.28

The de-tided vessel-mounted ADCP current data from the Flemish Cap transect on July 15-17, 2000 are from Han et al. (2008). The simulated currents are gridded onto the same positions as the observational data. There is reasonable agreement between the present model results and the ADCP observations, in terms of the spatial distribution pattern and the current strength for the southward inshore Labrador Current along the

coast (Fig. 5-4). The RMS difference is 6.6 and 7.0 cm/s for the eastward and northward components, respectively (Table 5-2). The speed difference ratio (SDR) and the velocity difference ratio (VDR) accounting for both the eastward and northward components are 0.2 and 0.6, suggesting good agreement in velocity magnitude and direction. The transport associated with the inshore Labrador Current was calculated from the coast to 100 m depth on the Grand Banks side of the Avalon Channel (AC in Fig. 5-1), the same segment as in Han et al. (2008). Fig. 5-5 shows the calculated transport for the inshore Labrador Current at 2000 and 2001. The mean transport is 0.37 and 0.27 Sv for 2000 and 2001 respectively, consistent with the estimation of 0.39 Sv (Greenberg and Petrie, 1988) based upon summer current meter data. The modelled inshore transport is relatively steady from May to September, with occasional strong transport events in September and even some reversals (Fig. 5-5).

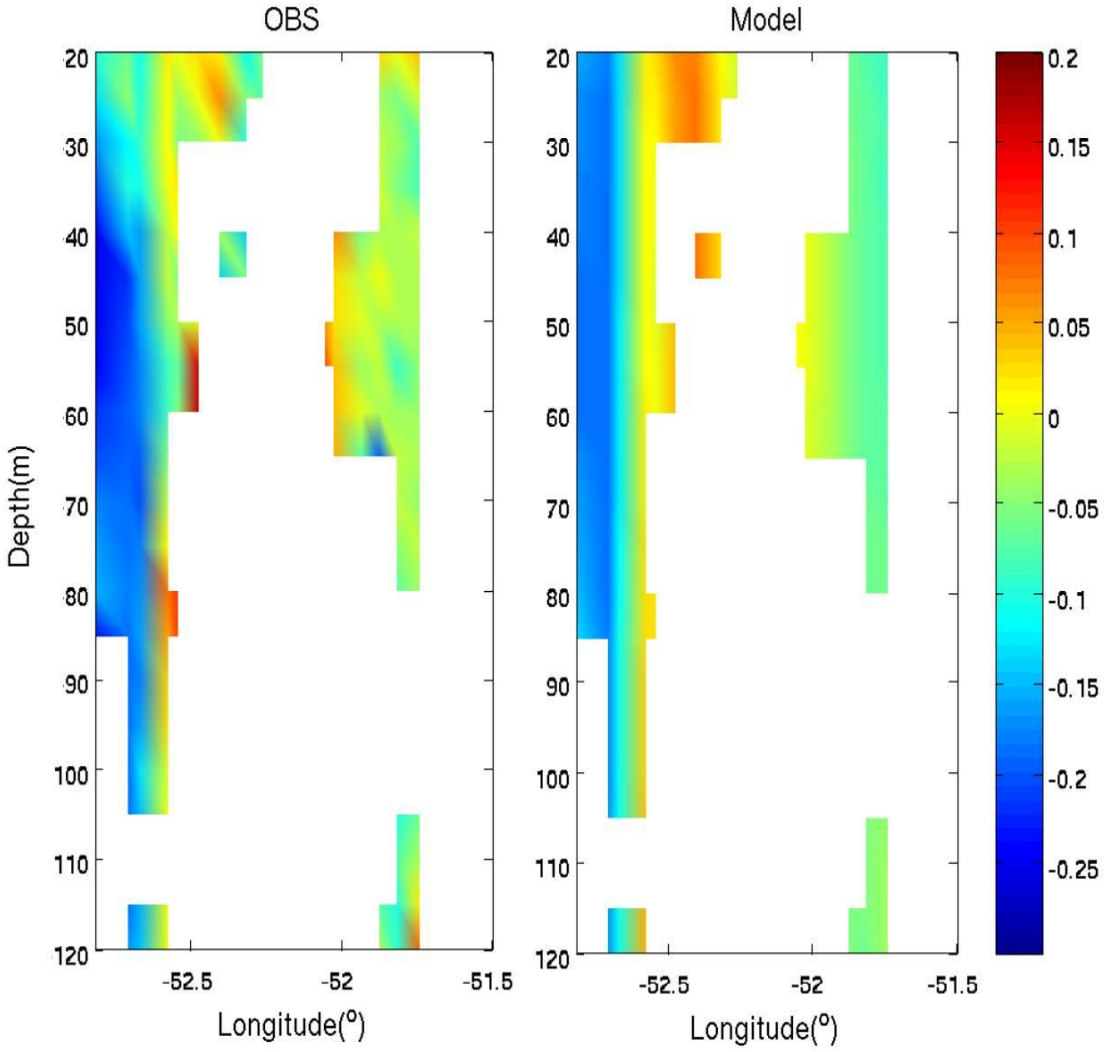

Fig. 5-4: Comparison between the vessel-mounted ADCP data and model currents along the Flemish Cap transect on July 15-17, 2000. Only the normal component (in m/s, positive northward) is shown.

Table 5-2: Statistics from the comparison between observed and model non-tidal currents along the Flemish Cap Transect in July, 2000. See Fig. 5-1 for the transect location. U is the eastward current and V is the northward current.

	U	V
RMS D (cm/s)	7.5	6.4
Observed RMS (cm/s)	6.3	10.8
Correlation	0	0.76
SDR	0.2	
VDR	0.6	

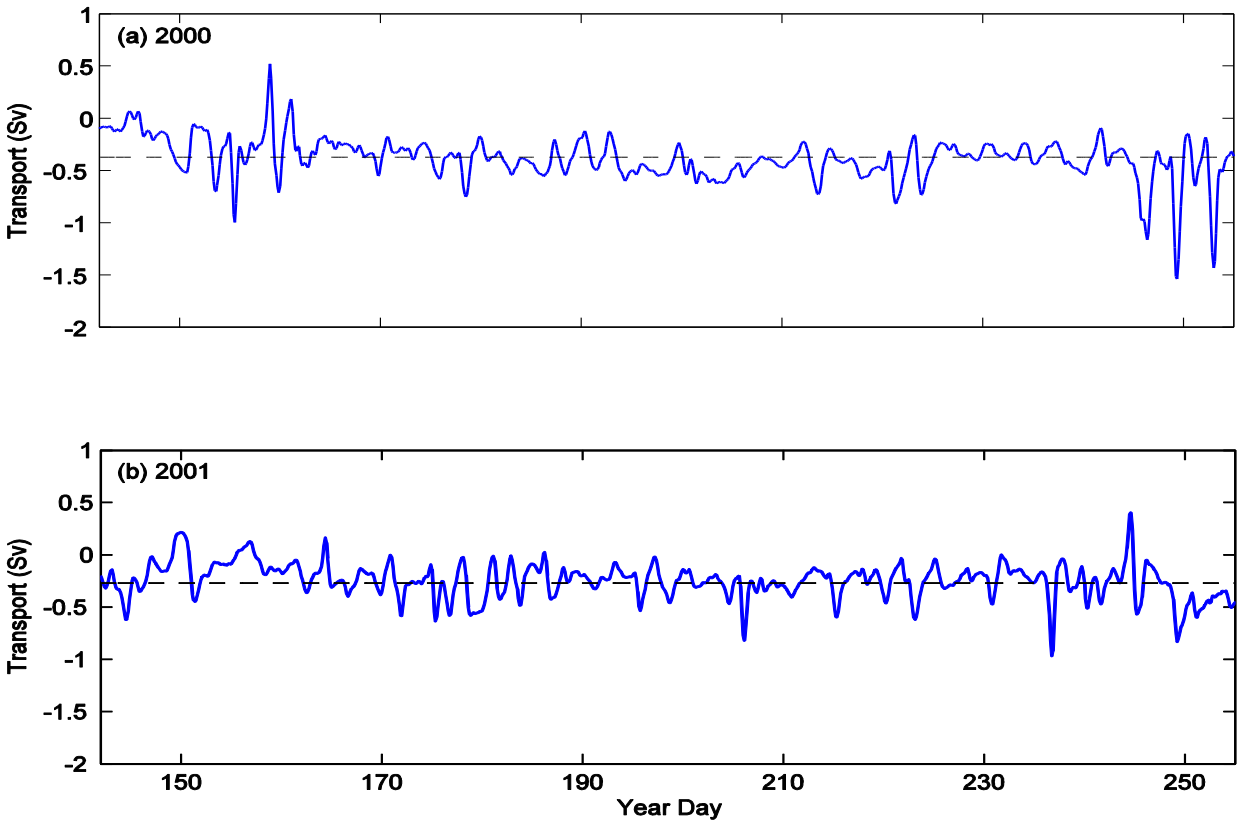

Fig. 5-5: Time series of the inshore Labrador Current volume transport at the Flemish Cap Transect (47^{o} N) in (a) 2000 and (b) 2001. The mean transport for the modelling period is also depicted (black dashed).

5.4.2 Evaluation of Hydrograph at Station 27

Station 27 (of Fig. 5-1) is located off St. John's at 47.55^{o} N and 52.59^{o} W, with a water depth of 176 m. Hydrographic data have been collected at Station 27 since 1946. Since the late 1990s, temperature and salinity data at Station 27 have regularly been collected by the Northwest Atlantic Fisheries Centre through the Atlantic Zone Monitoring Program (AZMP) of Fisheries and Oceans Canada (www.Meds-sdmm.dfo-mpo.gc.ca/isdm-gdsi.azmp-pmza/index-egn.html). The weekly data from May to September in 2000 and 2001 are used to evaluate the model. The surface layer temperature has strong seasonal variability, increasing from $4^{o}C$ in spring to $14^{o}C$ by late summer (Fig. 5-6, a and b). The modelled surface temperature from day 180 to 200 in 2000 shows a significant $4^{o}C$ drop associated with coastal upwelling, which is not clearly observed but consistent with observations available. The observed bottom temperature at Station 27 shows an increasing trend from $-1^{o}C$ to $2^{o}C$, primarily due to the accumulated heat flux during summer (Fig. 5-6, c and d). The simulated temperature reproduces approximately observational temperature at different depths, with an averaged RMS errors of $1.1^{o}C$ and $1.3^{o}C$ in 2000 and 2001, respectively (Table 5-3).

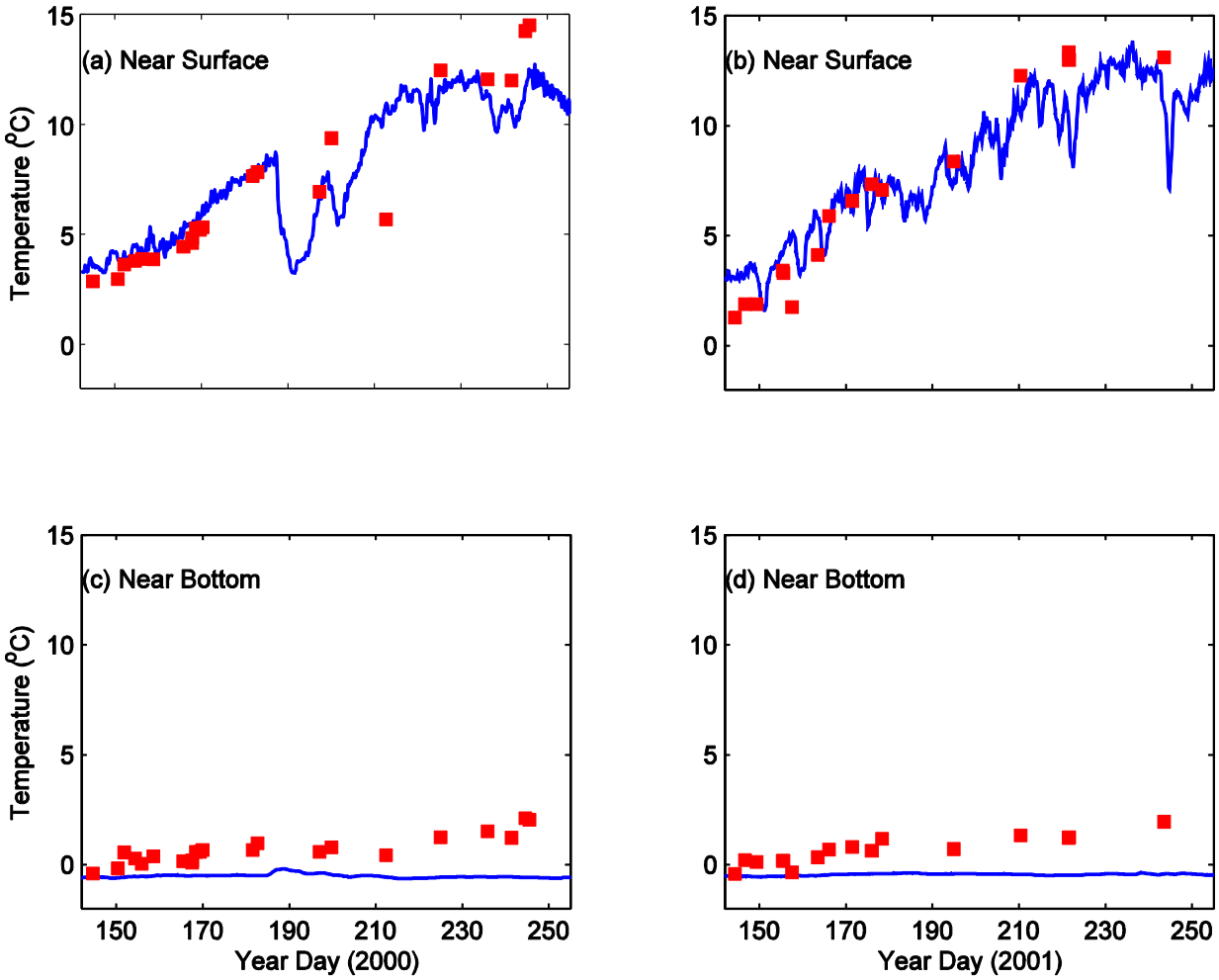

Fig. 5-6: Observed (red square) and model (blue) temperature at stations 27 for (a) near surface in 2000, (b) near surface but in 2001, (c) near bottom in 2000 and (d) near bottom but in 2001.

Table 5-3: Statistics from the comparison between observed and model temperature at Station 27 in 2000 and 2001. See Fig. 5-1 for the location.

	2000		2001	
	Temperature (^{o}C)		Temperature (^{o}C)	
	RMS difference	Observed RMS	RMS difference	Observed RMS
Surface Layer	1.6	7.5	1.8	7.9
Middle Layer	0.5	1.1	0.5	1.0
Bottom Layer	1.3	0.9	1.5	1.2

To further evaluate the vertical structure at Station 27, Fig. 5-7 shows the vertical temperature profiles in different months in 2000 and 2001. In early summer, the surface temperature is cold at around $4^{o}C$. With intensified heat flux over the summer, the surface temperature increases to $14^{o}C$ by September. The surface temperature in 2001 is warmer than that in 2000. Water below 70 m was nearly well mixed with temperature less than $0^{o}C$. The mixed layer depth is generally shallow (within 10 m) both in observation and model results, indicating the strong stratification during summer. The simulated temperature reasonably reproduces the observed temperature structure. Although the model temperature under-estimates the observed temperature at the surface in June and over-estimates in September, the model has overall good performance. Statistics for vertical profiles in four months are shown in Table 5-4. The averaged RMS difference is

1.1°C and 1.8°C for 2000 and 2001, respectively. The differences are larger in September than in June.

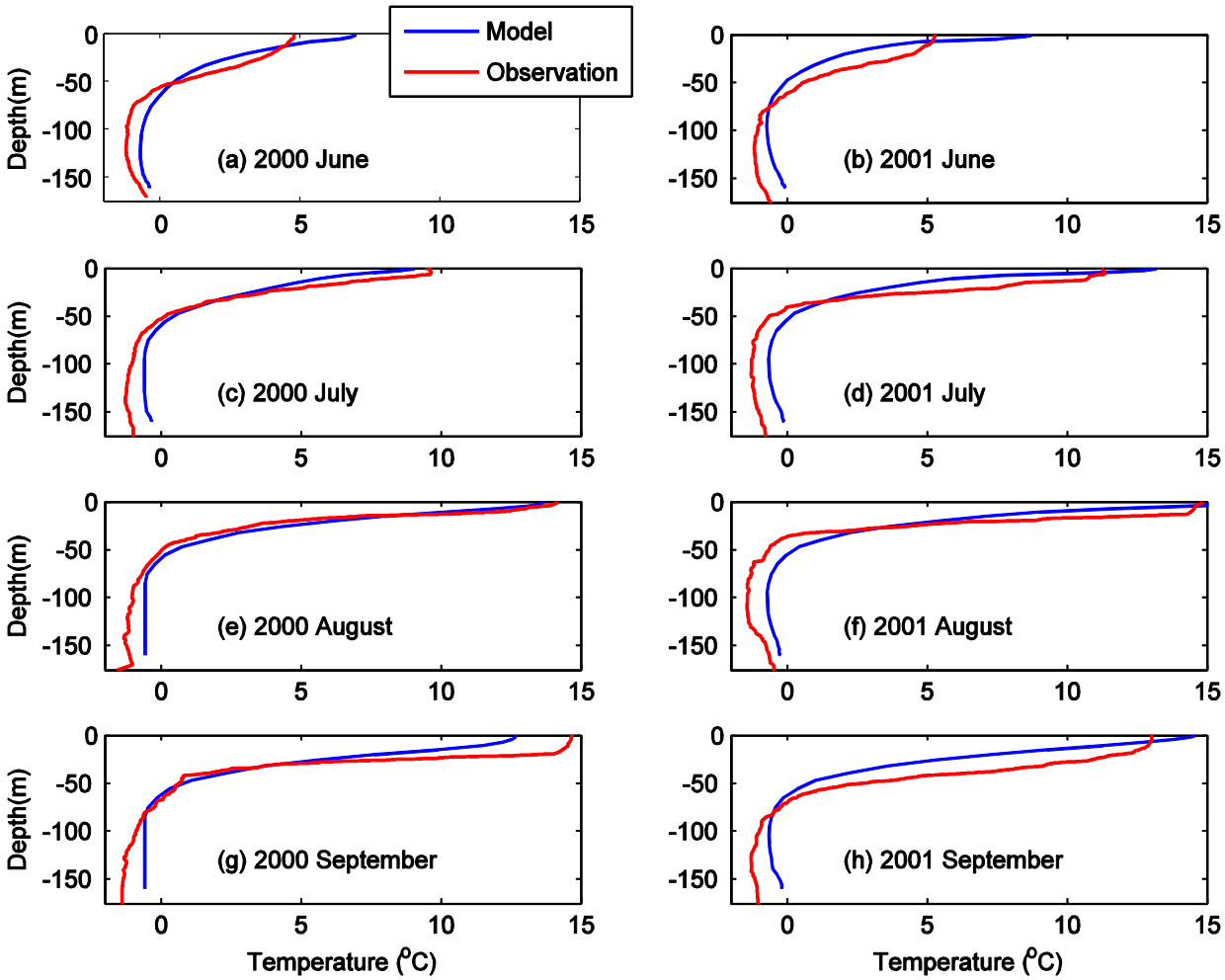

Fig. 5-7: Monthly mean vertical temperature profiles at Station 27 in (a) June, 2000, (b) June, 2001, (c) July, 2000, (d) July, 2001, (e) August, 2000, (f) August, 2001, (g) September, 2000 and (h) September, 2001.

Table 5-4: Statistics from the comparison between observed and model monthly-mean vertical temperature profiles at Station 27 in 2000 and 2001. See Fig. 5-1 for the locations.

	2000		2001	
	Temperature (^{o}C)		Temperature (^{o}C)	
	RMS difference	Observed RMS	RMS difference	Observed RMS
June	0.9	2.6	1.5	2.9
July	1.0	4.6	1.7	5.5
August	0.7	6.3	1.8	7.1
September	1.8	7.7	2.1	7.3

5.4.3 Comparison of hydrograph over Transects

Fisheries and Oceans Canada also regularly collects hydrographic data along the Bonavista and Flemish Cap Transects (of Fig. 5-1). The observed data are from July 15 to 19. Fig. 5-8 presents the temperature distribution along the Bonavista Transect from the model and the observation for 2000 and 2001. There is a sharp thermocline at 30 m, with a well mixed surface layer. The model underestimates the mixed-layer depth. Both the model and the observations show a cold water layer, nearly $0^{o}C$, extending from 30 m to 250 m with relative warm water around $3^{o}C$ from 250 m to bottom. Fig. 5-9 shows the temperature in both years along the Flemish Cap Transect. Modelled temperature shows a fair comparison with observations in the vertical, but with an underestimated mixed-layer depth. It should be noted that our model results reproduced cold surface temperature associated upwelling well near the coast (Fig. 5-9) for this transect, especially in 2000.

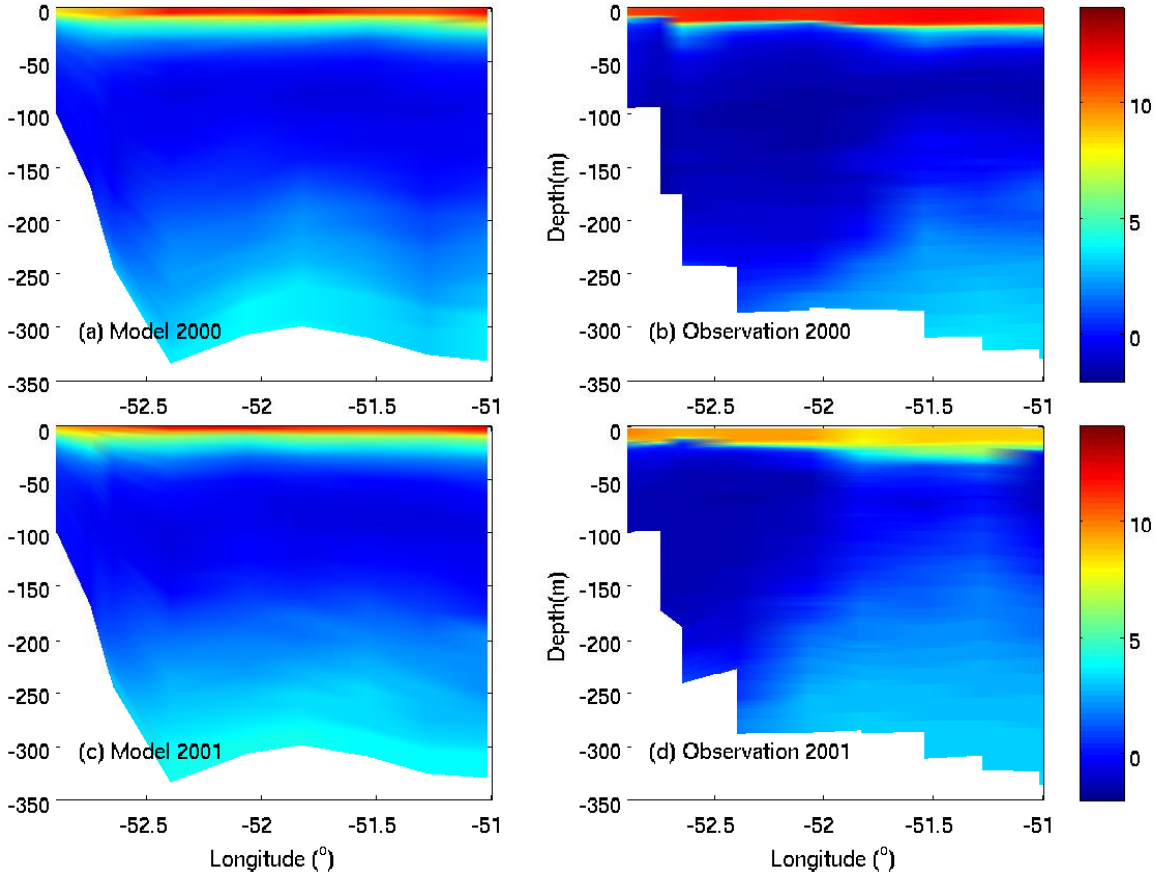

Fig. 5-8: Observed and model temperature (^{o}C) along the Bonavista Transect in 2000 and 2001.

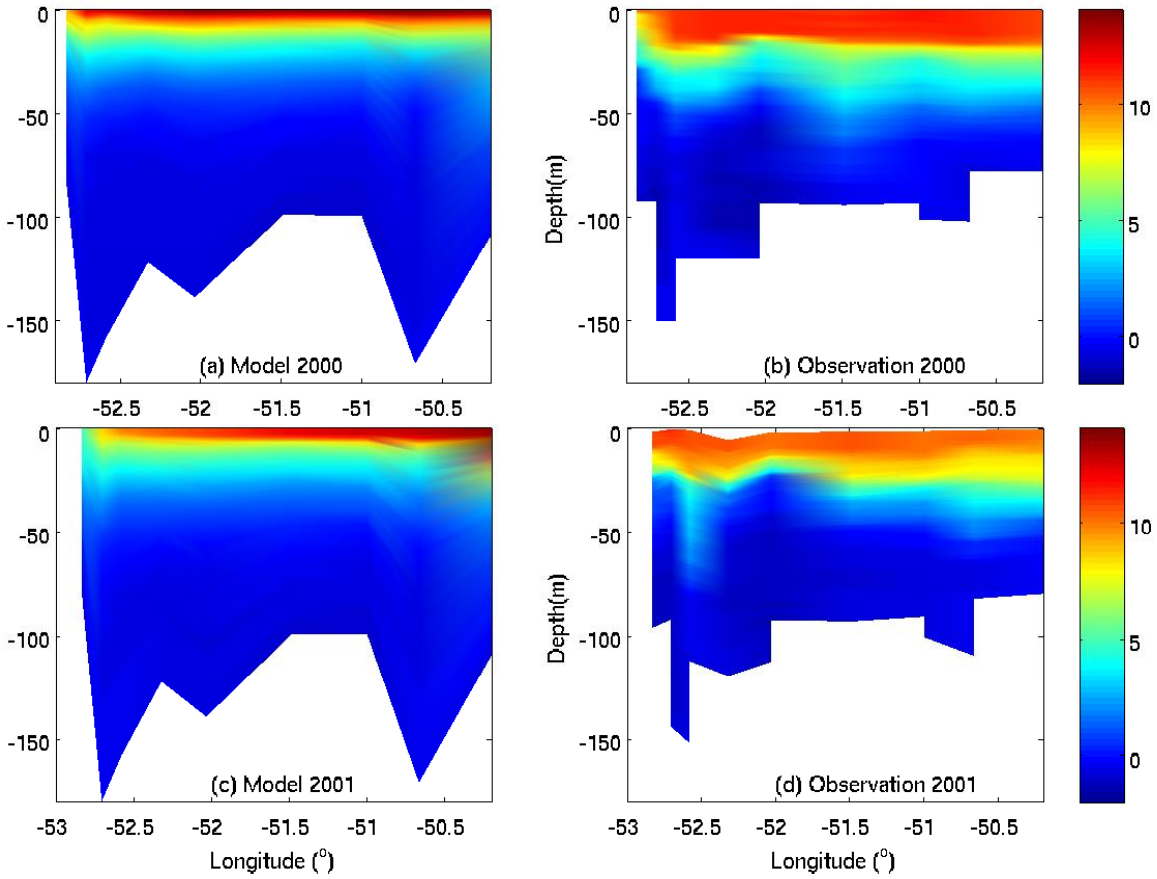

Fig. 5-9: Observed and model temperature (^{o}C) distribution along the Flemish Cap Transect in July, 2000 and 2001.

We apply statistical analyse to quantify the model performance (Table 5-5). To better evaluate the model temperature at different depths, transects were divided into three groups, the upper layer from surface to 20 m, the bottom layer within 20 m of the bottom, and the rest of the water column as the middle layer. The averaged model-observation temperature differences for the upper, middle and bottom layers are -1.3^{o}C , 1.1^{o}C , 0.9^{o}C and -0.9^{o}C , 0.7^{o}C , 1.2^{o}C along the Bonavista Transect for 2000 and 2001, indicating a colder temperature at the surface and warmer temperature below the surface in the model. The averaged temperatures in the three layers also

indicate the cold water at the middle depth of this transect. For the Flemish Cap Transect, the model-observed temperature differences are $-2.1^{o}C$, $-0.6^{o}C$, $-0.1^{o}C$ and $-2.2^{o}C$, $-0.2^{o}C$, $0.2^{o}C$ for 2000 and 2001, respectively. The model and observed temperatures agree well below the upper layer.

Table 5-5: Statistics from the comparison between observed and model temperature along Bonavista and Flemish Cap Transect. See Fig. 5-1 for the location.

	2000		2001	
Bonavista Transect	Averaged Temperature (^{o}C)		Averaged Temperature (^{o}C)	
	Model	Observed	Model	Observed
Upper Layer (0-20m)	7.3	8.6	6.8	7.7
Middle Layer	0.9	-0.2	1.0	0.3
Bottom Layer (20 m within bottom)	2.5	1.6	3.0	1.8
	2000		2001	
Flemish Cap Transect	Averaged Temperature (^{o}C)		Averaged Temperature (^{o}C)	
	Model	Observed	Model	Observed
Upper Layer	7.6	9.7	7.3	9.5
Middle Layer	0.6	1.2	0.7	0.9
Bottom Layer	-0.5	-0.4	-0.5	-0.7

5.4.4 Temperature in Trinity Bay

The modelled temperatures in Trinity Bay are evaluated against mooring data (Tittensor et al., 2002a) from May 21, 2001 to August 21, 2001. Ten thermistors measuring the water temperature were deployed (see Fig. 5-1). The data were sampled every 20 min. Both the model and observations are filtered with a 36 hour low-pass filter to remove the tidal effect and noise in the observations. Fig. 5-10 shows the comparison for the moorings M1, M2 and M5. The water temperature at 20 m is steady in May and June. With the increasing net heat flux toward summer, the water temperature at 20 m is increasing, with irregular temperature drops and recoveries associated with wind induced upwelling events. The water temperature at 50 m shows less variability with relatively steady temperature around $0^{o}\mathrm{C}$. The model has weakness in reproducing the temperature drop and recover at 20 m at M1 and 21 m at M5. This could be the over-mixing issue in MY-2.5 scheme that is documented in Han et al. (2011). An alternative $k-\varepsilon$ scheme can be used in the future. Fig. 5-11 shows the water temperature at 20 m and 50 m from M6, M8 and M9, together with observations at 33 m and 63 m from M7. Temperature data at 20m from M6 and M9 are missing due to instrument failure. Water temperatures at 20 m and 50 m show the same seasonal change and variability as seen in Fig. 5-10. Water temperature at 33 m and 63 m for M7 is steady around $0^{o}\mathrm{C}$. Fig. 5-12 shows the temperature comparison at 20m and 50m, but for M10, M11 and M12. Modelled water temperature reasonably captures the observed seasonal change, as well as the short-term variability. Especially at 20 m for M8 (Fig. 5-10 and 5-12), the model reproduces well the temperature decrease and increase between day 210 to 230, from $5^{o}\mathrm{C}$ to $2^{o}\mathrm{C}$ then to

$10^{o}C$. Quantitative statistics for temperature are shown in Table 5-6. The RMS differences are all within $2^{o}C$, indicating fair to good agreement with observations for temperature.

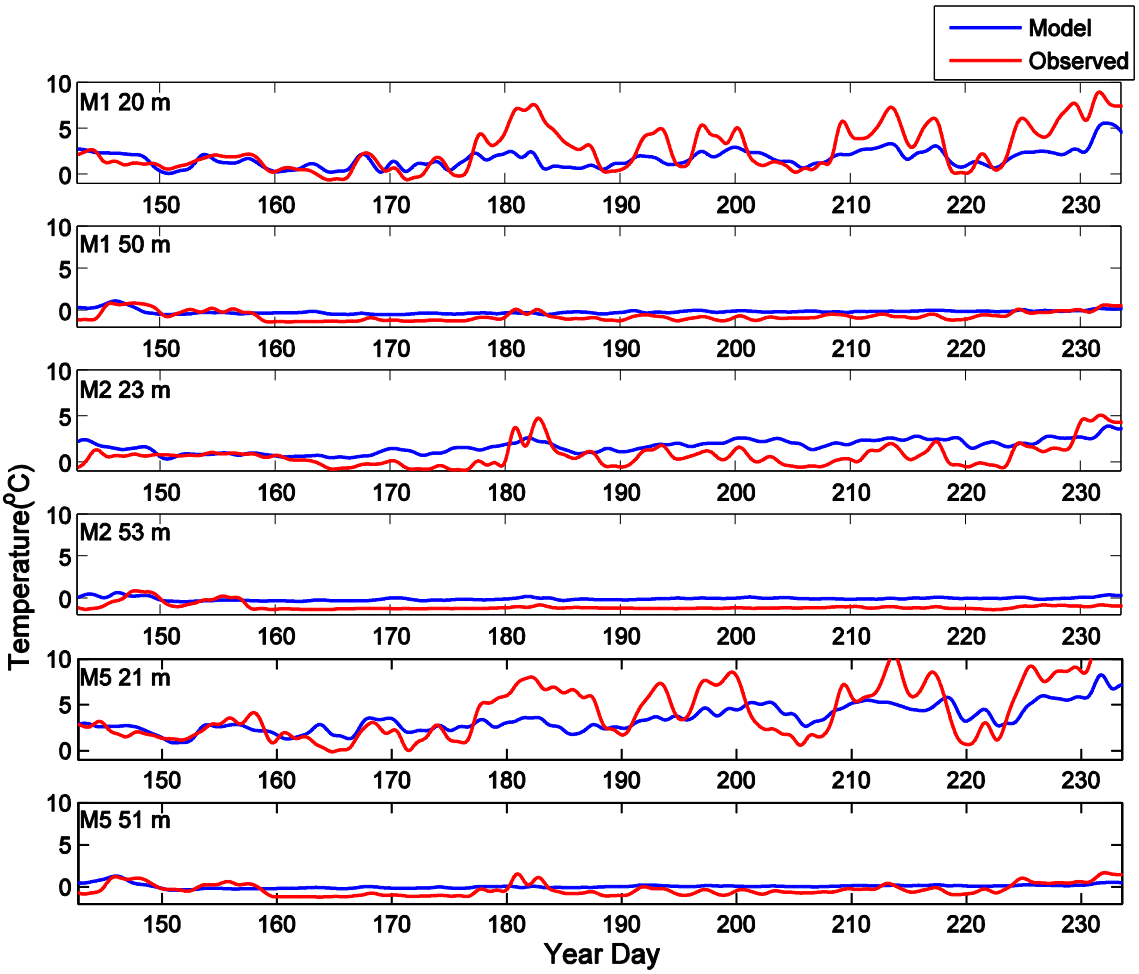

Fig. 5-10: Time series of observed (red) and model (blue) temperature (36 h low-pass filtered) at 20 m and 50 m for M1, M2 and M5.

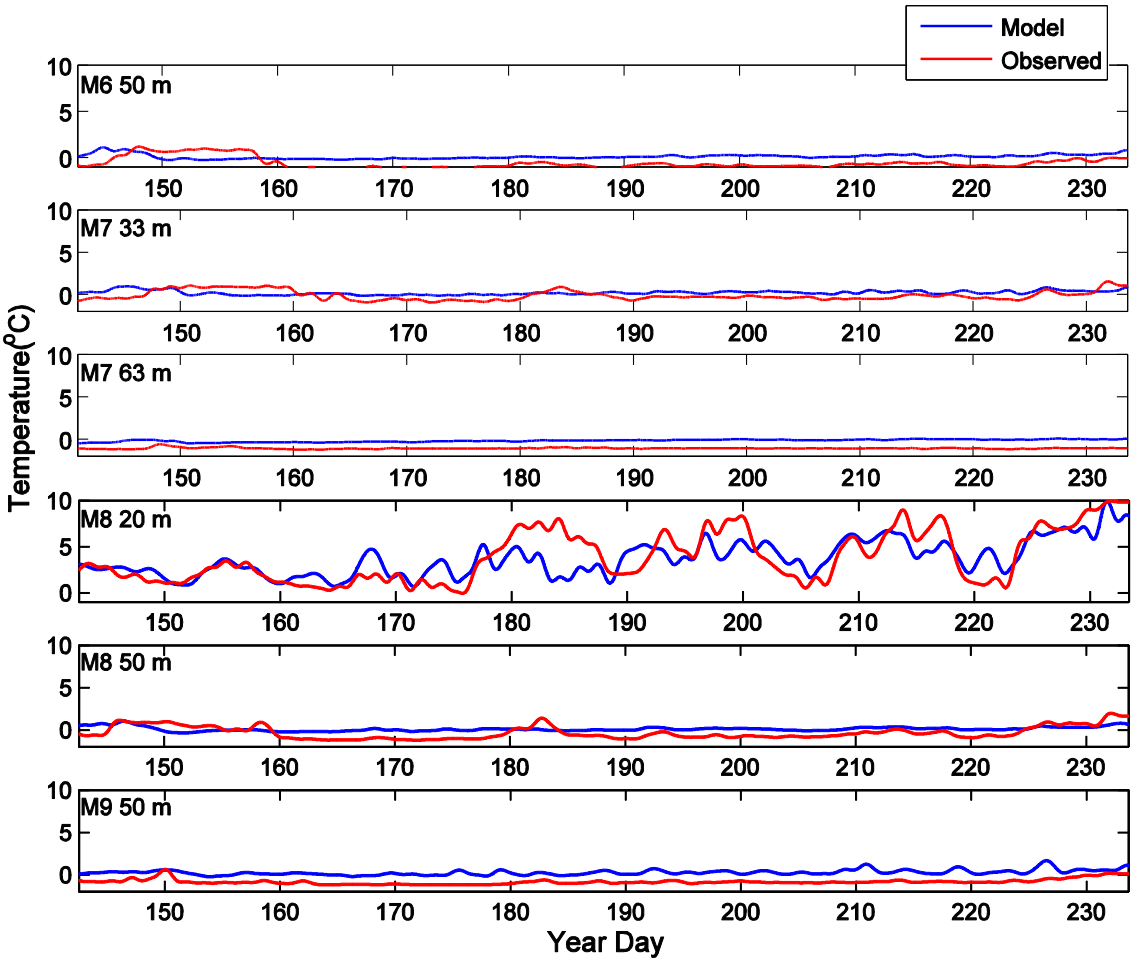

Fig. 5-11: Time series of observed (red) and model (blue) temperature (36 h low-pass filtered) at 50 m for M6, 33 m and 63 m for M7, 20 m and 50 m for M8 and 50 m for M9.

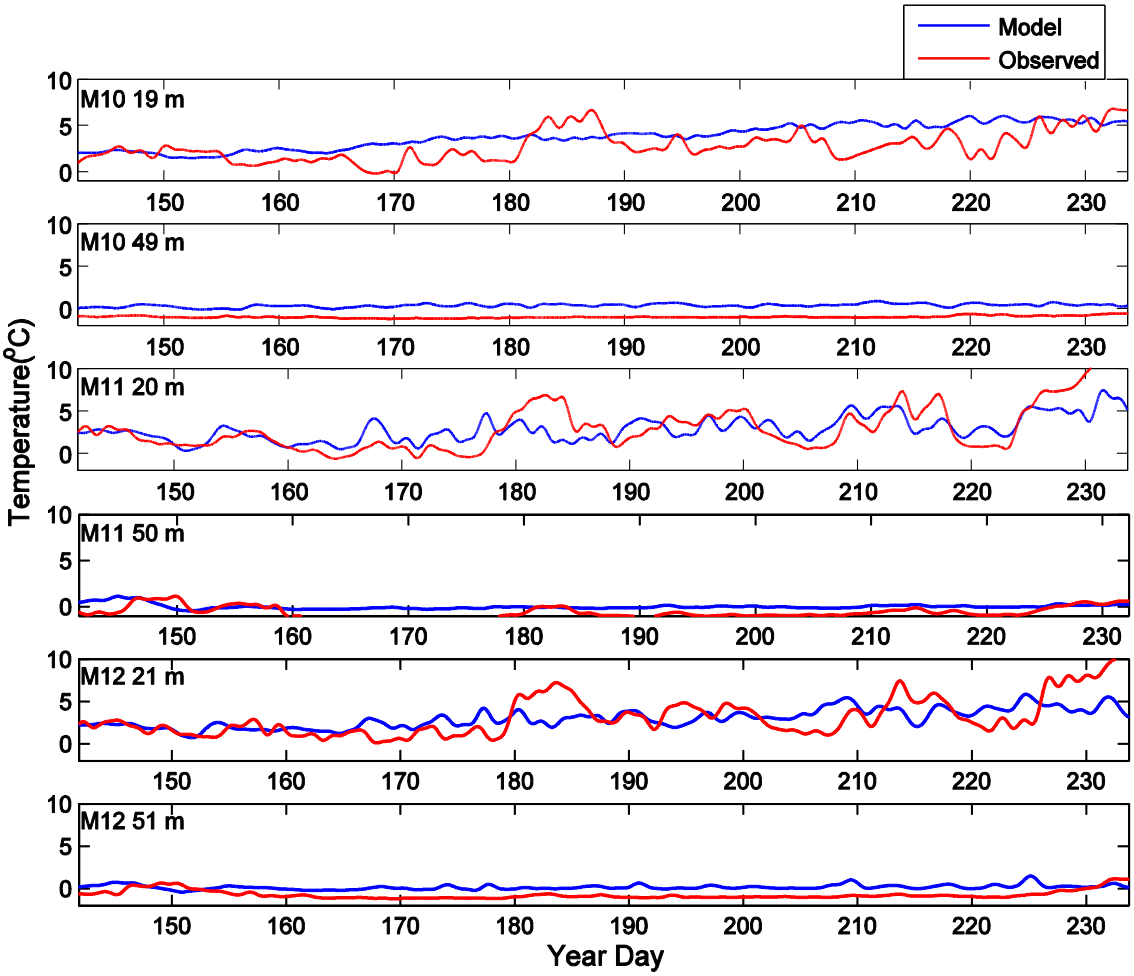

Fig. 5-12: Time series of observed (red) and model (blue) temperature (36 h low-pass filtered) at 19 m and 49 m for M10, 20 m and 50 m for M11, and 21 m and 51 m for M12.

Table 5-6: Statistics from the comparison between the observed and model temperature at M1, M2, M5, M6, M7, M8, M9, M10, M11 and M12. See Fig. 5-1b for the locations.

	Depth (m)	RMS difference (^{o}C)	RMS Observation (^{o}C)	Correlation
M1	21.5	1.9	3.6	0.7
	51.5	0.7	0.7	0.5
M2	23	1.4	1.5	0.5
	53	1.0	1.0	0.3
M5	21	2.3	2.3	0.7
	51	0.7	0.8	0.5
M6	50	0.9	0.8	0.1
M7	33	0.7	0.6	0.1
	63	0.9	1.1	0.03
M8	20	1.9	4.7	0.7
	50	0.8	0.8	0.5
M9	50	1.1	0.9	0.5
M10	19	1.8	3.1	0.5
	49	1.4	1.0	0.2
M11	20	2.0	4.1	0.7
	50	0.8	0.8	0.4
M12	21	2.0	3.9	0.5
	51	1.0	0.9	0.1

Vertical temperature profiles at M1, M10 and M11 from model and observations are shown in Fig.5-13. Both model results and observations are averaged into monthly

means (June and August, 2001). The model results agree well with the observed data. In particular, there is good agreement for the evolution of the stratification from June to August. In June, the temperature is relatively cold and below $5^{o}C$, even at the surface. In August, the surface temperature differs among these three sites. Surface temperature at M10 is $2^{o}C$ higher than at M11 and $4^{o}C$ higher than at M1 due to the coastal upwelling on the west side of the bay (see Section 5.5).

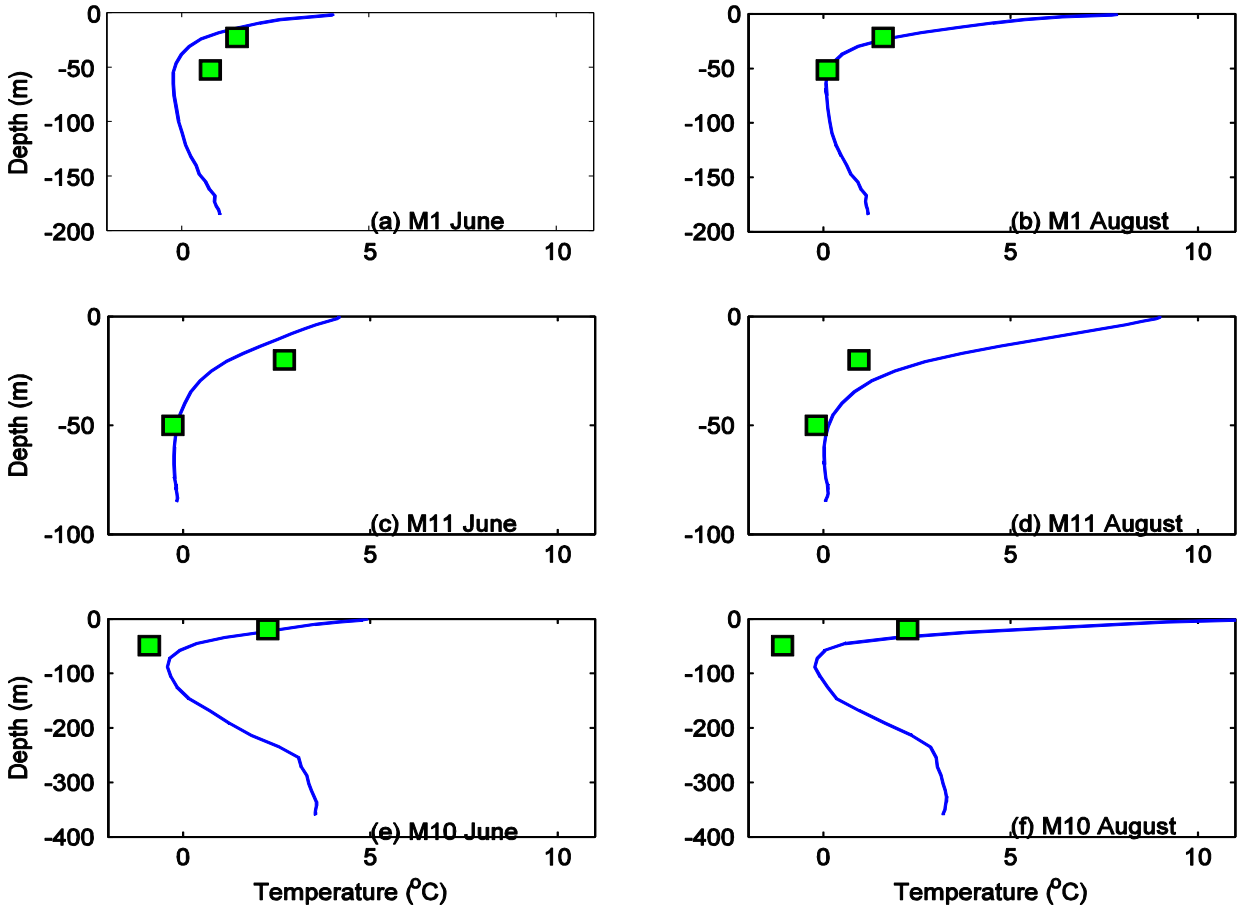

Fig. 5-13: Observed and model monthly mean vertical temperature profile at M1 in (a) June, (b) August, at M11 in (c) June, (d) August, and at M10 in (e) June and (f) August.

5.5 Circulation, Upwelling and Stratification

5.5.1 Circulation and Temperature Distribution

The model reveals two distinct surface circulation modes corresponding to difference in the wind direction from May to August for 2000 and 2001 (Fig. 5-14). Around day 150, in 2000 and around day 146, in 2001, the surface current was directed westward toward the coast in response to the northerly wind (Fig. 5-14a and c). The currents were blowing into Trinity Bay. Around day 236, 2000 and day 223, 2001, the dominant offshore surface flow was generated by a strong southwesterly wind. The circulation pattern for 2001 (Fig. 5-14 b and d) showed two eddies (Section 5.5.2).

The simulated surface temperatures were consistent with seasonal wind directions. The surface salinity was restored to the monthly mean climatology, and so the model salinity is not shown here. During May, the eastern Newfoundland coast including Trinity Bay was covered with cold water. Upwelling was weak and located on the eastern sides Trinity and Conception Bay. In contrast, when the wind turned southwesterly in the summer, the wind-induced coastal upwelling pumped low temperature water from a deeper layer up to the surface on the western side of Trinity Bay and also at Station 27 off St. John’s. A cold water front was clearly formed (Fig. 5-14 b and d).

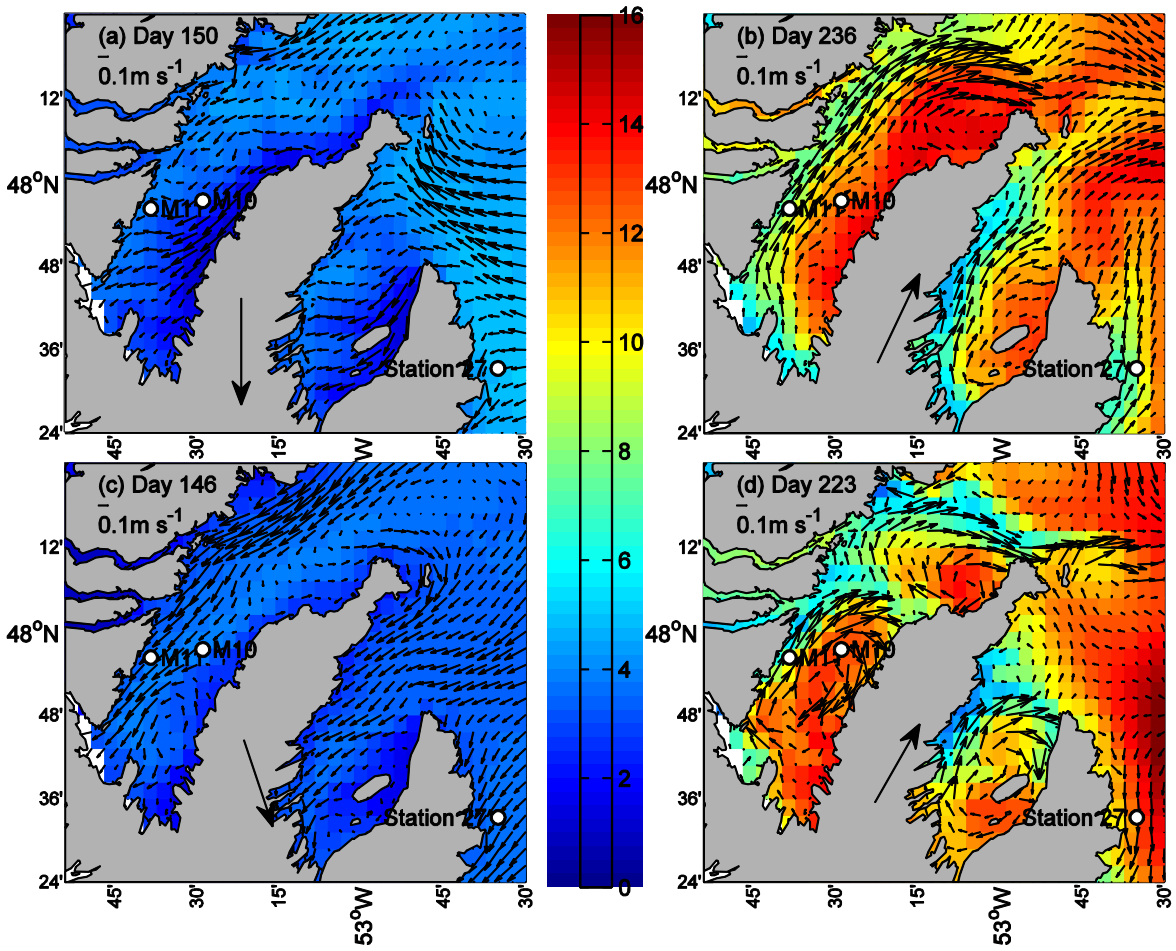

Fig. 5-14: Model surface temperature and currents distribution in Trinity Bay and neighbouring areas on (a) Day 150, 2000 with north wind, (b) Day 236,2000 with southwest wind, (c) Day 146, 2001 with northwest wind and (d) Day 223, 2001 with southwest wind. Three white circles are M11 and M10 in the Trinity Bay and Station 27.

5.5.2 Dynamics of Surface Eddies

Our model results show two persistent anti-cyclonic eddies at the surface from 20 July to 10 August, 2001, consistent with Davidson et al.'s (2001) model results. The mechanism for the eddies inside of the bay can be attributed to the geostrophy near the bay coast and wind driven Ekman drift over the gyre interior (Greatbatch and Otterson,

1991). The centre of the first eddy is located in the inner Trinity Bay, around 47.91°N - 53.55°W (Fig. 5-14d) and the centre of the second eddy is towards to the middle of the bay (48.15°N, -53.28°W), migrating 5 km towards the eastern shore of bay. The radius of the eddy is around 10 km with the maximum eddy current of 0.25 m/s. The mean relative vertical vorticity for the inner eddy was estimated to be 2.5e-5 1/s, and the vorticity normalized by the local Coriolis parameter f was 0.25. Taking this relative vorticity as a measurement of the Rossby number, it follows that the momentum balance is not strictly linear and geostropic. Instead, nonlinear effects were dominant.

5.5.3 Temporal and Spatial Variability of Stratification

The model simulations provide a detailed representation of the seasonal and spatial evolution of stratification during summer of 2000 and 2001. The seasonal development of stratification can be affected by the heat flux, with a steady trend from early to late summer. Spatially, the wind-driven turbulence can interrupt the strong stratification and penetrate more deeply in some areas.

To assess the strength of stratification quantitatively, the Richardson number (Ri) and buoyancy frequency (N) are used. The critical Ri is usually taken as 0.25. When Ri exceeds 0.25, the turbulence is suppressed. For Ri>1, the stratification is generally considered stable (Silva et al., 1999; Galperin et al., 2007). Time series of depth-averaged (0-20 m) N^2 and Ri values at M10 (on the western side of Trinity Bay), M11(in the middle of Trinity Bay) and Station 27 (east of St. John's) are shown in Fig. 5-15. Both of these parameters show the seasonal change in water column stratification and mixing in response to solar heating and wind forcing. During May and June extending to day 180,

Ri at the two locations inside Trinity Bay is below the critical value of 0.25 most of the time and Ri at Station 27 is below 1.0 most of the time. The water column stratification is weak and can be frequently disrupted as indicated by the N^2 time series plots. During summer from day 180 to 243, N^2 time series plots at the three locations show an increasing trend corresponding to increased stratification as a result of increasing short-wave radiation incident at the surface. However, N^2 becomes low in response to upwelling induced by southwesterly winds. During early fall, the stratification weakens again at the three stations.

Besides the seasonal change in stratification, the spatial differences and inter-annual changes in stratification can be seen in Fig. 5-15. For both years (2000 and 2001), Ri time series at M11 and M10 drop below 0.25 much more commonly than that at Station 27, suggesting stronger upwelling on the western side of Trinity Bay. With the same wind stress, the stronger upwelling on the western side could be related to the significant bottom slope change along the west coast of Trinity Bay, with around 300 m depth deepening within a 10 km horizontal distance. The inter-annual difference exists from spring to summer. The Ri time series at M10 clearly shows that stratification is weak between day 142 and 160 in 2000, but strong at the same period in 2001. From day 160 to 190, the stratification is weak in 2001, but strong in 2000, indicating the scale of upwelling event changes year by year.

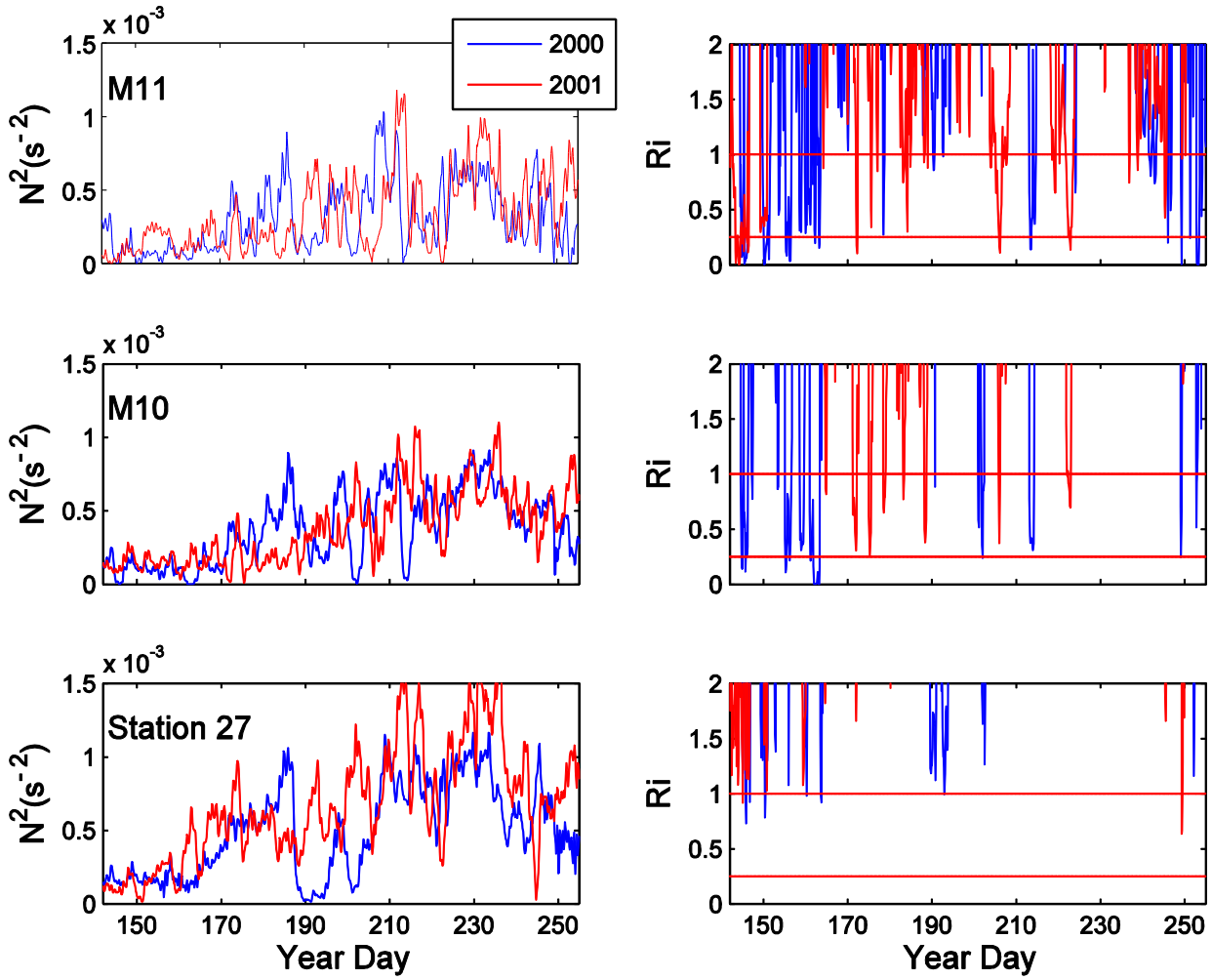

Fig. 5-15: Depth-averaged (0-15 m) buoyancy frequency squared N^2 and Richardson number (Ri) at M11, M10 and Station 27 for May-September 2001. In the plots of the Ri time series, the two red lines denote Ri=1 and Ri=0.25.

5.6 Conclusion and Summary

A three-dimensional finite-volume ocean model was developed to study the upper ocean response to wind off Eastern Newfoundland. The simulation period is from May to September, 2000 and 2001. The model results are compared with observations. Overall, the model simulated the non-tidal elevation, currents and temperature well.

The model results are firstly evaluated against the observed non-tidal sea level, with

an RMS difference of 5.6 cm. The model reproduced the sea surface elevation well, especially for the weekly to seasonal variability. Model currents are reasonable compared against ADCP data along the Flemish Cap Transect. The model transport for the inshore Labrador Current across the Avalon Channel is 0.32 Sv on average, consistent with previous observational estimate. The model temperature at Station 27 is compared with observations at different depths, especially at surface with temperature drop and increase corresponding to the upwelling and surface heat flux input. The statistics for different layers at Station 27 also indicated reasonable agreement between the model and observation, with all RMS differences within $2^{o}\mathrm{C}$. The monthly averaged vertical profiles were compared with observations at Station 27, both with well-developed vertical structure including the sharp thermocline and cold intermediate layer. Model temperatures along the Bonavista and Flemish Cap Transects are in fair comparison with observations, in spite of underestimation of the mixed-layer depth. Inside Trinity Bay, model temperatures agree reasonably well with measurements.

The model reproduces well the dominant inshore Labrador Current. The surface circulation patterns inside Trinity Bay respond strongly to the wind, with two eddies in a 10 km radius. These eddies have the Rossby number of 0.25, indicating the importance of the non-linear process. Wind-induced upwelling prevails inside Trinity and Conception Bay, weak in late spring and strong in summer. The location of upwelling events largely depends on the wind direction. The upwelling at Station 27 is also significant during summer. Stratification in response to surface heat flux and wind shows significant spatial, seasonal and interannual difference in this region.

This study reveals dynamical characteristics associated with upwelling and stratification off Eastern Newfoundland. It also offers improved understanding of the circulation and temperature changes relevant to ongoing biological and fisheries studies.

5.7Acknowledgement

We thank Dr. Changsheng Chen for providing the FVCOM code

5.8Reference:

Afargan, H., H. Gildor. 2015. The role of the wind in the formation of coherent eddies in the Gulf of Eilat/Aqaba. J. Mar. Syst. 142, 75-95.

Aggett, D., H. S. Gaskill,D. Finlayson, S. May, C. Campbell and J. Bobitt. 1987. A study of factors influencing availability of cod in Conception Bay, Newfoundland in 1985. Can. Tech. Rep. Fish. And Aquat. Sci., No. 1562, 123.

Chen, C., G. Cowles and R. C. Beardsley. 2004. An unstructured grid, finite-volume coastal ocean model: FVCOM User Manual. SMAST/UMASSD Technical Report-04-0601. 183.

Chen, C., Z. Lai, R.C. Beardsley, Q. Xu, H. Lin and N.T. Viet. 2012. Current separation and upwelling over the southeast shelf of Vietnam in the South China Sea. J. Geophys. Res. 117, C03033. doi: 10.1029/2011JC007150.

Curry, J.A. and P.J. Webster. 1998. Thermodynamics of atmospheres and oceans. International geophysics Series, Vol. 65, London, Academic Press, p. 471.

Davidson, F. J. M., R.J. Greatbatch, B. deYoung. 2001. Asymmetry in the response of a stratified coastal embayment to wind forcing. J. Geophys. Res. 106, 7001-7015.

deYoung, B., R. Greatbatch and K. Forward. 1993a. A diagnostic coastal circulation model with application to Conception Bay, Newfoundland. J. Phys. Oceanogr. 23, 2617-2635.

deYoung, B., T. Otterson and R.J. Greatbatch. 1993b. The local and nonlocal response of Conception Bay to wind forcing. J. Phys. Oceanogr. 23, 2636-2649.

deYoung, B and B. Sanderson. 1995. The circulation and hydrography of Conception Bay, Newfoundland. Atmosphere-Ocean 33:135-162.

Fairall, C.W.; E.F. Bradley, D.P. Rogers, J.B. Edson and G.S. Young. 1996. Bulk parameterization of air-sea fluxes for COARE. J. Geophys. Res. 101: 3747–3764.

Ferrer, L., A. Caballero. 2011. Eddies in the bay of Biscay: A numerical approximation. J. Mar. Syst. 87, 133-144

Fung, I.Y., D.E. Harrison and A.A. Lacis. 1984. On the variability of the net long-wave radiation at the ocean surface. Rev. Geophys. Space Phys. 22 (2): 177–193.

Galperin, B., S. Sukoriansky and P. Anderson. 2007. On the critical Richardson number in a stably stratified turbulence. Atmos. Sci. Lett. 8(3), 65-69.

Gan, J. and J.S. Allen. 2002. A modeling study of shelf circulation off northern California in the region of the Coastal Ocean Dynamics Experiment: response to relaxation of upwelling winds. J. Geophys. Res. 107:3123.

Geshelin, Y., J. Sheng and R.J. Greatbatch (1999), Monthly mean climatologies of temperature and salinity in the western North Atlantic. Can. Tech. Rep. Hydrogr. Ocean Sci. Report, No. 153. Ocean Sci. Div. of Fish. and Ocean Can., Dartmouth, NS, Canada.

Greatbatch, R.J., T. Otterson. 1991. On the formulation of open boundary conditions at the mouth of a bay. J. Geophys. Res. 96, 18431-18445.

Greenberg, D. A. and B. D. Petrie. 1988. The mean barotropic circulation on the Newfoundland shelf and slope. J. Geophys. Res. 93, 15541-15550.

Han, G. 2000. Three-dimensional modelling of tidal currents and mixing quantities over the Newfoundland Shelf. J. Geophys. Res. 105, 11407-11422.

Han, G. 2005. Wind-driven barotropic circulation off Newfoundland and Labrador. Cont. Shelf Res.. 25, 2084-2106.

Han, G., Z. Lu, Z. Wang, J. Helbig, N. Chen and B. deYoung. 2008. Seasonal variability of the Labrador Current and shelf circulation off Newfoundland. J. Geophys. Res.. 113, 1-23.

Han, G, Z. Ma, D. Chen, B. deYoung and N. Chen. 2012. Observing storm surges from space: Hurricane Igor off Newfoundland. Sci. Rep. 2, 1010; DOI:10.1038/srep010101.

Han, G., Z. Ma, B. de Young, M. Foreman, and N. Chen, 2011. Simulation of three-dimensional circulation and hydrography over the Grand Banks of Newfoundland, Ocean Modelling. 40, 199-210.

Lentz, S.J., D.C. Chapman. 2004. The importance of nonlinear cross-shelf momentum flux during wind-driven coastal upwelling. J. Phys. Oceanogr. 22(12), 1517-1539.

Li, J., J. Scinocca, J. Lazare, M. Mcfarlane, N. Mcfarlane, K. Von Salzen and L. Solheim.

2006. Ocean surface albedo and its impact on radiation balance in climate model. J. Clim. 19: 6314–6333.

Ma, Z., G. Han and B. deYoung. 2012. Modelling temperature, currents and stratification in Placentia Bay. Atmosphere-Ocean 50: 244-260.

Ma, Z., G. Han and B. deYoung. 2015. Oceanic responses to hurricane Igor over the Grand Banks: a modelling study. J. Geophys. Res. Oceans. 120:doi:10.1002/2014JC010322.

Mellor, G.L., T. Ezer and L.Y. Oey. 1993. The pressure gradient conundrum of sigma coordinate ocean models, J. Atmos. Ocean. Tech, 11: 1126–1134.

Monahan, E.G. and G. MacNiocaill. 1986. Oceanic whitecaps and their role in air-sea exchange processes. Springer-Verlag New York, LLC.

Pawlowicz, R., B. Beardsley, and S. Lentz. 2002. Classical tidal harmonic analysis including error estimates in MATLAB using T_TIDE. Computers and Geosciences 28, 929-937.

Rego, J.L. and C. Li. 2010. Storm surge propagation in Galveston Bay during Hurricane Ike, J. Mar. Syst., 82, 265-279

Resio, D.T. and J.J. Westerink. 2008. Modeling the physics of storm surges, Physics Today, 61 (9), 33–38.

Senciall, D., N. Chen, E. Cobourne, G. Han and J. Loder. 2006. ADCP currents along the Flemish Cap Transect. The National Science Workshop, Fisheries and Oceans Canada, Mont-Joli, Quebec.

Schillinger, D., B. deYoung and J. Foley. 2000a. Two-Yo and temperature data from Trinity Bay, May 2000. Physics and physical oceanography data report 2000-2, Memorial University, 29.

Schillinger, D., B. deYoung and J. Foley. 2000b. Physical and Biological TowYo data from Trinity Bay, July 2000. Physics and Physical oceanography data report 2000-4, Memorial University, 18.

Silva, I.P.D., A. Brandt, L. J. Montenegro and H. J. S. Fernando. 1999. Gradient Richardson number measurements in a stratified shear layer. Dynam. Atmos. Oceans. 20(1), 47-64.

Smith, R.L. 1995. The physical processes of coastal ocean upwelling systems. In: et al CPS (ed) Upwelling in the ocean: modern processes and ancient records. Wiley, New York, pp 39-64.

Tang, C. L., Q. Gui and I. K. Peterson. 1996. Modelling the mean circulation of the Labrador sea and adjacent shelves. J. Phys. Oceanogr. 26, 1989-2010.

Tittensor, D., R. Naud, B. deYoung and J. Foley. 2002a. Analysis of physical oceanographic data from Trinity Bay: May-August 2001. Physics and Physical oceanography data report 2002-1, Memorial Univeristy, 77.

Tittensor, D., R. Naud, B. deYoung and J. Foley. 2002b. Analysis of physical oceanographic data from Trinity Bay: May-August 2002. Physics and physical oceanography data report 2002-2, Memorial Univerity, 52.

Weisberg, R. H. and L. Zheng. 2006. Circulation of Tampa Bay driven by buoyancy, tides and winds, as simulated using a Finite Volume Coastal Ocean Model. J. Geophys. Res.. 111(C1).

6. Summary and Future Work

This study applies a finite volume ocean model (FVCOM) over the Newfoundland Shelf and in coastal embayments. The FVCOM model provided the ability to well-resolve the coastal ocean dynamics with high resolution grids near the coast. Three models are established to accomplish objectives in Chapter 1.4.

In Chapter 3, a 3-D, baroclinic, finite-volume ocean model was developed to study the upper-ocean responses to Hurricane Igor over the Grand Banks of Newfoundland. Reconstructed hurricane winds were applied to force this ocean model. The 3-D baroclinic ocean model reproduced the sea surface elevation before and after the storm reasonably well. Especially, the two surges generated by the passage of Hurricane Igor were well captured. Both the model and observations showed two surges at St. John's, Argentia and St. Lawrence. The first surge was attributed to the direct local wind forcing and the second one was the result of the propagating continental shelf wave generated by the storm. The model surface temperatures were compared with observations at three buoy stations over the Grand Banks. Both model and observation showed a significant decrease of $6^{\circ}C$ in the sea surface temperature. Furthermore, the calculated horizontal distribution of the sea surface temperature was compared with satellite observations. The model reproduced well the southward increase of temperature observed before the storm and the sharp decrease afterwards. The model near sea surface current was compared with observations at a point located in the outer Placentia Bay. The model was able to generate the observed variability of surface currents. The storm induced shelf wave was examined by analysing the sea level at tide-gauge stations and currents at a point far away from the

storm centre to prevent direct storm wind effects. Both observation and model results showed a propagation speed of 14-16 m/s and 0.5-0.7 CPD, consistent with the continental shelf-wave estimate from Han et al. (2012b). We further analyzed the vertically averaged currents in the outer Placentia Bay. The results highly support those from sea level data. The storm excited waves propagate equatorward along the Newfoundland coast. These waves can not only be observed from the sea surface elevation field but also from the horizontal currents. An examination of the Burger number and Ekman pumping parameters indicates that the entrainment due to turbulent mixing is the dominant process causing the sudden drop in SST. Upwelling associated with the wind stress curl plays a small supplementary role only. Results show that a 3-D baroclinic model simulates the storm surge slightly better than does an alternative 3-D barotropic model. The difference may be attributed to weaken bottom currents and thus friction in the 3-D baroclinic model. It is shown that sea surface cooling is well simulated with a k-ε turbulence closure, but is significantly underestimated with the commonly used MY2.5 closure.

In Chapter 4, a three-dimensional finite-volume ocean model was applied to study the upper-layer responses to two hurricanes in Placentia Bay, Newfoundland. The hurricanes chosen for the study are Hurricane Igor (2010) and Hurricane Leslie (2012). The two hurricanes feature different tracks, strength, and translation speed, resulting in quite different oceanic responses on sea level and upper-layer circulation. The finite-volume ocean model reproduced the water level rise before and after hurricanes. Especially, the surges generated by the passage of Hurricane Igor were captured well. The model sea level showed a good agreement with observations for Hurricane Leslie, in spite

of over-estimation of the storm-induced inertial oscillation. The model near-surface current was compared with observations at three different locations in Placentia Bay, two of which are located in the inner bay. Especially during hurricane events, simulated currents well capture the observed currents, in terms of magnitude and variability. The model reproduced the general cyclonic circulation in Placentia Bay before the two hurricanes. The upper 30 m circulation responding to the two hurricanes had opposite patterns. Upper-layer currents during Igor had strong outflow out of the inner bay while during Leslie strong inflow was observed. Cases without local atmospheric forcing were examined. The results showed the local atmospheric forcing contributed to the peak storm surges by over 50% during Leslie, but insignificantly during Igor, indicating that the local forcing may have much more influence in western-type storms than in eastern-type storms, depending on the distance from the landfall point to the bay. The remote coastally trapped wave contributes more to sea level rise for the Igor-like case. An examination of the circulation with and without stratification revealed the importance of baroclinicity for the hurricane response in Placentia Bay. The near surface currents during the two hurricanes were significantly decreased after removing the stratification. Thus, the local baroclinic effect was essential in reproducing the hurricane-induced current intensification and inertial oscillation in Placentia Bay. The recovery time is much longer for the baroclinic case, due to the reduced propagation speed of the baroclinic wave. This also suggests that the baroclinic wave and its propagation are an important process in generating the storm-induced surface current. Vertical structures of the model currents at the mooring stations show substantially different vertical energy distribution between the baroclinic and barotropic cases.

In Chapter 5, a three-dimensional finite-volume ocean model was developed to study the upper ocean response to wind off Eastern Newfoundland. The simulation period is from May to September, 2000 and 2001. The model results are compared with observations. Overall, the model simulated the non-tidal elevation, currents and temperature well. The model reproduced the sea surface elevation well, especially for the weekly to seasonal variability. Model currents are reasonable compared against ADCP data along the Flemish Cap Transect. The model transport for the inshore Labrador Current across the Avalon Channel is 0.32 Sv on average, consistent with a previous observational estimate (Greenberg and Petrie, 1988). The model temperature at Station 27 is compared with observations at different depths, especially at surface with temperature drop and increase corresponding to the upwelling and surface heat flux input. The monthly averaged vertical profiles were compared with observations at Station 27, both with well-developed vertical structure including the sharp thermocline and cold intermediate layer. Model temperatures along the Bonavista and Flemish Cap Transects are in fair comparison with observations, in spite of underestimation of the mixed-layer depth. Inside Trinity Bay, model temperatures agree reasonably well with measurements. The model reproduces well the dominant inshore Labrador Current. The surface circulation patterns inside Trinity Bay respond strongly to the wind, with two eddies in a 10 km radius. These eddies have a Rossby number of 0.25, indicating the importance of the non-linear process. Wind-induced upwelling prevails inside Trinity and Conception Bay, weak in late spring and strong in summer. The location of upwelling events largely depends on the wind direction. The upwelling at Station 27 is also significant during summer. Stratification in response to surface heat flux and wind shows significant spatial,

seasonal and interannual difference in this region.

This thesis has documented a successful effort at setting up a model framework for the Newfoundland Shelf with the finite volume modelling approach and offers new insights into modelling oceans' responses to hurricanes and into coastal dynamics on different time scales in coastal embayments such as Placentia Bay and Trinity Bay. However, there remain some limitations in the application of this model.

One improvement could be on the addition of a method to reconstruct the high resolution hurricane winds field for application over the Newfoundland Shelf. A more accurate wind field could perform better in reproducing the storm surges. In the future, by applying the observed hourly and high-resolution wind data in the hurricane model (Regio and Li, 2010), the reconstructed local winds should be improved to generate more accurate high-frequency sea level. By assimilation of the observed winds in the hurricane model, the asymmetry of the hurricanes can be applied to produce the intensified wind speed at the right side of the storms.

The second improvement could be to increase the resolution of the atmospheric forcing. The present model uses wind and heat flux data from NARR to force the model. The resolution of the atmospheric model results is 32km in space and three hourly time step in output. Higher-resolution atmospheric filed can improve the ocean model results before and after the storms.

The last improvement could be the parameterization of the turbulent mixing scheme. The model results show the surface cooling with mixed layer depth deepening is sensitive to the turbulent mixing scheme. A more accurate turbulent mixing scheme is helpful to improve the evolution of stratification during the hurricanes (Marques and Ozgokmen,

2014).

Reference:

Afargan, H., H. Gildor. 2015. The role of the wind in the formation of coherent eddies in the Gulf of Eilat/Aqaba. *J. Mar. Syst*. 142, 75-95.

Aggett, D., H. S. Gaskill, D. Finlayson, S. May, C. Campbell and J. Bobitt. 1987. A study of factors influencing availability of cod in Conception Bay, Newfoundland in 1985. *Can. Tech. Rep. Fish. And Aquat. Sci*., No. 1562, 123.

Blumberg, A.F., and G.L. Mellor. 1987. A description of a three-dimensional coastal ocean circulation model, in Three-Dimensional Coastal Ocean Models, Vol. 4, edited by N.Heaps, pp. 208, American Geophysical Union, Washington, D.C.

Blumberg, A. F. A primer for Ecom-si. 1994. Technical Report of HydroQual, Inc., 66 pp.

Bradbury, I.R.; P.V.R. Snelgrove and S. Fraser. 2000. Transport and development of eggs and larvae of Atlantic cod, Gadus morhua, in relation to spawning time and location in coastal Newfoundland. *Can. J. Fish. Aquat. Sci*. 57: 1761–1772.

Burchard, H. 2001. Simulating the wave-enhanced layer under breaking surface waves with two-equation turbulence models. *J. Phys. Oceanogr*., 31, 3133-3145.

Csanady,G.T., 1972. Response of large stratified lakes to wind. *J. Phys.Oceanogr*. 2, 3-13.

Casey, K.S., T.B. Brandon, P. Cornillon and R. Evans. 2010. The Past, Present and Future of the AVHRR Pathfinder SST Program, in Oceanography from Space: Revisited, eds. V. Barale, J.F.R. Gower, and L. Alberotanza, Springer, doi: 10.1007/978-90-481-8681-5_16.

Chen, C., H. Liu and R.C. Beardsley. 2003. An unstructured grid, finite volume primitive equation coastal ocean model: application to coastal ocean and estuaries. J. Atmos. Ocean. Technol, 20, 159–186.

Chen, C., G. Cowles and R. C. Beardsley. 2004. An unstructured grid, finite-volume coastal ocean model: FVCOM User Manual. SMAST/UMASSD Technical Report-04-0601. 183.

Chen, C., Xie, L., 1997. A numerical study of wind-induced, near-inertial oscillations over the Texas-Louisiana shelf. *J. Geophys. Res*. 102, 15583-15593.

Chen, C., Z. Lai, R.C. Beardsley, Q. Xu, H. Lin and N.T. Viet. 2012. Current separation and upwelling over the southeast shelf of Vietnam in the South China Sea. *J. Geophys. Res.* 117, C03033. doi: 10.1029/2011JC007150.

Colbourne, E., B. deYoung, S. Narayanan et al. Comparison of hydrography and

circulation on the Newfoundland Shelf during pages 1990-1993 with the long-term mean. Canadian Journal of Fisheries and Aquatic Sciences. 54, 68-80.

Curry, J.A. and P.J. Webster. 1998. Thermodynamics of atmospheres and oceans. International geophysics Series, Vol. 65, London, Academic Press, p. 471.

Davidson, F. J. M., R.J. Greatbatch, B. deYoung. 2001. Asymmetry in the response of a stratified coastal embayment to wind forcing. J. Geophys. Res. 106, 7001-7015.

deYoung, B., and C. Tang. 1990. Storm-forced baroclinic near-inertial currents on the Grand Bank, *Journal of Physical Oceanography*, 20: 1725-1741.

deYoung, B., R. Greatbatch and K. Forward. 1993a. A diagnostic coastal circulation model with application to Conception Bay, Newfoundland. Journal of Physical Oceanography. 23, 2617-2635.

deYoung, B., T. Otterson and R.J. Greatbatch. 1993b. The local and nonlocal response of Conception Bay to wind forcing. *Journal of Physical Oceanography*. 23, 2636-2649.

deYoung, B and B. Sanderson. 1995. The circulation and hydrography of Conception Bay, Newfoundland. Atmosphere Ocean 33:135-162.

Emanuel, K.A. 2005. Increasing destructiveness of tropical cyclones over the past 30 years. *Nature*. 436, 686-688.

Fairall, C.W.; E.F. Bradley, D.P. Rogers, J.B. Edson and G.S. Young. 1996. Bulk parameterization of air-sea fluxes for COARE. *J. Geophys. Res*. 101: 3747–3764.

Ferrer, L., A. Caballero. 2011. Eddies in the bay of Biscay: A numerical approximation. *J. Mar. Syst*. 87, 133-144

Foreman, M., P. Czajko, D.J. Stucchi and M. Guo. 2009. A finite volume model simulation for the Broughton Archipelago, Canada, *Ocean Modelling*, 30: 29–47.

Fung, I.Y., D.E. Harrison and A.A. Lacis. 1984. On the variability of the net long-wave radiation at the ocean surface. *Rev. Geophys. Space Phys*. 22 (2): 177–193.

Galperin, B., L. H. Kantha, S. Hassid, and A. Rosati. 1988. A quasi-equilibrium turbulent energy model for geophysical flows. *J. Atmos. Sci*., 45, 55-62.

Galperin, B., S. Sukoriansky and P. Anderson. 2007. On the critical Richardson number in a stably stratified turbulence. Atmos. *Sci. Lett*. 8(3), 65-69.

Gan, J. and J.S. Allen. 2002. A modeling study of shelf circulation off northern California

in the region of the Coastal Ocean Dynamics Experiment: response to relaxation of upwelling winds. *J. Geophys. Res.* 107:3123.

Geshelin, Y., J. Sheng and R.J. Greatbatch. 1999. Monthly mean climatologies of temperature and salinity in the western North Atlantic. Can. Tech. Rep. Hydrogr. Ocean Sci. Report, No. 153. Ocean Sci. Div. of Fish. and Ocean Can., Dartmouth, NS, Canada.

Gill, A.E. 1984. On the behavior of internal waves in the wakes of storms. *J. Phys. Oceanogr.* 14, 1129-1151.

Greenberg, D. A. and B. D. Petrie. 1988. The mean barotropic circulation on the Newfoundland shelf and slo;pe. *J. Geophys. Res*. 93, 15541-15550.

Greatbatch, R.J., T. Otterson. 1991. On the formulation of open boundary conditions at the mouth of a bay. *J. Geophys. Res*. 96, 18431-18445.

Greatbatch, R.J. 1983. On the response of the ocean to a moving storm: the nonlinear dynamics. *J. Phys. Oceanogr*. 13, 357-367.

Han, G. 2000. Three-dimensional modelling of tidal currents and mixing quantities over the Newfoundland Shelf. *J. Geophys. Res*. 105, 11407-11422.

Han, G. 2005. Wind-driven barotropic circulation off Newfoundland and Labrador. *Cont. Shelf Res*. 25, 2084-2106.

Han, G., Z. Lu, Z. Wang, J. Helbig, N. Chen and B. deYoung. 2008. Seasonal variability of the Labrador Current and shelf circulation off Newfoundland. *J. Geophys. Res*. 113, 1-23.

Han, G., S. Paturi, B. de Young, S. Yi, and C.-K. Shum. 2010. A 3-D data-assimilative tide model of Northwest Atlantic. *Atmosphere-Ocean*. 48, 39-57.

Han, G., Z. Ma, B. de Young, M. Foreman, and N. Chen. 2011. Simulation of three-dimensional circulation and hydrography over the Grand Banks of Newfoundland. *Ocean Modelling*. 40, 199-210.

Han G., Z. Ma and N. Chen. 2012a. Hurricane Igor impacts on the stratification and phytoplankton bloom over the Grand Banks, *Journal of Marine System*, 100-101, 19-25.

Han, G., Z. Ma, D. Chen, B. deYoung and N. Chen. 2012b. Observing storm surges from space: Hurricane Igor off Newfoundland, *Scientific Report*, doi: 10.1038/srep01010.

Han, G., Z. Ma, N. Chen, R. Thomson and A. Slangen. 2015. Changes of mean relative sea level around Canada in the 20th and 21st centuries. Atmosphere-ocean. Accepted.

Hart, D.J., B. deYoung, and J. Foley. 1999. Observations of currents, temperature and salinity in Placentia Bay, Newfoundland. Physics and Physical Oceanography Data Report 1998–9, Memorial University of Newfoundland, St. John's: Newfoundland.

Hannah, C.G., D.A. Greenberg, J.W. Loder and Z. Xu. 1995. Seasonal baroclinic circulation in the scotia-maine and Grand Banks regions. *Can. Tech. Rep. Hydrogr. Ocean Sci*. 169, 81-85, Ocean Sci. Div. of Fish. And Ocean Can., Dartmouth, N. S., Canada.

Holland, G. J. 1980. An analytic model of the wind and pressure profiles in hurricanes, *Mon, Weather Rev*., 108, 212–1218.

Hubbard, M. E. 1999. Multidimensional slope limiters for MUSCL-type finite volume schemes on unstructured grid. J. Comput. Phys. 155, 54-74.

Jones, J.E., and A.M. Davies. 2004. On the sensitivity of computed surges to open-boundary formulation, *Ocean Dynamics*, 54 (2), 142–162.

Kobayashi, M. H., J. M. C. Pereira and J. C. F. Pereira. 1999. A conservative finite volume second order accurate projection method on hybrid unstructured grids. J. Comput. Phys. 150, 40-75.

Krajcar, V., Orlic, M., 1995. Seasonal variability of inertial oscillations in the Northern Adriatic. *Cont. Shelf. Res*. 15, 1221-1233.

Kraus, E. B. 1972. Atmosphere-Ocean Interaction. *Clarendon Press*, 275pp.

Lentz, S.J., D.C. Chapman. 2004. The importance of nonlinear cross-shelf momentum flux during wind-driven coastal upwelling. *J. Phys. Oceanogr*. 22(12), 1517-1539.

Li, J., J. Scinocca, J. Lazare, M. Mcfarlane, N. Mcfarlane, K. Von Salzen and L. Solheim. 2006. Ocean surface albedo and its impact on radiation balance in climate model. *J. Clim*. 19: 6314–6333.

Liu, Y., P. MacCready, B.M. Hickey, E. P. Dever, P.M.Kosro, and N.S. Banas. 2009. Evaluation of a coastal ocean circulation model for the Columbia River plume in summer 2004. *J. Geophys. Res.* 114, C00B04, doi: 10.1029/2008JC004929.

Loder, J. W., B. D. Petrie, and G. Gawarkiewicz. 1998. The coastal ocean off northeastern North America: A large-scale view, in The Global Coastal Ocean: Regional Studies and Synthesis, vol. 11, edited by K. H. Brink and R. Robinson, chap. 5, pp. 105–133, John Wiley, Hoboken, N. J.

Lynch, D. R., and C. E. Naimie. 1993. The M2 tide and its residual on the outer banks of the Gulf of Maine, J. Phys. Oceanogr., 23, 2222-2253.

Ma, Z., G. Han and B. deYoung. 2012. Modelling temperature, currents and stratification in Placentia Bay. *Atmosphere-Ocean.* 50: 244-260.

Ma, Z., Han, G., deYoung, B., 2015. Oceanic responses to hurricane Igor over the Grand Banks: a modelling study. *J. Geophys. Res. Oceans*. 120:doi:10.1002/2014JC010322.

Madala, R. V., and S. A. Piacsek. 1977. A semi-implicit numerical model for baroclinic oceans, *J. Cornput. Phys*., 23, 167-178.

Marques, G.M., and T.M. Ozgokmen. 2014. On modeling turbulent exchange in buoyancy-driven fronts. *Ocean modelling*. 83, 43-62.

Mellor, G. L. and A. Blumberg. 2004. Wave breaking and ocean surface layer thermal response. *J. Phys. Oceanogr*., 34, 693-698.

Mellor, G.L., T. Ezer and L.Y. Oey. 1993. The pressure gradient conundrum of sigma coordinate ocean models, *J. Atmos. Ocean. Tech*, 11: 1126–1134.

Mellor, G. L. and T. Yamada. 1982. Development of a turbulence closure model for geophysical fluid problem. Rev. *Geophys. Space. Phys*., 20, 851-875.

Mesinger, F., Dimego, G., Kalnay, E., Shafran, P., Ebisuzaki,W., Jovic,D., Wollen,J., Mitchell, K., Rogers, E., Fan, M., Ek,Y., Grumbine, R., Higgins, W., Li, H., Lin, Y., Manikin,G., Parrish,D., Shi,W., 2006. North American Regional Reanalysis. Bull. Amer. Mereor. Soc. 87, 343-360.

Monahan, E.G. and G. MacNiocaill. 1986. Oceanic whitecaps and their role in air-sea exchange processes. Springer-Verlag New York, LLC.

Morey, S.L., S. Baig, M.A. Bourassa, D.S. Dukhovskoy and J.J. O'Brien. 2006. Remote forcing contribution to storm-induced sea level rise during Hurricane Dennis. *Geophysical Research Letters*, 33, L19603, doi: 10.1029/2006GL027021.

Naimie, C. E. 1996. Georges Bank residual circulation during weak and strong stratification periods: prognostic numerical model results. *J. Geophys. Res*. 101(C3), 6469-6486.

Pasch, R.J. and T.B. Kimberlain. 2011. Tropical Cyclone Report Hurricane Igor (AL112010).

Pawlowicz.R, B. Beardsley and S. Lentz. 2002. Classical tidal harmonic analysis including error estimates in MATLAB using T_TIDE. *Computers and Geosciences*. 28:929-937.

Pedlosky, J. 1974. Longshore currents, upwelling and bottom topography. *J. Phys. Oceanogr*., 4, 214-226.

Phadke, A. C., C. D. Martino, K.F. Cheung, and S. H. Houston. (2003). Modelling of tropical cyclone winds and waves for emergency management. *Ocean Engineering*. 30, 553-578.

Pepin, P. and J.A. Helbig. 1997. Distribution and drift of Atlantic cod (Gadus morhua) eggs and larvae on the northeast Newfoundland shelf, Can. *J. Fish. Aquat. Sci*, 54, 670–685.

Peng, M., L. Xie and J. Pietrafesa. 2006a. A numerical study on hurricane induced storm surge and inundation in Charleston, South Carolina, *J. Geophys. Res*, 111, C08017. doi:10.1029/2004JC002755.

Peng, M., L. Xie and J. Pietrafesa. 2006b. Tropical cyclone induced asymmetry of sea level surge and fall and its presentation in a storm surge model with parametric wind fields, *Ocean Model*,14, 81–101.

Price, F. 1981. Upper ocean response to a hurricane, *J.Phys.Oceanogr*. 11, 153-175.

Rego, J.L. and C. Li. 2010. Storm surge propagation in Galveston Bay during Hurricane Ike, *Journal of Marine System,* 82, 265-279

Resio, D.T. and J.J. Westerink. 2008. Modeling the physics of storm surges. *Physics Today*, 61 (9), 33–38.

Senciall, D., N. Chen, E. Cobourne, G. Han and J. Loder. 2006. ADCP currents along the Flemish Cap Transect. The National Science Workshop, Fisheries and Oceans Canada, Mont-Joli, Quebec.

Shen, J., W. Gong and H.V. Wang. 2006. Water level response to 1999 Hurricane Floyd in the Chesapeake Bay. *Cont. Shelf. Res*, 26, 2484–2502.

Sheng, J., X. Zhai and R. Greatbatch. 2006. Numerical study of storm –induced circulation on the Scotian Shelf during Hurricane Juan using a nested-grid ocean model. *Progress in Oceanography* , 70, 233-254.

Sheng, J. and K.R. Thompson. 1996. Surface circulation on the Newfoundland Shelf and Grand Banks: The roles of local density gradients and remote forcing. *Atmosphere-ocean.* 43, 257-284.

Schillinger, D., B. deYoung and J. Foley. 2000a. Two-Yo and temperature data from Trinity Bay, May 2000. Physics and physical oceanography data report 2000-2, Memorial University, 29.

Schillinger, D., B. deYoung and J. Foley. 2000b. Physical and Biological TowYo data from Trinity Bay, July 2000. Physics and Physical oceanography data report 2000-4, Memorial University, 18.

Schillinger, D.J., Simmons,P., deYoung, B., 2000c. Analysis of the mean circulation in Placentia Bay: spring and summer 1999. Physics and physical oceanography data report 2000-1, Memorial University of Newfoundland: St. Johns, Newfoundland.

Silva, I.P.D., A. Brandt, L. J. Montenegro and H. J. S. Fernando. 1999. Gradient Richardson number measurements in a stratified shear layer. *Dynam. Atmos. Oceans*. 20(1), 47-64.

Simpson, J. J. and T. D. Dickey, 1981a: The relationship between downward irradiance and upper ocean structure. *J. Phys. Oceanogr*., 11, 309-323.

Simpson, J. J. and T. D. Dickey, 1981b: Alternative parameterizations of downward irradiance and their dynamical significance. *J. Phys. Oceanogr*., 11, 876-882.

Smagorinsky, J. 1963. General circulation experiments with the primitive equations, I. The basic experiment. Monthly Weather Review, 91:99-164.

Smith, R.L. 1995. The physical processes of coastal ocean upwelling systems. In: et al CPS (ed) Upwelling in the ocean: modern processes and ancient records. Wiley, New York, pp 39-64.

Stacey, M. W. 1999. Simulation of the wind-forced near-surfacee circulation in Knight Inlet: a parameterization of the roughness length. *J. Phys. Oceanogr*., 29, 1363-1367.

Tang, C. L., Q. Gui and I. K. Peterson. 1996. Modelling the mean circulation of the Labrador sea and adjacent shelves. *J. Phys. Oceanogr*. 26, 1989-2010.

Tang, C.L., Q. Gui and B.M. Detracey. 1998. Barotropic response of the Labrador/Newfoundland Shelf to a moving storm, *J. Phys. Oceanogr*, 28, 1152-1172.

Terray, E. A., M. A. Donelan, Y. C. Agrawal, W. M. Drnnan, K. K. Kahma, A. J. Williams, P. A. Hwang, and S. A. Kitaigorodski. 1996. Estimates of kinetic energy dissipation under breaking waves. *J. Phys. Oceanogr*., 26, 792-807.

Terray, E. A., M. A. Donelan, Y. C. Agrawal, W. M. Drnnan, K. K. Kahma, A. J. Williams, P. A. Hwang, and S. A. Kitaigorodski. 1997. Reply. *J. Phys. Oceanogr*., 27, 2308-2309.

Terray, E. A., W. M. Donelan, and M. A. Donelan. 2000. The vertical structure of shear and dissipation in the ocean surface layer. Proc. Symp. On Air-Sea Interaction Sdyney, Australia, University of New South Wales, 239-245.

Tittensor, D., R. Naud, B. deYoung and J. Foley. 2002a. Analysis of physical oceanographic data from Trinity Bay: May-August 2001. Physics and Physical oceanography data report 2002-1, Memorial Univeristy, 77.

Tittensor, D., R. Naud, B. deYoung and J. Foley. 2002b. Analysis of physical oceanographic data from Trinity Bay: May-August 2002. Physics and physical oceanography data report 2002-2, Memorial Univerity, 52.

Thiebaut.S and R. Vennell. 2010. Observation of a fast continental shelf wave generated by a storm impacting Newfoundland using wavelet and cross-wavelet analyses, *J. Phys. Oceanogr*, 40, 417-428.

Urrego-Blanco, J. and J. Sheng. 2012. Interannual variability of the circulation over the Eastern Canadian Shelf. *Atmosphere-Ocean*. 50, 277-300.

Wada, A. 2005. Numerical simulations of sea surface cooling by a mixed layer model during the passage of Typhoon Rex. *J. Oceanogr*. 61. 41-57.

Webster, P.J., G.J.Holland, J.A.Curry, and H.R.Chang. 2005. Changes in tropical cyclone number, duration, and intensity in a warming environment. *Science.* 309, 1844-1846.

Weisberg, R.H. and L. Zheng. 2006a. Hurricane storm surge simulation for Tampa Bay, *Estuaries Coasts*. 29 (6), 899–913.

Weisberg, R.H. and L. Zheng. 2006b. A simulation of the Hurricane Charley storm surge and its breach of North Captiva Island, *Fla. Sci.* 69, 152–165.

Weisberg, R. H., Zheng, L., 2006c. Circulation of Tampa Bay driven by buoyancy, tides and winds, as simulated using a Finite Volume Coastal Ocean Model. *J. Geophys. Res.* 111, C1005, doi:10.1029/2005JC003067.

Weisberg, R.H. and L. Zheng. 2008. Hurricane Storm surge simulations comparing three-dimensional with two-dimensional formulations based on an Ivan-like storm over the Tampa Bay, Florida region, *J. Geophys. Res*. 113, C12001, doi: 10.1029/2008JC005115.

Westerink, J. J., R. A. Luettich, J. C. Feyen, J. H. Atkinson, C. Dawson, H. J. Roberts, M. D. Powell, J. P. Dunion, E. J. Kubatko and H. Pourtaheri. 2008. A basin- to channel-scale unstructured grid hurricane storm surge model applied to Southern Louisiana. *Mon. Weather Rev*, 136, 833–864.

Willmott, C.J. (1981). On the validation of models. *Phys. Geogr*., 2, 184-194.

Xie, L., L. Pietrafesa and M. Peng. 2004. Incorporation of a mass-conserving inundation scheme into a three dimensional storm surge model. *J. Coast. Res*. 20 (4), 1209–1223.

Xie, L., S. Bao, L. Pietrafesa, K. Foley and M. Fuentes. 2006. A real-time hurricane surface wind forecasting model: formulation and verification. *Mon.Weather. Rev*, 134, 1355–1370.

Yao, T. 1986. The response of currents in Trinity Bay, Newfoundland, to local wind forcing. *Atmosphere-Ocean.* 24,235–252.

Zhang, J.A. and E. W. Uhlhorn (2012). Hurricane sea surface inflow angle and an observation-based parametric model. *Mon.Weather. Rev.* 140, 3587-3605.